AEDC-TR-80-25

Computer Controlled Life Testing of Light-Emitting Diodes (LED's)

A. E. Lennert and J. B. Puckett
ARO, Inc.

February 1981

Final Report for Period January 1976 – December 1979

Approved for public release; distribution unlimited.

ARNOLD ENGINEERING DEVELOPMENT CENTER
ARNOLD AIR FORCE STATION, TENNESSEE
AIR FORCE SYSTEMS COMMAND
UNITED STATES AIR FORCE

APPROVAL STATEMENT

This report has been reviewed and approved.

Marshall K. Kingery

MARSHALL K. KINGERY
Project Manager
Directorate of Technology

Approved for publication:

FOR THE COMMANDER

Marion L. Laster

MARION L. LASTER
Director of Technology
Deputy for Operations

REPORT DOCUMENTATION PAGE		READ INSTRUCTIONS BEFORE COMPLETING FORM
1 REPORT NUMBER AEDC-TR-80-25	2 GOVT ACCESSION NO.	3 RECIPIENT'S CATALOG NUMBER
4 TITLE (and Subtitle) COMPUTER CONTROLLED LIFE TESTING OF LIGHT-EMITTING DIODES (LED's)		5 TYPE OF REPORT & PERIOD COVERED Final Report-January 1976 to December 1979
		6 PERFORMING ORG. REPORT NUMBER
7 AUTHOR(s) A. E. Lennert and J. B. Puckett, ARO, Inc., a Sverdrup Corporation Company		8 CONTRACT OR GRANT NUMBER(s)
9 PERFORMING ORGANIZATION NAME AND ADDRESS Arnold Engineering Development Center/DOT Air Force Systems Command Arnold Air Force Station, Tennessee 37389		10 PROGRAM ELEMENT, PROJECT TASK AREA & WORK UNIT NUMBERS Program Element 65807F
11 CONTROLLING OFFICE NAME AND ADDRESS Arnold Engineering Development Center/DOS Air Force Systems Command Arnold Air Force Station, Tennessee 37389		12 REPORT DATE February 1981
		13 NUMBER OF PAGES 128
14 MONITORING AGENCY NAME & ADDRESS(if different from Controlling Office)		15 SECURITY CLASS. (of this report) UNCLASSIFIED
		15a DECLASSIFICATION/DOWNGRADING SCHEDULE N/A

16 DISTRIBUTION STATEMENT (of this Report)

Approved for public release; distribution unlimited.

17 DISTRIBUTION STATEMENT (of the abstract entered in Block 20, if different from Report)

18 SUPPLEMENTARY NOTES

Available in Defense Technical Information Center (DTIC)

19 KEY WORDS (Continue on reverse side if necessary and identify by block number)

life tests	output	current density
light emitting diodes	degradation	
measurement	voltage	
light	temperature	

20 ABSTRACT (Continue on reverse side if necessary and identify by block number)

An automated, computer-controlled, test complex was designed and built to life test a large number of light-emitting diodes (LED's). One of the objectives of the test was to determine the minimum burn-in time required to estimate the lifetime of the LED's. The test setup, experimental hardware, operating details, and the problems that arose during the test program are described. Experimental and theoretical results of attempts to estimate the life-

20. ABSTRACT (Continued)

times of the devices are presented and discussed. It was found that if the light output power degraded by more than 15 percent of the initial light output power and if there was a voltage change exhibited by the LED's of more than 100 mv, within a period of 200 hr, then the light output power of the LED's would fall below 50 percent of the original light output power within 2,000 hr of operation. The initial degradation rate was found to be proportional to the operating temperature and current density, whereas the degradation rate of those devices that passed the screening criteria appeared to be independent of these parameters after 2,000 hr of operation. The double-heterojunction devices had a longer mean time to failure than did the homojunction devices. The time to obtain 50 percent of the initial light output power was used as a criterion of failure.

AFSC
Arnold AFS Tenn

PREFACE

The work reported herein was conducted by the Arnold Engineering Development Center (AEDC), Air Force Systems Command (AFSC), under the sponsorship of the Naval Ocean Systems Center (NOSC). The results of the research were obtained by ARO, Inc., AEDC Group (a Sverdrup Corporation Company), operating contractor for the AEDC, AFSC, Arnold Air Force Station, Tennessee, under ARO Project Nos. P34L-02 and B34I-03. Mr. Marshall Kingery was the Air Force project manager, and Dr. Steve A. Miller was the NOSC project manager. The data analysis was completed on December 20, 1979, and the manuscript was submitted for publication on May 29, 1980.

The authors wish to acknowledge the assistance of Mr. H. T. Bentley, III, for his contribution to the thermal resistance measurements, Mr. B. W. Bomar and Mr. D. S. Peterson for their assistance in computer programming and data formatting, Mrs. L. Vandergriff and Mr. Marc Smotherman for the myriad of computer operations they performed, and Mr. Ed Harding, Mr. Franklin Hornsby, Mr. Don Inglish, and Mr. Roger Johnson for constructing, operating, and trouble shooting the complicated circuitry so that smooth-running, long-term, test programs could be run.

CONTENTS

ILLUSTRATIONS

TABLES

1.0 INTRODUCTION

1.1 GENERAL

Light-emitting diodes — LED's — and injection lasers are expected to play an important role in future communication systems. Their small size and weight, high frequency response, electromagnetic (EMI) and electric field immunity, and security make the LED's and associated fiber optics extremely attractive for both military and commercial use. During the past decade, considerable progress has been made in lengthening the lifetime of these devices from approximately several hundred hours to thousands of hours. What is still required, however, is a method for estimating the reliable operating lifetime of these devices, particularly by means of simple voltage, temperature, and light output measurements that can be made during pretest periods or at some time after a relatively short burn-in period. The purpose of this report is to describe the results of an attempt to meet this requirement.

1.2 BACKGROUND

Initially, 240 commercially available LED's from five different manufacturers were selected and operated at carefully controlled chamber temperatures of -65, 30, 90, and 120°C at constant current densities ranging from 495 amp/cm^2 to 4,700 amp/cm^2 for 6,000 hr. At the end of the first 6,000 hr of testing, a number of analyses were performed to determine indicators of the operational lifetimes of the LED's. The Arrhenius relationship (Ref. 1) could not be used to provide a conclusive predictive method. Although the time to reach 50 percent (t 1/2) of the original light output power, L(1), is temperature sensitive, there did not appear to be a direct correlation with temperature. This is illustrated in Figs. 1 through 4. In these figures, t 1/2 vs junction temperature is plotted as a function of operating current. The data reveal large variations both at a given junction temperature and between junction temperatures.

A correlation between the change in forward voltage, V_f, and the change in light output from pretest and posttest data, was found for several LED's that were arbitrarily selected for testing under specified operating conditions. These were RCA C30123 LED Nos. 204, 205, and 206. These LED's were tested in the 90°C chamber and were operated at 200-ma drive current. The pretest I-V characteristics were essentially the same, as may be seen in Fig. 5a. Figure 5a reveals that the posttest I-V characteristics of Diode No. 204 changed dramatically and that the light output degradation was somewhat proportional to the change in voltage. Diode No. 206 failed after approximately 450 hr of operation and indicated a forward voltage change of 1.5 v at the time of failure. The light output vs time and forward voltage vs time characteristics of this LED are shown in Fig. 5b. The selection of these diodes for study

may have been fortuitous since this trend was not evident when all the LED's were considered. In addition to the change in forward voltage, another indicator was the rate of degradation of light output power during the early portion of the test program (i.e., after approximately 200 hr of operation). A complete evaluation of the LED's revealed that (1) if the light output power degraded to approximately 0.85 of the original light output power, L(1), or less, after approximately 200 hr burn-in, and/or (2) if the forward voltage changed by more than 100 mv during this same period, then the light output of the LED would fall to less than 0.5 L(1) within 2,000 hr of operations.

Based on these findings, a second test program was designed in which more than 300 LED's were tested for over 5,400 hr of continuous operation. The program was begun on December 11, 1978, and ended on July 25, 1979. The following sections summarize the work that was performed in this attempt to formulate a method for estimating the operational lifetime of the LED's from data acquired solely from pretest data and data acquired during the first 200 hr of operation of the tests.

Section 2 describes the test articles, test configuration, and procedures established to conduct the test. Section 3 details the instrumentation used and the problems that developed during the tests. Section 4 briefly describes the two types of pulse tests performed, as well as the apparatus used. Section 5 summarizes the procedures and hardware affecting the light output measurements. Section 6 contains descriptions of the LED's that were tested plus schematic diagrams of the devices and infrared (IR) photographs illustrating their light output characteristics. Section 7 contains a summary of the pretest and posttest thermal resistance measurements. The experimental results are presented in Section 8. In Section 9, the many analyses performed in both test programs are briefly reviewed; the conclusions drawn from these analyses are given in Section 10.

Because of the large volume of data amassed during the program, a number of data packages were compiled comprised of detailed characteristics of each LED within a given lot. The contents of each data package are described in the relevant sections that follow but, because of their bulk, are not included in this report.

2.0 DESCRIPTION OF TEST ARTICLES, CONFIGURATION, AND GENERAL PROCEDURES

Life tests were performed on 314 commercially available LED's obtained by the Naval Ocean Systems Center (NOSC) for the second test program. Test samples included 43 Mitsubishi MEK 104 LED's; 54 Texas Instruments, Inc., TIES 35's; 52 Texas Instruments Special diodes; 32 RCA C30123's; 36 RCA C30119's; 31 Spectronics Corp. SPX 2231's; 12

Spectronics 2234's, and one injection laser diode. Five additional LED's were included in the continuous-pulse mode portion of the program. The types of LED's tested at the various ambient temperatures are included in Table 1.

2.1 TEST ARTICLES

The LED's were tested in five dry-nitrogen purged environmental chambers operated at predetermined temperatures. The heat sinks and connection configurations for all five chambers are consistent with those used in the first test (Ref. 2). The optical scanner was modified to include both silicon and germanium photodetectors which were monitored through special low-thermal relays by an autoranging digital multimeter. The optical scanner was also nitrogen purged. The multimeter BCD output was connected directly to a Hewlett Packard 2100A computer that operated the system and transferred all data to punched paper tape and to magnetic disks with a Tektronix PDP 11/02. Details concerning the test complex and the computer program have been published (Ref. 2).

2.2 PRETEST PROCEDURES

The second test program was conducted as follows:

a. The pretest rise and fall times were obtained automatically with use of the digital processing oscilloscope (DPO); the data were stored on magnetic disks.

b. The pretest thermal resistance data were obtained with equipment that yielded shorter transient pulses, and, hence, higher thermal resistance values than the data from the first test in which longer transient pulses were used.

c. The forward current-forward voltage (I-V) and the forward current-light output (I-L_o) characteristics of each LED were obtained at two different temperatures. (In the first test, these characteristics were obtained at one temperature.) The environmental chamber temperatures were closely controlled during the test by means of specially designed circuitry.

d. The calibration constant was obtained for each LED at the time of installation by means of an in-house-built calibration box (Cal-Box). The light output was measured outside the chamber where the LED was directly coupled to the photodetector. Then, the diode was immediately installed in the chamber and the light output reading was taken by means of the fiber optics and respective couplers with the optical scanning system. The data were then compared and recorded and are tabulated in the analysis data package.

2.3 CONTINUOUS-OPERATION TEST CONFIGURATION

Figure 6 shows a block diagram of the continuous-operation test complex, consisting of the following:

a. *Environmental Chambers*: The five environmental chambers shown in Fig. 7 contained identical heat sink racks in which the devices to be tested were installed.

b. *Optical Scanner System*: The light output of each LED was coupled through a fiber-optics bundle and lens system to a specially designed optical scanner containing silicon and germanium photodetectors. (An exploded view of the scanner system is given in Fig. 8.)

c. *Current Regulators and Instrument Racks*: The LED's were operated at the designated forward drive currents by means of separate current regulators. These, along with their associated reference cells and operating power supplies, were contained in an instrument rack (Fig. 9) close to the environmental chambers.

d. *Data Recording Equipment*: A 1,000-point, computer operated, random-access multiplexer (MUX) scanned the test parameters and transmitted the measurements to a 5-1/2-digit autoranging digital multimeter (DMM). The DMM transferred the readings in a BCD format to an online computer that recorded the data on paper tape, which was then transferred to an associated computer that re-recorded the data on magnetic disks. (The computer/manual operating console is shown in Fig. 10.)

e. *Scanner Modifications*: The optical scanner was modified to include a germanium photodetector (PD) so that data could be acquired at longer wavelengths (i.e., exceeding the sensitivity range of the silicon PD). A mechanical counter was added to the scanner to help determine the positions of the PD's.

f. *50°C Chamber*: A fifth environmental chamber, operating at 50°C, was added during the second test to replace the -65°C chamber used in the first test program. Selected LED's that had been tested in the -65°C chamber and a number of new LED's were installed in the 50°C chamber.

g. *Temperature Cycling (-65°C) Chamber*: The control circuits for the 65°C chamber were modified to permit chamber operation at four different

temperatures, each for an 8-hr period, on a 32-hr timing cycle. Utilization of this chamber permitted comparison of the data from a constant temperature environment with that from a cycle varying environment. The cycling temperatures were -30, 20, 60, and 100°C.

h. *Data Calendar*: The computer program provided a special data calender to permit making automatic data runs at 8-hr intervals during the first 200 hr and at any other predetermined time intervals. Also, manually initiated data runs could be made at any time. These data runs were made 2 hr into a temperature cycle to ensure that the diodes were stablized at the required temperature.

i. *Circuit/Program Modifications*: Circuits were designed and the computer program was modified to permit obtaining I-V and I-L_o characteristics of selected diodes at any time during the test period.

j. *PD Monitor*: An LED was mounted on the optical scanner, with no fiber-optics accessories, to permit monitoring the germanium and silicon PD's. The LED was operated at very low forward current and had power applied only during data acquisition. Thermocouples were attached to this LED's heat sink to monitor the scanner temperature throughout the test.

k. *Fiber-Optics Cables*: A standard-length, fiber-optics cable was installed in each chamber, both ends of which were accessible from outside the chamber. This made it possible to monitor any degradation of the cables at the various temperatures.

l. *Standby Generator*: A three-phase, 120/208 v, 60-Hz diesel generator was added as a standby power source in case of a power failure. Auxiliary battery supplies were included to furnish the operating power to the current regulators and LED's during the transition time (approximately 12 sec) between a commercial power failure and the startup of the generator.

m. *Temperature Monitor*: A special six-channel, continuous-operation temperature recorder was installed to monitor the chamber temperatures and the scanner temperature during the test. The operating temperatures for this phase of the test were the following:

Chamber A—50°C

Chamber B—20°C

Chamber C—90°C

Chamber D—120°C

Chamber E—cycling (previously described)

2.4 POSTTEST PROCEDURES

The same control type of data as that taken during the pretest studies was sought for all the operable LED's that had completed the 6,000- and 5,400-hr continuous tests.

At the end of the extended test periods, the calibration constants of each operable LED were obtained before and immediately after the LED's were removed from the chambers by using the same hardware and circuitry with which the pretest data were obtained. Rise and fall time measurements were made with use of the same pulse generator for each LED but also with use of a digital processing oscilloscope and a hard copier for data retrieval during the second test, rather than by photographing an oscilloscope record and manually analyzing the data. The posttest I-V and I-L_0 characteristics data, in addition to the LED thermal resistance data, were obtained with the same hardware and circuitry as were used for obtaining the pretest data.

3.0 INSTRUMENTATION

3.1 DESCRIPTION

To minimize the quantity of data-gathering instruments in the LED complex, a Hewlett-Packard 2100A computer was used with a computer/manual control panel wired to a random-access, reed-relay operated, 1,000-point multiplexer (MUX). A specific input channel of the MUX could be connected to the input of an autoranging digital multimeter (DMM) by either manual or computer control. The BCD output of the DMM was wired back to the computer. Light output of the test LED's was monitored by photodetectors (PD's) that were precisely positioned by a specially designed optical scanner so that they aligned with terminal strips containing fiber-optics bundles (one for each LED). The output voltages of the PD's were amplified by in-house-built, temperature controlled amplifiers whose outputs were connected by means of computer or manually controlled low thermal relays connected through coaxial cables to the DMM.

The shields on all cables (except coaxial) used in wiring the test complex were insulated from ground and were common to the guard terminal of the DMM. A 1,000-μf decoupling capacitor was connected between the DMM guard terminal and ground. All power supplies used in the system were the floating type and were not grounded at any point.

Mercury cells (Mallory type RM42R) were used as references for the individual in-house-designed current regulators. The current regulators contained fixed, precision, current set

resistors. The regulators were adjustable over approximately 10 percent of their desired operating ranges by trim potentiometers. The low current drain of the voltage dividers used in the mercury cell reference circuits ensured very stable, long-life, reference potentials.

During both test periods, the results of all data runs were printed out. The printouts were used mainly to monitor the LED operating characteristics; however, if the data indicated rapid LED degradation or other unusual behavior, then the characteristics could be rechecked manually before beginning the next data run. The data were then stored on punched tape and magnetic disks for further analysis. In addition, a printout of all data points was made immediately following each data run so that the system operation could be checked.

Since the 1,000-point MUX and the DMM were used, only minimal instrumentation was required for the extended DC test, thus reducing the chances for error.

A "piggyback" reverse-bias test was initially run on extra LED's operating in the C and D environmental chambers in the first test. This reverse-bias test was performed to ascertain any changes in the degradation characteristics by reversing the polarity of the LED operating voltages for different periods of time. Data were acquired on these LED's during the initial portion of the test period with special runs made at half-hour intervals after the reversal process was begun. Since no useful data were obtained from this piggyback experiment, it was discontinued.

3.2 SPECIAL INSTRUMENTATION

The operation of a test complex for extended periods of time, such as those required for the LED degradation study, posed several problems in regard to maintaining instrument calibration. The uninterrupted test time exceeded the interval at which the instruments would ordinarily have been scheduled for recalibration at AEDC. The operating time also exceeded the recalibration and preventive maintenance period recommended by the manufacturer for the refrigeration-heater-type environmental chambers. In-place calibrations were therefore performed on the DMM by reading known voltages and comparing the system DMM readings to those of an identical DMM calibrated at the same time as the test system DMM. Posttest calibration of the two DMM's revealed that their respective calibrations were unchanged.

Relative light readings were obtained for all operable LED's during each data run by monitoring the dark current of the PD and subtracting this reading from each L_0 data point.

Small thermal voltages generated by the MUX caused slight negative L_o readings to be obtained from the failed LED's, but these negative readings caused no discernible error in the data. A comparison of the PD's at the end of the tests made with use of a reference LED (i.e., an LED that did not undergo the tests) showed no discernible variations from their pretest values.

The 0°C thermocouple referencing system had to be replaced with a 150°F system at approximately 1,950 hr into the first test because of the presence of cross talk in the 0°C system. The computer program was changed and the 150°F referencing system was used for the duration of the first test. In the second test, a floating thermocouple referencing system was used that obviated this problem.

Errors were discovered in the calibration procedures prescribed in the operation manuals of environmental chambers B and E. Notified of the errors, the manufacturers initiated corrections to their calibration procedures. Posttest calibration showed that the chambers were operating well within their rated values.

The computer operated 1,000-point MUX performed flawlessly during the extended DC tests. A manual mode of operation indicated an intermittent contact problem; however, this in no way affected data quality. Multiplexing all measurements to the DMM minimized the amount of instrumentation required.

There were no failures with the forward current, I_f, regulator referencing system that used the 1.35-v mercury batteries. Only slight trimming was required of some current regulator set point values that could not be related to the referencing batteries. Filter decoupling was required in some circuits to eliminate stray oscillations caused by small millivolt differences at the points where the reference potentials were connected to the main buses. A forced-air cooling system for the current regulators was never put into operation since normal convection cooling was found to be sufficient.

During the course of the second test, a printout of the data revealed sporadic fluctuations in the light output vs time data acquired from the silicon photodetector output. The fluctuations disappeared after approximately 800 to 1,000 hr of testing. The data log book was examined to ascertain the cause of these fluctuations. A number of events occurred during this interval of time, including rezeroing the digital voltmeter and changing a power plug that was a possible cause of ground loop problems. Attempts to duplicate the fluctuations over a period of several weeks proved fruitless. The data were replotted using the germanium photodetector output, in which the fluctuations were not evident.

A control relay in the refrigeration position of the temperature cycling chamber also malfunctioned during the second test program. This prevented the chamber temperature from attaining the 100°C requirement for a number of cycles during the 1979 Christmas holidays. The relay was repaired, and an analysis of the data indicated that the slope of the light output vs time curve could be extended, throughout the malfunction period, to the time when normal operation resumed without noticeable variations. During the first test a malfunction occurred in the -65°C chamber and the temperature increased to ambient temperature conditions. The light output characteristics did not fully recover upon resumption of normal operations.

The temperature of the entire test area was maintained to a close tolerance in order for all the systems to stabilize and to maintain the PD's at as constant a temperature as possible.

4.0 PULSE MODE TESTS

The pulse mode tests were of two types. First, all the LED's were subjected to pretest and posttest rise and fall time measurements. Then, a few diodes of each LED type were arbitrarily selected for lifetime testing at specified pulse repetition rates and duty cycles. One set of LED's was pulsed at a 1-mHz repetition rate and 50-percent duty cycle, and the other set was pulsed at 20 kHz on a 1-percent duty cycle. A photograph of the pulse test setup is given in Fig. 13. The rise and fall times and the light output of each LED were periodically monitored and recorded throughout the tests.

4.1 RISE AND FALL TIME MEASUREMENTS

The necessary hardware for the fast rise and fall time circuitry is given in block diagram form in Fig. 11 and photographed in Fig. 12. A model HP8004A pulse generator was used to to provide a pulse with a transition time of less than 1.5 nsec with a 50-ohm source and 50-ohm load. Type GR fittings were used in the hardware to adapt the LED to the pulse generator. The pulse generator rise and fall times were recorded. Photographs of the scope traces are shown in Fig. 14. The photodiode assembly was comprised of a photodiode adapter (Spectronics Model SPX1631) having a rise and fall time of less than 1.5 nsec. The photodiode responsivity was 50 v/w with a nominal bias of 100 v and could range as high as 170 v. The assembly utilized a Spectronics Model SD5426 silicon photodiode with a compensating network within a BNC fitting.

The amplification was provided by staged Avantek, high-bandwidth amplifiers. A circuit diagram of the amplifier is shown in Fig. 15. Considerable care was taken to shield the amplifier from extraneous EMI by using ground planes, foil shielding, and ferrite beads.

The pulse amplifier response is illustrated in Fig. 16; here, the response time is shown to be on the order of 1.5 nsec. This is the combined response time of the pulse generator and the amplifier only. For this measurement, the amplifier output was fed to a Tektronix 7904 oscilloscope main frame with a 7A19 vertical amplifier. Rise and fall time data were taken with a Tektronix Digital Processing Oscilloscope (DPO) and stored on magnetic disks for further analysis. An example of the data displayed on the DPO is given in Fig. 17. The numbering system used in the test is illustrated clearly in this figure for diode number 100171. The first two numbers represent the lot number — in this case, 10, which is the Spectronics type SPX 2231 — and the last three digits indicate the diode number, 171. A separate oscilloscope was used to establish the initial operating conditions. The LED's were pulsed to an 80-ma level as measured by the voltage drop across a 50-ohm load. Both 0- and 1-v biases were applied to the LED and the rise and fall times were measured. The 1-v bias is lower than the normal operating voltage; therefore, extremely low bias currents are drawn.

4.2 CONTINUOUS-PULSE TEST

The continuous-pulse mode of the LED test utilized the pulse circuitry that is illustrated schematically in Fig. 18. The periodicity of pulsing the LED on and off was controlled by two one-shots in an oscillator configuration. The on and off time was controlled by the RC time constant for each of the one-shots. Two hex inverters were driven in parallel by means of buffering logic gates to provide the relatively high current required to drive the LED. The current level was limited by a series resistor in the circuit. The relative light output was monitored daily except on weekends. Relative light output measurements were made with use of a Tektronix J16 photometer and an assembly to maintain accurately the relative position between the LED being tested and the photometer.

5.0 LIGHT OUTPUT MEASUREMENTS

5.1 GENERAL

The primary purpose of the tests was to obtain accurate light output measurements of the LED's over the duration of the test program. These measurements were to be accurate to within 10 percent. Relative light output measurements were to be recorded periodically for each of the LED's. The measurement philosophy pursued is illustrated in Fig. 19.

Test hardware was developed (including the fixtures for mounting the LED's, the computer control relay panels, interface connecting wiring, and amplifiers), and the photodiodes were selected and purchased. A computer controlled current source was developed to supply a number of predetermined current settings over several orders of magnitude for acquiring I-V and I-L_0 characteristics. Computer software was developed to

acquire the data and to control the measuring instruments through the computer controlled MUX and special low thermal relays. Absolute light output (photocurrent) data were taken for each LED, including light output vs current and light output at the fixed test current. All pretest data were taken both at room temperature and at a temperature of approximately 45°C. The data, together with the detector calibration from United Detector Technology (UDT) verified by NOSC, were used to determine the absolute light output for each of the LED's. The in-house-developed optical scanner, together with the data-acquiring computer software, automatically acquired pretest data of the LED's after they were installed in their chambers. The ratio of the pretest data to the absolute light output of each LED is the transmission coefficient due to fiber-optics and other coupling losses. An absolute power calibration coefficient for each LED was computed for later use. This permitted translating the test data (i.e., the relative light output readings) to absolute light output power for each of the LED's.

The test setup for preliminary current light output measurements is shown in block diagram form in Fig. 20. The test setup is similar to that used for the current-voltage measurements, which were made at the same time. The computer controlled current source was used to vary the current over several orders of magnitude. Under direction of a basic computer program (Ref. 3), the HP2100A computer stored the data on magnetic tape and disks and punched paper tape. Data were input through a keyboard and output was obtained via a CRT graphics display with hard copy available.

The photodetector was a United Detector Technology PIN 10 DF CAL photodiode. It was kept as close to the test LED as was physically possible. The detector's spectral response is shown in Fig. 21. Since the light output for each of the LED's varied in wavelength, an average responsivity was calculated by using a weighted average over the spectral output and the responsivity curve. The calibrations from UDT and NOSC agreed to within 5 percent. The photocurrent from the photodiode went to a transimpedance amplifier, which converted the photocurrent into a voltage that could be accurately measured by a Fluke 8800A autoranging voltmeter connected with a BCD input to the computer. The transimpedance amplifiers are shown schematically in Fig. 22. The photodetectors were operated in the short circuit, or current, mode in which the input voltage was kept very close to zero. The output voltage was related to the input current as it showed up as an IR drop across the feedback resistor.

5.2 TEST OPERATION

The interface between the LED's located within the test chambers and the photodetector was made by means of fiber-optics bundles and suitable couplers (Fig. 23). The fiber-optics

bundles consisted of 212 individual glass fibers, 5 ft long and wrapped in a high-temperature-resistant material, TEFZEL®. Optical coupling to the fiber optics was achieved by means of lens cans located at both ends of the fiber-optics cable. These were held in place by coupler-ferrule assemblies that were epoxied directly to the heat sink at the chamber end and threaded directly to a terminal strip at the scanner end. Once in place, the fiber optics were bound so that no further motion could occur and possibly change the attenuation. Essential components of the interconnect between the LED and the photodetector are shown in Fig. 24. Approximately 2 percent or less of the light output of the LED's was transmitted through the fiber-optics coupling system to the scanner. Precise positioning of the scanner was required to obviate variations in light output attributable to coupling misalignment of the LED and the fiber-optics bundle. This was achieved with an external detent system on the optical scanner's stepping motor and position transducer. Furthermore, using lens cans to focus the output of the fiber optics onto the photodetector greatly increased the sensitivity of the system to correct for slight misalignments.

The data from the lifetime tests were stored both on magnetic tape and on punched paper tape. At the time of data acquisition, a hard copy teletype printout was obtained. Data in the latter form were used primarily for diagnostics of the data-handling system. Parameters against which data could be plotted include heat sink temperature, operation current, time, LED type, and forward voltage, in addition to any other derived quantities. (Detailed light output vs time plots, pretest and posttest I-V plots, and L_0 vs V plots for all the LED's tested were included in the data packages for each LED lot.)

6.0 DESCRIPTION OF LED'S TESTED

The following paragraphs present brief descriptions of the LED's that were tested in the program. The LED's may be generally classified as either homojunction or double-heterojunction devices. Of all the LED types, three were double-heterojunction devices, i.e., the RCA C30119 (lot 90), the RCA C30123 (lot 30), and the Mitsubishi MEK 104 (lot 14). The remaining LED's, those manufactured by Texas Instruments, Inc., and by Spectronics, Inc., were the homojunction type.

6.1 HOMOJUNCTION DEVICES

6.1.1 Spectronics, Inc. (SPX Types)

Five different types of LED's manufactured by Spectronics, Inc., were used in the test program: the SPX 2231, SPX 2231F, SPX 2234, SPX 2354, and SPX 2354F. The F-denoted devices are steep-junction devices characterized by fast rise and fall times (on the order of 10

nsec), whereas the remaining types have a graded junction and relatively slow rise and fall times (on the order of 50 nsec). The SPX 2231 and 2234 LED's are similar in construction; each is a planar diffused, circular, edge-emitting LED with a chip diameter of 0.018 in., mounted in a parabolic reflector and sealed in a TO-46 package with a flat-glass window. Each type of LED was ultrasonically cut from the same gallium-arsenide (GaAs) wafer and then etched to remove the surface damage. The LED's were constructed by means of zinc-gallium diffusion process and are rated at a power output of 3 mw in the 900-nm range, at a current density of 3,100 amp/cm^2 (100-ma drive current).

The 2231F LED's have the same general geometrical configuration as the 2231's, but they are fabricated instead by means of a zinc/arsenide diffusion process. The rated output power is 0.7 mw at 100-ma drive current with a junction area of 3.2 x 10^{-5} cm^2. The LED's are classified as edge-emitting devices having a thermal resistance of approximately 170°C/w. The results of the AEDC thermal resistance measurements agreed with the Spectronics measurements for the SPX 2231 (Lot No. 10) LED's. However, in the cases of the SPX 2231F (Lot No. 11) and the SPX 2234 (Lot No. 34), the AEDC measurements were somewhat higher, approximately 200°C/w. Since the LED's are of similar construction, a representative schematic is given (Fig. 25). Figure 25 also shows typical infrared photographs of the light output of the SPX types 10 and 11.

The remaining two Spectronics devices — SPX types 2354 (Lot No. 40) and 2354F (Lot No. 41) — are quite different in construction from the devices previously described. They were manufactured in chip configuration approximately 0.010 in. square with a junction area of 6.45 x 10^{-4} cm^2, a relatively large area in comparison to the previous types. The SPX 2354 types were also manufactured by use of the same diffusion process as the SPX 2231 types having zinc/gallium diffusion and a graded junction, whereas the SPX 2354F was constructed with a zinc/arsenide diffusion and a steep junction. Neither of these devices was etched (e.g., saw damage was present), and both are highly stressed mechanically. The two LED types are illustrated schematically in Fig. 26. Included in the figure is a typical microphotograph of the light output of Lot Nos. 40 and 41. The effects of surface roughness are clear in the IR photographs of these two devices. The rated power output is 1 mw at a forward current of 100 ma, and the current density is approximately 155 amp/cm^2 at this current level.

6.1.2 Texas Instruments (TI Types)

Three different types of LED's manufactured by Texas Instruments (TI) were used in the test program. These were the TIXL 35 (Lot No. 51); TIES 35 (Lot No. 50), and a TI Special (Lot No. 52). All three types are Ga/Al/As surface emitters. Both the TIXL 35 and TIES 35

have n-type domes, whereas the TI Special has a flat surface. The main difference between the TI 35 types is that different bonding techniques are used in the fabrication. The junction area for both was approximately 2 x 10^{-4} cm^2, yielding a current density of 500 amp/cm^2 at 100-ma drive current. Schematics of the two TI 35 types are given in Fig. 27 along with a typical IR photograph. Figure 28 gives a schematic of the TI Special and a typical IR microphotograph.

6.2 DOUBLE-HETEROJUNCTION DEVICES

6.2.1 RCA, Inc.

Two types of RCA LED's were tested in the program. Both RCA LED types were fabricated by use of liquid-phase epitaxy and are Ga/Al/As double-heterojunction, restricted, edge-emitting rectangular chips 0.006 in. wide and from 0.010 to 0.015 in. long. The surface area of the devices is approximately 5.4 x 10^{-4} cm^2. The major difference between the two types — RCA C30119 (Lot No. 90) and RCA C30123 (Lot No. 30) — is the amount of p-type dopant used. The former are heavily p doped, whereas the latter are lightly p doped. Heavier doping results in a faster rise time in pulse mode operation. The devices are similarly constructed and are illustrated schematically in Fig. 29. Infrared microphotographs were not obtained for these diodes.

6.2.2 Mitsubishi

A number of Mitsubishi MEK 104 double-heterojunction LED's were tested in the program. The MEK 104 is a restricted-surface emitter from which the light is transmitted through a 50-μm aperture. The rated power output at a drive current of 75 ma is 0.5 mw. Figure 30 presents a schematic of this LED type and contains an IR microphotograph of the light output.

6.3 LASER INJECTION DIODE

One Ga/A1/As multi-heterostructure injection laser diode was tested in the program. The unit, LCW 10, is manufactured by Laser Diode Laboratories, Inc., and has a rated output of 14 mw at a forward current of 300 ma. The dimensions of the active region are given by the manufacturer as 0.01 by 0.5 mils. No further details concerning the injection laser are available. It is unfortunate that the device failed (i.e., the light output fell below 50 percent of the initial light output) within the first 24 hr of operations. The unit and all pertinent data were returned to the manufacturer.

7.0 THERMAL RESISTANCE

Excessive junction temperatures, caused by large operating current levels, have been considered a debilitating factor in the operating lifetime of LED's. Knowledge of the thermal resistance provides a means for determining the rise in junction temperature above ambient conditions; thus, it appears possible to correlate the lifetime of the device with the junction temperature. Thermal resistance data were obtained in accordance with the procedures outlined in Mil. Spec. 883A method 1012 (November 15, 1974) and Ref. 4. Modifications to the circuitry were made as suggested by Speer (Ref. 5) to reduce the time lag between the initial drop to the low current level of operation and the time at which the voltage V_f is measured. In the first test program, the time lag was about 10 to 20 μsec, whereas, after the modifications were incorporated, the time lag was about 2 μsec. The modifications yielded higher values of thermal resistance in the second test than in the initial test program. The second test measurements more nearly represented the LED's junction thermal resistance than their bulk resistance properties.

7.1 TEST EQUIPMENT

Figure 31 is a block diagram of the thermal resistance measurement setup. The thermal resistance test set detailed in Fig. 32 was obtained from Spectronics, Inc. An external pulse generator provided 1-μsec pulses at 100-μsec intervals to the thermal resistance test set; an oscilloscope was used for measuring the voltages. A precision voltage source was compared with the signal level offset by 1.35 v furnished by a mercury battery. All the voltage measurements were made with a 5-1/2-digit multimeter (DMM). The DMM was connected through the computer controlled MUX to the Hewlett Packard 2100A for data storage and later analysis. The test LED was mounted in close thermal contact with a temperature controlled aluminum heat sink electrically isolated from the LED. The temperature was monitored automatically by the HP 2100A by a thermocouple embedded in the heat sink.

Junction voltage was measured at a low current, nominally 1 ma, and was used to indicate the junction temperature. The voltage coefficient of the temperature was obtained by measuring the voltage at the 1-ma level at two different temperatures. The thermal resistance could then be inferred from the voltage measured at 1 ma when a nominal 100-ma heating current was applied. The major difference between the test programs was that the voltages were measured an order of magnitude faster in the second test.

The pretest vs posttest thermal resistances, in °C/w, were plotted and are given in Figs. 33a through j. As the figures show, for those diodes that did not fail, the thermal resistance

tended to decrease with time. This is in opposition to the trend observed during the first test program, in which the thermal resistance increased. The variance could probably be attributed to the fact that bulk properties were measured in the initial test, whereas junction properties were measured in the second test program. Since the data indicate considerable scatter, this conclusion is somewhat tentative.

It was found, however, that the thermal resistance measurements were reproducible to within 2 percent for those cases that were tested more than once. Variation from LED to LED for any given type could be as great as 100 percent or more. This appeared to be true for all the LED's, regardless of the manufacturer. The measured average thermal resistance also varied considerably for each LED type.

8.0 SUMMARY OF RESULTS

8.1 EXPERIMENTAL RESULTS - PULSE TEST

The rise and fall times of the LED's generally decreased with time, somewhat in proportion to the degree of degradation. Figure 34 gives a plot of the rise and fall time as a function of operating time for several types of devices tested. Attempts made to correlate the rise and fall time with degradation appear promising. Plots of the percent degradation vs change in rise time are included in Figs. 35 and 36 for the Spectronics 2231F and the RCA C30123 LED's, respectively. The results of a least-squares fit to the data and of a linear regression analysis performed on all the LED's in the lot showed that the RCA C30123 yielded a correlation coefficient of 0.769 and the Spectronics 2231F, a coefficient of 0.712. Detailed studies of the screened LED's are being performed by G. Zaeschmar of NOSC to verify this trend and to determine the radiative lifetime and other physical parameters from the rise and fall time data. During the course of measuring the pretest and posttest rise and fall times, it was noticed that instances occurred in which oscillations were present in the characteristics, as can be seen in a typical example shown in Fig. 37. The drive current, for all the rise and fall time measurements, was 80 ma. The operating current for this particular RCA C30119 diode was 300 ma during the test. At the rated current, the light output was initially only 0.2 mw — relatively low.

Figure 38a contains a plot of the pretest rise and fall times of an SPX type 2231, and it is to be noted that the characteristics are devoid of oscillations. The pretest light output power of this LED was approximately 1.1 mw at a drive current of 125 ma: The posttest rise and fall time characteristics of this SPX 2231 LED shown in Fig. 39 exhibit large-scale oscillations. Figure 40a, containing a plot of the light output power vs time for this same LED, indicates that the diode had suffered considerable degradation. The posttest light

output power had degraded to approximately 0.002 mw. Figure 40b is a posttest rise and fall time plot of an SPX 2231 LED that had not suffered severe degradation. Oscillations are not evident in this figure. It may be concluded, generally, that the oscillations become evident when the light output power levels are relatively low.

It was assumed that the LED's that exhibited these oscillations had suffered capacitance changes during the course of operation. Since capacitance measurements were not made before testing but were only belatedly included in posttest measurements, this hypothesis could not be verified. Nevertheless, there were a number of SPX 2354 LED's that were not used in the test program and that were stored at ambient temperatures for about two years. Some of these SPX 2354 devices were included in the second test program. Similar values were indicated by comparing the average value of the measured capacitance of the stored devices with the average value of those that were tested for 5,400 hr. Speer (Ref. 5) reported that there were no variations in measured capacitance between the pretest and posttest values for the Spectronics LED's tested. It is therefore assumed that the oscillations may not be attributed to changes in LED capacitance. It is possible that at these low power levels (0.1 mw or less) circuit limitations could introduce oscillations in the data.

8.2 CONTINUOUS TEST AT CONSTANT TEMPERATURE

Of all the LED's tested, the double-heterojunction devices indicated the greatest reliability of operation. These devices were the RCA C30119, RCA C30123, and MEK 104. Of these, the RCA C30119, characterized by a large amount of p dopant, had the shortest lifetime. What is interesting is that the RCA C30119 LED's that were operated at elevated temperatures and at current densities greater than approximately 1,000 amp/cm^2 exhibited improvement in light output, with time, after completing an initial rapid rate of degradation. The characteristics are displayed in Figs. 41, 42, and 43. In Fig. 41, the light output is plotted as a function of time for devices operating at various current densities in an ambient temperature environment of approximately 30°C. This figure shows that the initial light output is proportional to the current density. The degradation of the LED's operating at a current density of 495 amp/cm^2 appears to be linear in time; however, the devices operating at higher current densities exhibit a decreasing degradation rate until they ultimately stabilize at a rate comparable to that of devices operating at a current density of 495 amp/cm^2. The degradation rate of those LED's operating at a current density of 1,485 amp/cm^2 had not stabilized after 6,000 hr of operation.

Figure 42 contains a plot of the light output vs time for a number of LED's operating at various current densities in an ambient environment of 90°C. In this figure the LED's

operating below a current density of 1,000 amp/cm^2 exhibit a degradation rate that varies with time, then tends to stabilize at approximately 2,000 hr of operation. Those LED's operating at a current density greater than approximately 1,000 amp/cm^2 exhibit an improvement in light output as time progresses. Stabilization appears to occur after 5,500 hr of operation, at which the LED's exhibit a recovery of approximately 50 percent from the light output of their lowest point. Figure 43 contains similar plots for data obtained when the ambient operating temperature was approximately 120°C. In this figure, there first occurs a rapid drop in light power output; then all the devices appear to recover as time progresses but at a rate lower than that of the LED's in the 90°C environment. This recovery was not evidenced by the LED's comprising other lot numbers. (Detailed plots for all the LED's are included in their respective data packages.)

Several of the LED's that survived the first 6,000 hr of testing were also included in the second test program. These LED's were stored at room temperature for approximately 9,000 hr before the second test was begun. Representative plots of these devices are included in Figs. 44a through g. Figure 44a shows the light output vs time characteristics of an RCA C30123 operating initially in a 30°C environment, then in a 20°C environment. It can be seen from this figure that there is an initial increase in light output power at the initiation of the second test and that the ensuing decay rate is approximately the same as the initial 6,000-hr decay rate. Figures 44b and c are light output vs time characteristics at operating environmental temperatures of 90 to 120°C, respectively. These two figures show that there appears to be a recovery in the light output after a storage period of approximately 9,000 hr.

The decay rate of the devices becomes essentially the same as the final decay rate evidenced in the initial test. Figures 44d and e contain the light output vs time characteristics of the RCA C30119 at 20 and 90°C, respectively. Both figures show an increase in the initial light output after the storage period had ended; in the case of the 20°C device, the light output degrades at a rate similar to its initial decay rate. In the case of the 90°C device, there was the initial increase; however, the light output continued to increase, as previously discussed. Figures 44f and g show the light output vs time characteristics of the SPX 2231 devices operating at ambient temperatures of 20 and 90°C, respectively. Again there is an initial increase in the light output power of the device after 9,000 hr of storage, at which time the devices degrade at approximately the same rate as in the initial test.

8.3 VARIABLE AMBIENT TEMPERATURE

During the second test, a number of LED's were tested in a temperature-cycling environment to evaluate their performance and to compare their degradation characteristics with those devices tested in a constant temperature environment. The chamber was cycled at

four different temperatures: -30, 20, 60, and 100°C. The temperatures were changed every 8 hr, and the measurements of the light output were taken after the chamber had stabilized at the new temperature. The general characteristics of the devices (e.g., light output vs time) are included in Figs. 45a, b, and c, and 46a, b, and c. Figures 45a, b, and c illustrate the light output vs time characteristics of the Mitsubishi MEK 104 devices operating at current densities of 2.5 x 10^3 amp/cm^2, 3.8 x 10^3 amp/cm^2, and 5 x 10^3 amp/cm^2. Figures 46a, b, and c are the light output vs time characteristics of the TI Special LED's operating in the temperature cycling chamber at current densities of 425, 850, and 1,700 amp/cm^2, respectively. From these figures it can be seen that the TI Special devices tend to degrade more rapidly than do the double-heterojunction MEK 104 devices. Included in these figures are the forward voltages as a function of time and temperature.

At approximately 250 hr, the relay engaging the refrigeration system in the environmental chamber suffered a malfunction. The unit continued to operate, but the 100°C cycle could not be attained. The operation of the LED's was not curtailed during this period. It can be seen, particularly in Fig. 46b, that the slope of the 100°C curve continued, upon repair of the relay, as though the perturbation had not occurred.

A plot of the percent degradation vs junction temperature of the TI Special devices is included in Fig. 47. It can be seen that the degradation behavior of the devices, in the temperature cycling chamber, was similar to that produced with a junction temperature of approximately 110°C. (Detailed plots of all the devices tested in the temperature cycling chamber are included in the respective data packages by lot numbers.)

9.0 DISCUSSION OF TEST RESULTS

9.1 DEFINITION OF PROBLEM

During the experimental program, attempts were made to evaluate the LED performance by following the logical path of analyzing pretest characteristic data, continuously evaluating the variations of LED performance as a function of time, and attempting to correlate degradation with measured values of temperature, current, voltage, light output, and efficiency. The objective was to determine a means for estimating the operating lifetime of the LED's at the earliest possible time after test startup. The lifetime of the LED's is defined as the time that the light output would degrade to 0.5 of the initial light output, L_o. Furthermore, the additional restrictions were that only pretest and arbitrary 200-hr burn-in data could be used for estimating the lifetime of the devices.

The literature was continuously evaluated to determine whether lifetime estimates had been previously published by other workers. Although a number of publications were

uncovered, these did not include methods of estimating the lifetime within the constraints that were imposed. Reviews covering the pre-1975 work are included in the books by Bergh and Dean (Ref. 6), Kressel and Butler (Ref. 7), Casey and Panish (Ref. 8), and the publications of Mataré (Ref. 9). The models proposed by Jordon and Ralston (Ref. 10), Zaeschmar (Ref. 11), Hersee (Ref. 12), Ishikawa (Ref. 13), and others were also evaluated for application to early estimation of reliable LED operation. None of the references specifically addressed the problem of estimating the lifetime from the pretest data and/or from early burn-in data. Therefore, attention was focused on developing a technique for the early determination of LED lifetimes.

9.2 ANALYSIS OF CONSTANT TEMPERATURE TEST DATA

9.2.1 Evaluation of Diode Parameters

The ideal-diode equation was modified to include the bulk resistance of the semiconductor and other nonideal effects. If it is assumed that the diode bulk resistance, R, is fixed, then the diode equation becomes (Ref. 9)

$$I = I_o \left[\exp\left(\frac{qV_j}{nkT}\right) - 1 \right] \tag{1}$$

where

I = Current, amp

I_o = Saturation current

q = Charge on the electron

k = Boltzmann constant

T = Temperature, °K

n = $1 \leq n \leq 3$

V_j = Junction voltage = $V - IR$

where V is the applied voltage and R is the bulk resistance.

In the high current density region of operation — the region of interest — the value of the exponential $>>$ 1, and the unity term will be neglected in what follows. If it is assumed that there is little change in R and n with forward voltage, then

$$\frac{d(\ell n\ I)}{dV} = \frac{q}{nkT}\left(1 - R\frac{dI}{dV}\right) \tag{2}$$

$$= \frac{q}{nkT}\left[1 - IR\ \frac{d(\ell n\ I)}{dV}\right] \tag{3}$$

$$= \left(\frac{nkT}{q} + IR\right)^{-1} \tag{4}$$

For the case of light output vs voltage, the following is generally true (Refs. 6 and 7):

$$L = \eta I \tag{5}$$

where L is the light output and η is the external quantum efficiency. Substituting the modified form of Eq. (1) into Eq. (5) yields

$$L = \eta I_o \exp\left(\frac{qV_j}{kT}\right) \tag{6}$$

where in this instance n = 1, the radiative portion of the current. If η is assumed to be a weak function of voltage, then

$$\frac{d(\ell n\ L)}{dV} = \frac{q}{kT}\left(1 - R\frac{dI}{dV}\right) \tag{7}$$

It follows from Eqs. (2) and (7) that

$$n = \frac{d(\ell n\ L)}{d(\ell n\ I)} \tag{8}$$

The bulk resistance, R, is then obtained from Eq. (4) as

$$R = \frac{1}{I\,\dfrac{d(\ell n\ I)}{dV}} - \frac{nkT}{qI} \tag{9}$$

Equation (9) determines the bulk resistance from the slope of the I-V characteristic curve minus the dynamic resistance of the p-n junction. Numerous plots of the parameters in Eqs. (2), (7), and (8) were made with partial success, particularly in determining the value of n in Eq. (8). A value of n greater than unity (e.g., n = 1.8) indicates that a significant portion of the total current is nonradiative. Pretest and posttest values of n are illustrated in Figs. 48 and 49 for an RCA C30119 LED and an SPX 2231F. In Fig. 48, the value of n decreased

from pretest and posttest measurements, thus indicating that the light output had increased, a behavior typical of this highly p-doped type of LED.

Another interesting example is presented in Fig. 49. In this case, the value of n increased from the pretest to the posttest measurements; however, the results indicate a somewhat greater than 2-kT slope. It was found in this latter case that the external quantum efficiency was initially about 0.08 percent, whereas the posttest external quantum efficiency had degraded to approximately 0.001 percent, signifying an essentially "dead" LED.

The slope of the $\ln(L_1)$ with respect to the V vs I curve indicates that at low current levels the light output is essentially 1 kT (40) and rapidly approaches 2 kT (20) as the bulk resistance becomes appreciable. This is illustrated in Figs. 50 and 51, which contain, for the SPX 2231 LED's, representative plots of the various parameters contained in Eqs. (2), (7), and (8). In these two figures, parameter variations are compared with the light output at the end of the test program. There first appeared to be some correlation, but a more detailed evaluation of all the diodes (including the different types of LED's) did not produce any definite conclusions.

In randomly selected LED's, the bulk resistance derived from the slopes of the $d(\ln I)/dV$ and the $d(\ln L_0)/dV$ vs I curves revealed that the LED's with short lifetimes generally had higher values of bulk resistance around the operating point. It is unfortunate that this behavior was not consistent for all the LED's.

9.2.2 External Quantum Efficiency

Another concern was the parameters affecting the external power quantum efficiency, defined as

$$\eta = \frac{L}{IV} \tag{10}$$

where L is the light output power and I and V the drive current and the forward voltage, respectively. The effects of the bulk resistance are included in this relationship. Plots of the LED efficiency vs forward current revealed that the efficiency tended to peak at different drive currents both within each lot and between lots. However, there was no correlation between the lifetime of the devices and the point of peak efficiency.

It was also surmised that the peak efficiency-current product might provide a useful basis for performance evaluation. Positive results were obtained in the case of the RCA C30123 LED's operating in the 90°C chamber, but, again, no consistency was found in the results for all of the LED's in the 90°C chamber or in the results for all of the RCA LED's

operating at other temperatures. Representative plots of these parameters are included in Figs. 52 and 53. Data are presented for three diodes in each figure; the data include the peak efficiency, the current at peak efficiency, and the product of the forward voltage (V_f) and light output divided by the current and bulk resistance. Additional parameters included are (1) the change in efficiency between the peak and drive current, (2) the change in L between the peak and drive current, and (3) the change in the slope of the efficiency between the peak and drive current. These results did not demonstrate any specific trend. The results of the numerous analyses that were performed are summarized in Table 2.

9.2.3 Temperature Effects

In Ref. 14, Henry, Petroff, et al. attributed catastrophic damage to light absorption in the crystal lattice. However, the operating power of the LED's used in the test program described herein was much lower than that used in their experiments. Attempts to correlate lower power densities and longer periods of operating time with higher power densities and much shorter periods of operation were also fruitless. This is shown by the fact that some of the double-heterojunction devices, such as the Mitsubishi MEK 104's, appeared insensitive to temperature over the range of operation. Part of the difficulty could be attributed to the assumption, in this case, of a uniform temperature distribution in the junction. In general, this is not valid since many geometries (such as stripe, restrictive edge-emitting, and restricted surface-emitting) produce inhomogeneous resistive heating (Ref. 15). Even for the case of an ideal diode with uniform heat generation and uniform thermal conductivity, the temperature in the center of the recombination region would be higher than in the periphery. With a hotter central region, the bandgap energy and, hence, the effective resistance would be somewhat lower than in the periphery; this would produce greater current flow near the center and greater nonuniformity.

It is reasoned that, if the rate of nonradiative center generation was proportional to the temperature, then such centers would develop more rapidly in the hotter region. As time progressed, the central region of the junction would degrade more rapidly than the periphery, and this would result in redistributing the light output (Ref. 15). This is confirmed by evaluating the pretest and posttest IR microphotographs taken of the light output on the surface-emitting LED's (TIXL 35). Representative photographs are included in Figs. 54 through 56. The dark line defects on these devices, operated at different current levels, are quite distinct. Note that the light intensities cannot be compared since the exposure times of the posttest microphotographs were much longer than the pretest exposure times.

In view of these findings, attempts were then made to apply the heating model proposed by Pankove (Ref. 16) and used by others such as Ettenberg, Wittke, and Kressel (Ref. 15) to

estimate LED performance. The model tends to correlate fairly well with the data. In short, the light emitted by an LED is given by Eq. (5) as $L = \eta I$. At constant current (forcing function in the test), the rate of change in light output with temperature is

$$\frac{dL}{dT} = I \frac{d\eta}{dT} \tag{11}$$

Furthermore (Ref. 16),

$$\eta = \eta_o \exp\left(\frac{-T_j}{\theta}\right) \tag{12}$$

where

T_j = Junction temperature, °C

η_o = A constant (extrapolated to 0 °C)

θ = Temperature coefficient of efficiency

The junction temperature is defined (Ref. 15) as

$$T_j = T_a + \Delta T \tag{13}$$

$$\Delta T = IVZ \tag{14}$$

where

T_a = Ambient temperature, °C

Z = Thermal resistance, °C/w

The second approach involves calculating the temperature coefficient of efficiency rather than measuring the thermal resistance in accordance with the Mil. Spec. Std. 883A recommendations.

Taking the derivative of Eq. (12) and rearranging yields

$$\frac{d\eta}{dT_j} = -\frac{\eta_o}{\theta} \exp\left(-\frac{T_j}{\theta}\right) \tag{15}$$

$$= -\frac{\eta}{\theta} \tag{16}$$

$$\frac{dL}{dT_j} = I\frac{d\eta}{dT_j} = -\frac{L}{\theta} \tag{17}$$

and

$$\theta = -\frac{dT_j}{\frac{dL}{L}} = \frac{IZdV}{\frac{dL}{L}} \tag{18}$$

The voltage and light output are measured either at two different times during the test or at two different temperatures at the beginning of the test program, and θ is calculated with the aid of Eq. (18). In the latter case, the current is kept relatively small, on the order of 1 ma, so that the heating effects attributed to current stressing are minimal and can be neglected.

Values of θ have been published ranging from 60 to over 100°C (Refs. 15 and 16). The results obtained in the first test correspond to these values. In the second test programs θ had a wider range of values both within each lot and between lots. The half-lifes of the LED's vs junction temperature were plotted in the form of a scatter diagram. A linear least-squares fit to the data in each lot was performed. The results of a regression analysis, made with use of both methods of determining junction temperature, indicated comparable values of correlation coefficient, slope, and intercept. The results of the analyses are included in Figs. 57a through 63b. In these figures the half-lifes determined by the application of Eq. (20) for the value of T_j are shown in the "a" figures. The values of T_j determined from the thermal resistance measurement [Eq. (14)] are included in the "b" figures.

The comparable values of correlation coefficient, obtained with use of the two techniques, suggests determining the junction temperature from I-$\dot{L}_0$ and I-V characteristics at two different temperatures and calculating the value of θ in lieu of the recommended procedures. The determination of the thermal resistance from the measurements suggested by Mil. Spec. Std. 883 is a time-consuming and costly effort. Additional studies of the accumulated data should be made to determine the relationship of these two types of measurements.

The analysis data package includes a tabulation of pretest and posttest values of both thermal resistance and θ for each LED. Large variations in pretest and posttest values are shown by both sets of data. Additional studies, particularly on the LED's in the temperature cycling chamber, are suggested to determine whether θ and/or Z varies with time and/or temperature and whether they are related.

9.2.4 Correlation of Variables with Degradation

The next phase of the analysis was to determine whether there were measurable quantities within the first 200 hr of operation that would indicate reliable LED operation. The light output ratios L(100)/L(1) and L (200)/L(1) were compared to the light output ratio L(6,000)/L(1) at the end of 6,000 hr of operation. Changes in voltage at the end of 100 and 200 hr of operation were also compared to L(6,000)/L(1), the light output ratio at the end of 6,000 hr of operation. Variations in efficiency at the end of 200 hr and the changes in junction temperature during these two time periods were also compared to L(6,000)/L(1). The data from the diodes in each lot were plotted in a scatter diagram, a least-squares fit was applied, and a linear regression analysis was performed to yield the correlation coefficient. The results of the analysis are given in Table 3, which gives correlation coefficients for all the parameters evaluated.

The interesting point in the analysis is that there were two consistent indicators that could be used to estimate the operating lifetime of the devices. In some diode lots it was found that if the light output degraded by more than 15 percent within the first 200 hr of operation, then the LED would fail within 2,000 hr of operation. Failure is defined as the time when the light output ratio becomes $L(t) \leq 0.5\ L(1)$.) It was also found that there were cases in which the light output had not degraded to any extent within the first 200 hr (e.g., less than 1 percent of the original light output); however, the light output power had degraded to less than 0.5 L(1) within the first 2,000 hr of operation. In these cases a change in forward voltage resulted.

In the case of the RCA C30123 lot, it was found that if the forward voltage changed more than 0.05 v during the first 200 hr of operation, then the LED would not meet the screening criteria. In the other lots a voltage change greater than 0.100 v was required. (Note that the voltage changes are absolute values.) In some instances the forward voltage decreased during the first 200-hr period. If the voltage variation exceeded the screening criteria, then the LED failed within 2,000 hr regardless of whether the voltage increased or decreased.

It appeared that these two conditions would serve to detect short-lived LED's during the first 200 hr of operation so that they could be eliminated. The performances of the LED's in both tests were then evaluated to verify these findings. The results of this screening test are included in Table 4 for those LED's operated in a constant temperature environment. Of approximately 304 LED's evaluated, 145 indicated a light output degradation greater than 15 percent during the first 200 hr of operation. In addition, 28 LED's indicated a voltage

change greater than 0.1 v (with the exception of the RCA C30123, for which 0.05 v was the criterion within this burn-in period). Table 4 shows that 95 percent of the LED's predicted to do so did degrade below the failure criteria within the first 2,000 hr of operation. The remaining 5 percent of the LED's operated more than 2,000 hr.

The results of additional analyses are included in Table 5. This table includes, for each diode lot, the correlation coefficients of the half-life vs T_j, obtained by using both techniques for determining T_j, and the half-life vs $\Delta V(200)$. In addition, Table 5 includes other parameters such as the MTTF and the current density at peak efficiency. As the table shows, the correlation coefficient for the half-life vs T_j is quite high for all the lots except the MEK 104, which appears to be insensitive to temperature.

It is suggested that future efforts consider the time to reach a specific minimum ouput power level (e.g., 0.1 mw) instead of the time to attain 0.5 L(1). In the case of the homojunction devices, the MTTF was quite short in comparison to that of the double-heterojunction devices. In many cases the light output power of the homojunction LED's was at least a factor of two greater than the light output power exhibited by the double-heterojunction LED's.

It was also observed during the studies that the light output power is proportional to the current density, at a given ambient temperature, until a critical value is reached. Operating the LED's at higher values produces accelerated degradation rates somewhat proportional to the current density. The degradation rates of the devices operating below the critical value appear to be independent of current density. This characteristic is illustrated in Fig. 41 for the RCA C30119 in which the critical current density appears to be 1,250 amp/cm^2. Figure 64 contains a plot of the light output vs time for the TIXL 35 as a function of current densities ranging from 855 to 2,564 amp/cm^2. The diodes operating at a current density greater than 1,700 amp/cm^2 have a faster rate of degradation than those operating at less than 1,700 amp/cm^2.

Figures 65 and 66 contain plots of the light output power vs time as a function of current density and ambient temperatures of -65 and 90°C, respectively, for the SPX 2231 LED's. Below a critical current density of approximately 3,900 amp/cm^2, the decay rate is independent of current density and temperature. Additional evidence is given in Figs. 67 and 68, which contain similar plots of the RCA C30123 LED's operating in ambient temperature environments of 30 and 90°C, respectively. In this example, the LED's operating at an ambient temperature of 30°C have not attained the critical current density. In the 90°C environment, the critical current density is above approximately 1,260 amp/cm^2. Figure 69

contains a plot of the light output vs time of the Mitsubishi MEK-104 operating at a current density of 5,000 amp/cm^2 and various ambient temperatures. It appears that these LED's are on the verge of exhibiting variations. Below this value of current density, the degradation is almost immediately established at a rate below 10^{-5}/hr.

Figure 70 contains a summary plot of the characteristics of several LED types operating at essentially the same current density, although the forward current is markedly different between lots. Except for the TIXL 35 (considered a faulty lot by the manufacturer), the LED's exhibit essentially the same degradation rate after approximately 2,000 hr of operation, regardless of type or manufacturing process.

Figure 71 summarizes the operating reliability of the LED's tested in the second program. In this figure, the half-life is plotted for each LED. The LED's are subdivided into their respective lot numbers, and the total number in the lot and the cumulative total are indicated. It can be seen that the double-heterojunction devices (Lot Nos. 14, 30, and 90) exhibit the longest operating lifetime in regard to the assumed failure criteria. Those LED lifetimes greater than 6,000 hr are only estimated lifetimes, as the tests were not conducted over longer periods of time.

9.3 LIFETIME ESTIMATES OF LED OPERATION

From the discussions and results presented in the previous section it appears possible to estimate the operating lifetime of the LED's. The screening process eliminates those LED's that have a lifetime of 2,000 hr or less. Those LED's that stabilize within the first 200 hr of operation tend to have a constant degradation rate. The decay characteristics can be adequately described by

$$L(t) = L(200) \exp(-\lambda t) \tag{19}$$

In general, $\lambda << 1$ (in the present case λ was found to be on the order of 10^{-5}/hr or lower); hence, the relationship may be simplified to

$$L(t) = L(200)(1 - \lambda t) \tag{20}$$

for time periods up to approximately 20,000 hr. Those LED's operating above a critical current density level will exhibit initial degradation rates (within the first 200 hr of operation) of less than 7.5×10^{-4}/hr and greater than approximately 5×10^{-5}/hr. In this operating regime, the time that the degradation rate stabilizes appears to be proportional to the current density or the junction temperature. Furthermore, a preliminary evaluation of the data indicates that the light output power level, attained upon reaching the stability

region, is also functionally inversely proportional to the current density. It is suggested that additional studies of the accumulated data should focus on the characteristics of the LED's having degradation rates between these two regimes (i.e., from 7×10^{-4}/hr to 5×10^{-5}/hr).

9.4 LASER DIODE

One injection laser from Laser Diode Laboratories, Inc., was tested in the 20°C chamber at the rated current level. Within 24 hr of operation the light output had degraded to approximately 20 percent of its initial value. The light output vs time characteristic for this device is plotted in Fig. 72. The unit and all the accumulated data were returned to the manufacturer. Although a test of only one unit may be considered to be statistically insignificant or to be part of a freak distribution in a manufactured lot, indications are that injection lasers also tend to yield a high percentage of unreliable devices. Chen et al. (Ref. 17) note that following a burn-in of 300 hr in a test involving nine injection lasers selected for use in a 70-MHz communication link, three of the devices could not be used in the field tests.

10.0 SUMMARY OF RESULTS

The myriad of detailed data that were acquired during the course of the two test programs are included in data packages, one for each LED lot or manufacturer. In general, these data did not provide the indicators necessary to estimate the operating lifetime of the LED's during a burn-in period — 200 hr. The following paragraphs summarize the salient results of the two tests performed to meet the objective of estimating the lifetime of the devices.

1. Approximately 390 LED's were subjected to life tests in constant temperature environments for 6,000 hr and for 5,400 hr of continuous operation. More than 50 percent of the devices degraded to a light output power of less than 0.5 L(1) within 2,000 hr of operation.
2. Detailed analysis of the data showed that if within 200 hr of operation the light output of the LED's had degraded by more than 15 percent [(e.g., L(200)/ L(1) $\leq$ 0.85], then the light output power of the device would fall below 0.5 L(1) within 2,000 hours of operation. The analyses also showed that if there was a voltage change greater than 0.100 v during this same period of time (0.05 v, in the case of the RCA C30123), then the light output power of the device would also fall below 0.5 L(1) before 2,000 hr of operation had elapsed. Applying this

criterion to all the LED's tested indicated that it was 95-percent effective in eliminating the short-lived LED's. Approximately 5 percent of the rejected LED's survived the 2,000-hr period of operation.

3. An evaluation of the light output power characteristics indicated variances both among LED's of the same type and between the two different types. The double-heterojunction devices exhibited the greatest reliability in operation, particularly the Mitsubishi MEK 104 and RCA C30123 types. The RCA C30119, characterized by a heavy p-type dopant, exhibited a recovery of light output power with time after the initial decrease stabilized. As expected, the external quantum efficiency of the double-heterojunction LED's (fractions of a percent) was considerably lower than the homojunction LED's (in the percent range). The homojunction LED's, however, exhibited much lower mean time to failure than did the heterojunction LED's. The Spectronics SPX 2231 LED's that survived the screening test did provide reliable operation for periods extending beyond 6,000 hr.

4. The results of the studies indicate that comparable results may be obtained by determining the temperature coefficient of efficiency, θ_i rather than by performing thermal resistance measurements, which is a time-consuming process. In the second test program, the values of the thermal resistance of the LED's decreased by a factor of two from pretest to posttest measurements. This indicates that the junction temperature was reduced. The values of θ also changed markedly but generally increased. This also indicates that the junction temperature was lowered as testing progressed. Additional studies are necessary to determine the relationship of the two parameters.

5. The rise and fall times of the devices decreased with time. Preliminary evidence indicates that this is not attributable to changes in measured capacitance.

6. The results of the studies indicated that, below a critical current density, the degradation rate is independent of current density or junction temperature, and the lifetime of the devices can be estimated by a simple linear relationship (the degradation rate was on the order of 10^{-5}/hr or less). When the initial degradation rate was less than 7.5×10^{-4}/hr and greater than 10^{-5}/hr, there would be a continuously variable degradation rate decreasing with time. The degradation rate of the devices would ultimately stabilize at 10^{-5}/hr or less. Additional studies and correlation of the accumulated data should help define the relationship between current density and/or junction temperature with the time when the degradation rate stabilizes.

7. The coupling coefficient of the light output power from the LED operating in its respective position in the test chamber and the photodetector was relatively poor — 2 percent or less. It was recently learned (Ref. 18) that a newly developed coupler considerably improves the coupling efficiency (from 60 to 80 percent). Using such an efficient coupler in future tests should result in considerably improved data quality.

REFERENCES

1. Gladstone, S., Laidler, K. J., and Eyring, H. *The Theory of Rate Processes*, McGraw-Hill Book Co., New York, 1941.

2. Puckett, J. B. and Miller, S. "Automated Long Term, Uninterrupted, LED Test Complex." *Proceedings*. Advanced Test Techniques in Failure Analysis, Los Angeles, California, November 6 — 9, 1978.

3. Batte, Z. "Automatic Data Acquisition System for an LED Test." AEDC-TR-77-112, (AD-A055872), April 1978.

4. Meiners, L. "Thermal Resistance Measurement of Light Emitting Diodes." NELC Technical Note TN-2971, June 3, 1975.

5. Speer, R. S. "Research and Development Program to Characterize and Control Degradation of Ga/As Light Emitting Diodes." Final Technical Report Contract Number N00123-76-C-1111. Prepared for NOSC, November 1977.

6. Bergh, A. A., and Dean, P. J. *Light-Emitting Diodes*. Clarendon Press, Oxford, England, 1976.

7. Kressel, H. and Butler, J. K. *Semiconductor Lasers and Heterojunction LED's*. Academic Press, New York, 1977.

8. Casey, H. C., Jr., and Panish, M. B. *Heterostructure Lasers*. Academic Press, New York, 1978.

9. Mataré, H. F. "Light Emitting Devices, II." *Advances in Electronics and Electron Physics*, Vol. 45, Academic Press, New York, 1978.

10. Jordan, A. S. and Ralston, J. M. "Diffusion Model for GaP Red LED Degradation." *Journal of Applied Physics*, Vol. 47, No. 10, October 1976, pp. 4518-4527.

11. Zaeschmar, G. and Speer, R. S. "Mechanical-Stress-Induced Degradation in Homojunction GaAs LED's." *Journal of Applied Physics*, Vol. 50, No. 9, September 1979, pp. 5686-5690.

12. Hersee, S. D. "The Reliability of High Radiance GaAs LED's." *AGARD Conference Proceedings No. 219: Optical Fibres, Integrated Optics and their Military Applications*, London, May 16 — 20, 1977.

13. Ishikawa, H. et al. "Accelerated Aging Test of $Ga_{1-x}Al_xAs$ DH Lasers." *Journal of Applied Physics*, Vol. 50, No. 4, April 1979, pp. 2518-2527.

14. Henry, C. H., Petroff, P. M., et al. "Catastrophic Damage of $Al_xGa_{1-x}AS$ Double-Heterostructure Laser Material." *Journal of Applied Physics*, Vol. 50, No. 5, May 1979, pp. 3721-3732.

15. Ettenberg, M., Wittke, J. P., and Kressel, H. "High Speed Light Emitting Diodes." PRRL-75-CR-37 (AD-A018757), Vol. 1, June 1975.

16. Pankove, J. I. "Temperature Dependence of Emission Efficiency in Lasing Threshold in Laser Diodes." *IEEE Journal of Q.E.* QE-4, No. 4, April 1968.

17. Chen, F. S. et al. "Laser Transmitters for 70-MHz Entrance Links." *The Bell System Technical Journal*, Vol. 58, No. 7, September 1979, pp. 4617-1629.

18. Kuwahara, H. and Furuta, H. "Efficient Light Coupling from Semiconductor Lasers into Tapered Hemispherical End Fibres." *Proceedings of the IEEE*, October 1979.

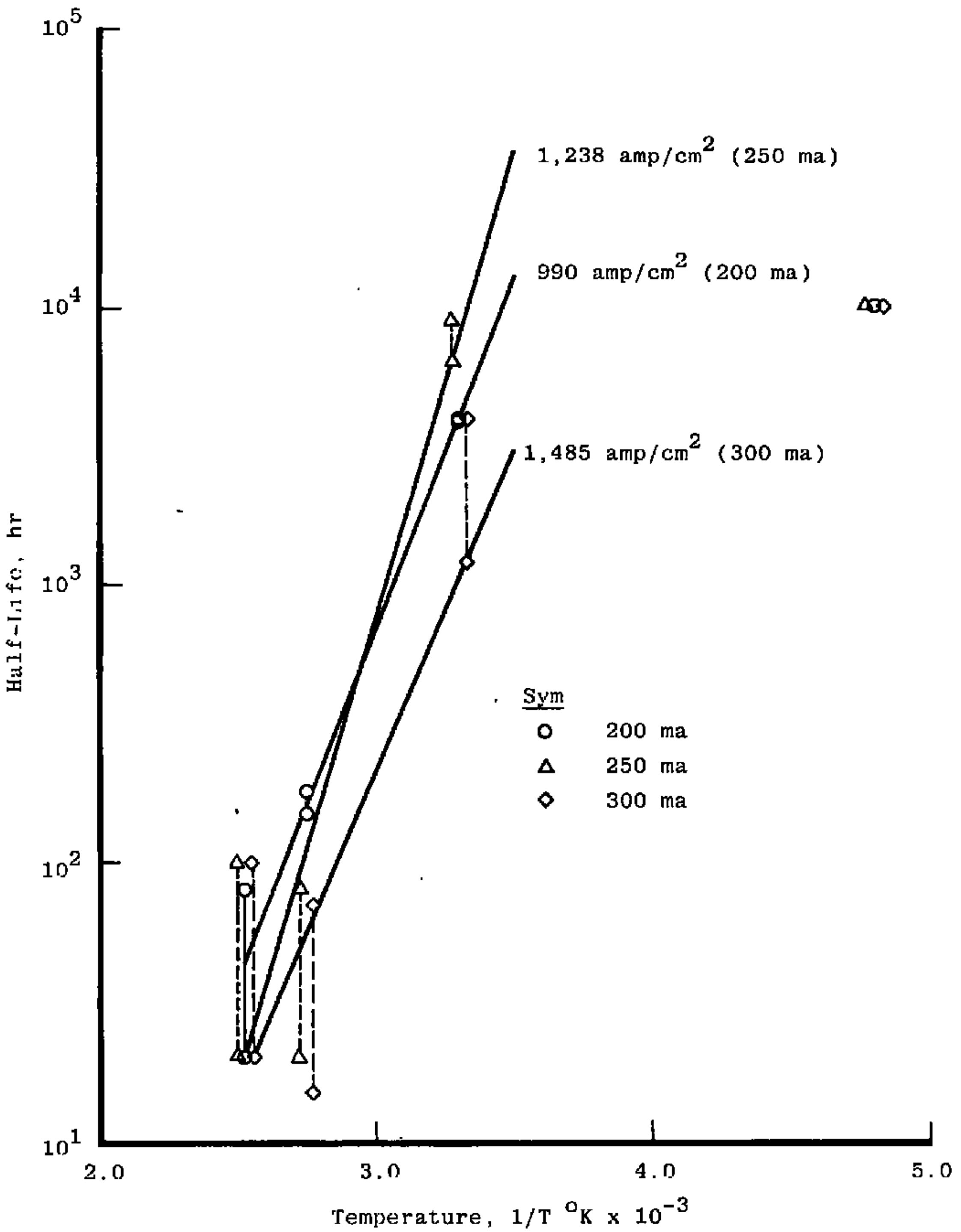

Figure 1. Half-life (t 1/2) vs temperature — RCA C30119.

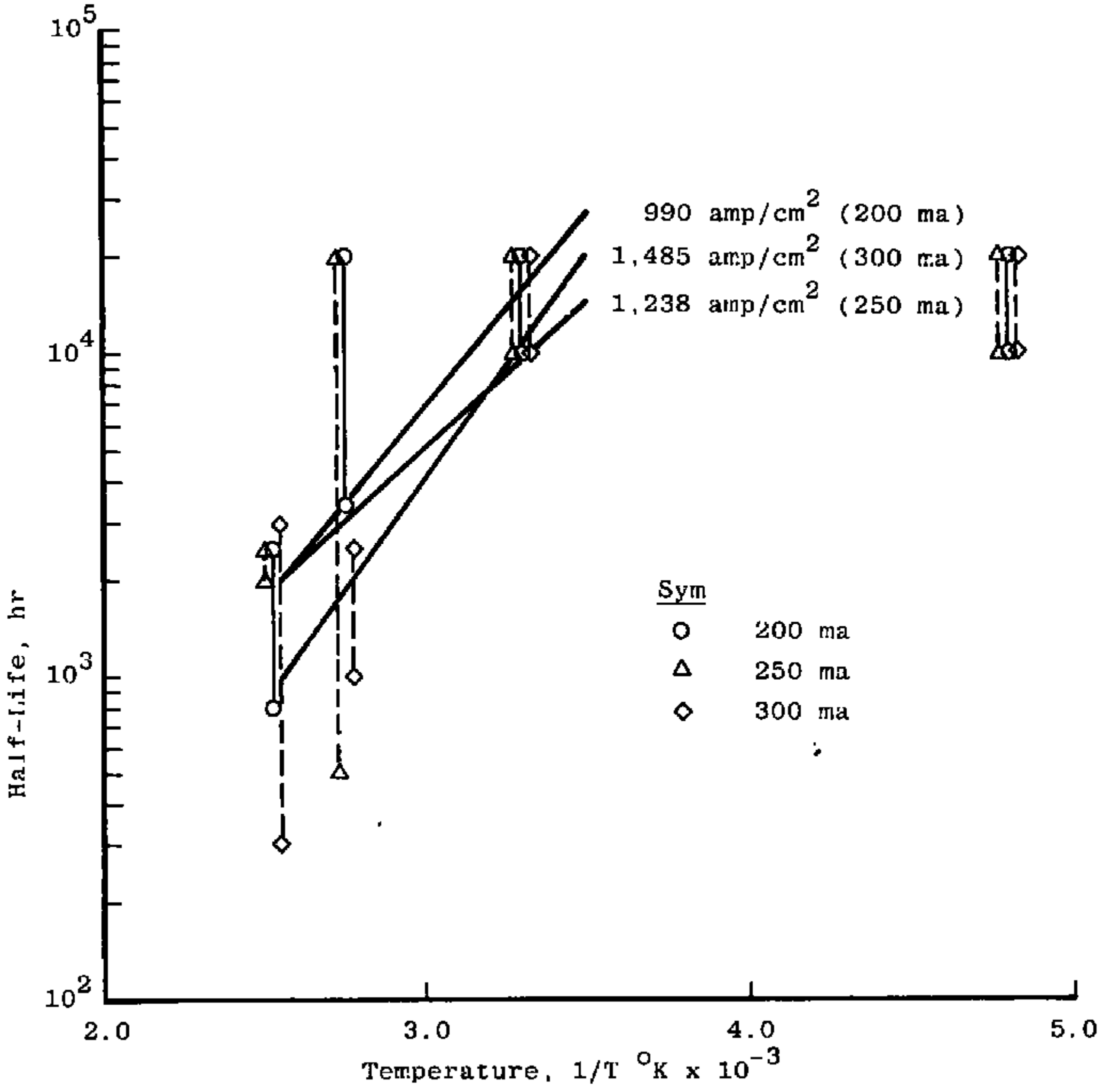

Figure 2. Half-life (t 1/2) vs temperature — RCA C30123.

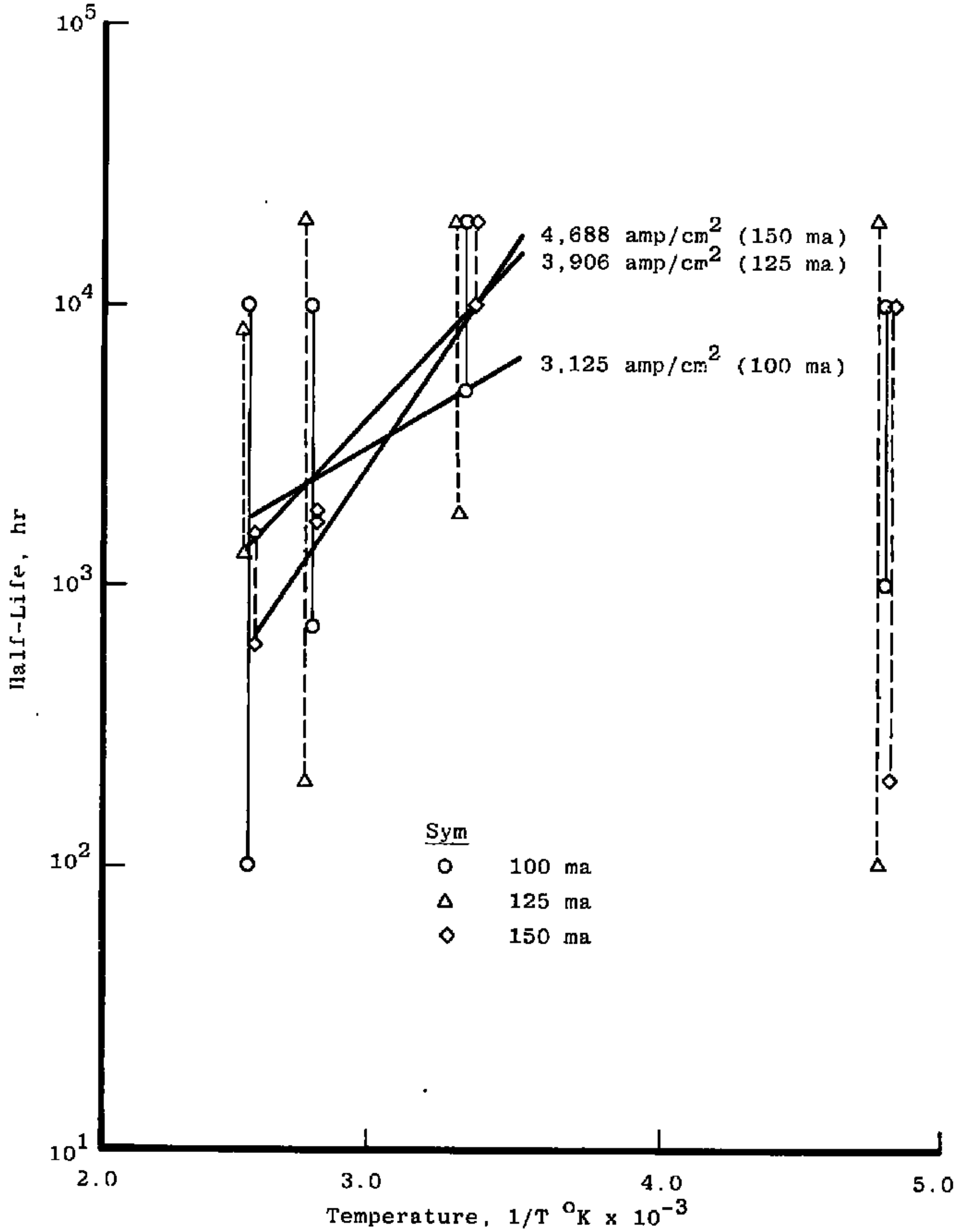

Figure 3. Half-life (t 1/2) vs temperature – SPX 2231.

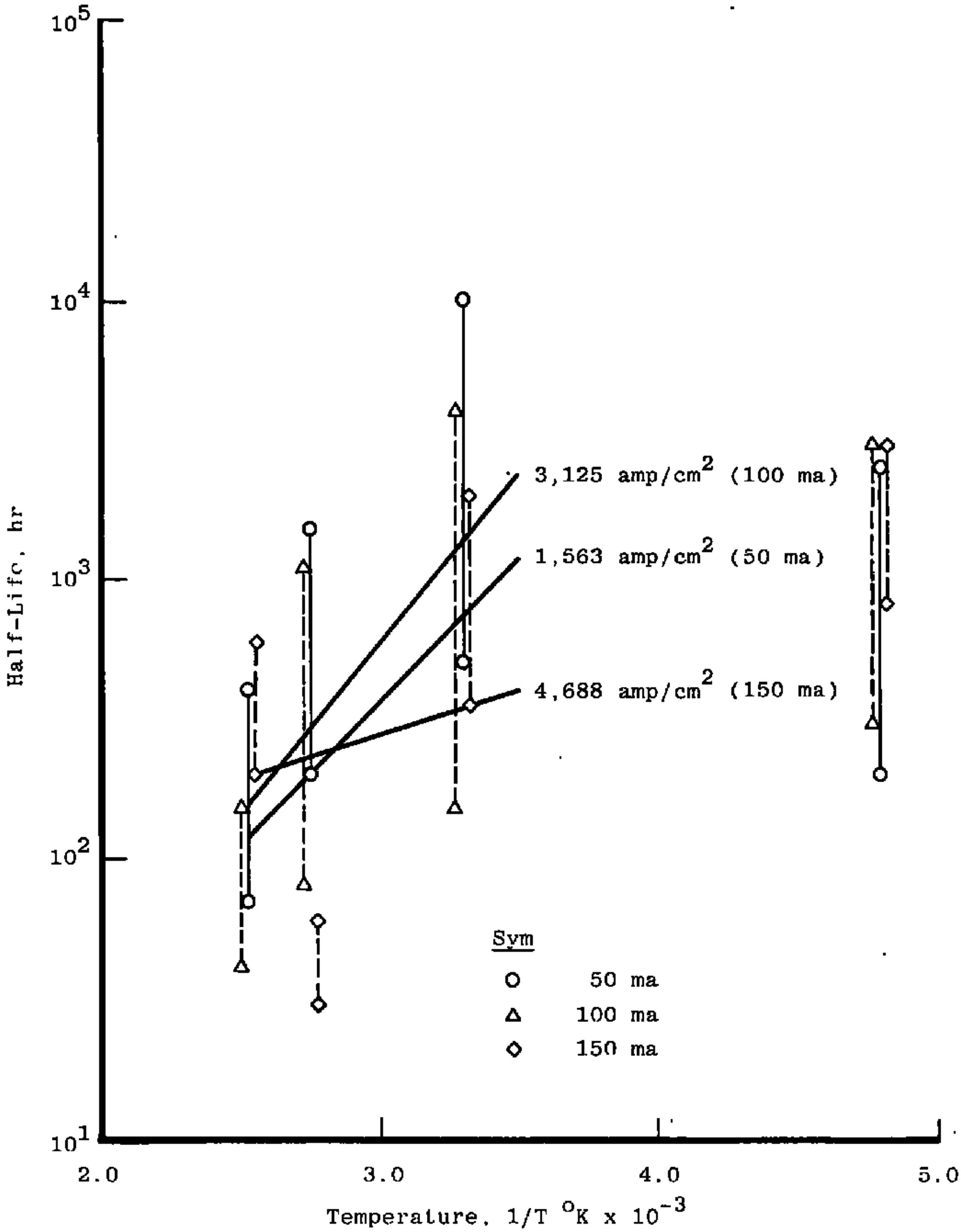

Figure 4. Half-life (t 1/2) vs temperature — SPX 2231F.

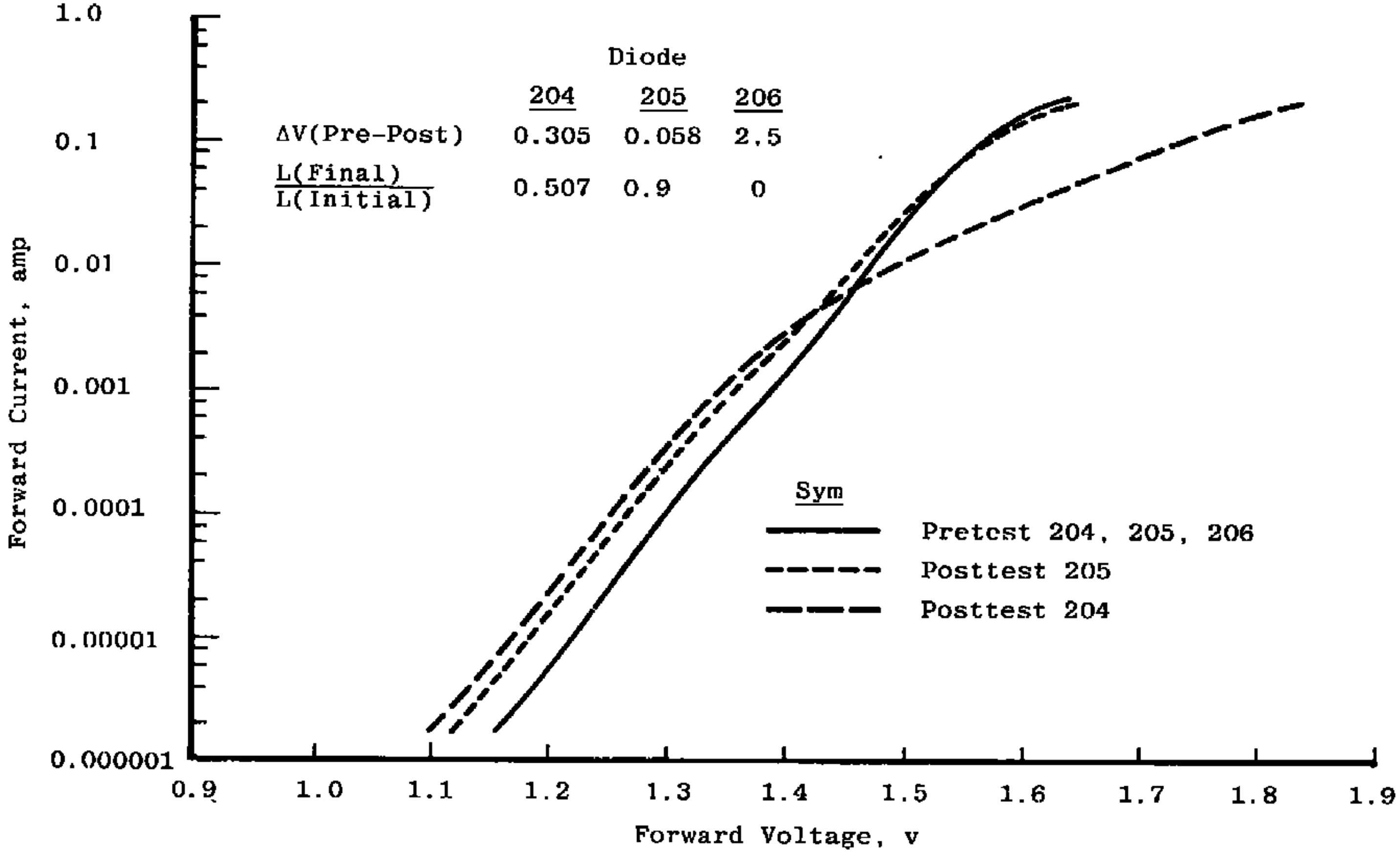

a. Forward current vs forward voltage

Figure 5. Pretest and posttest characteristics – RCA C30123.

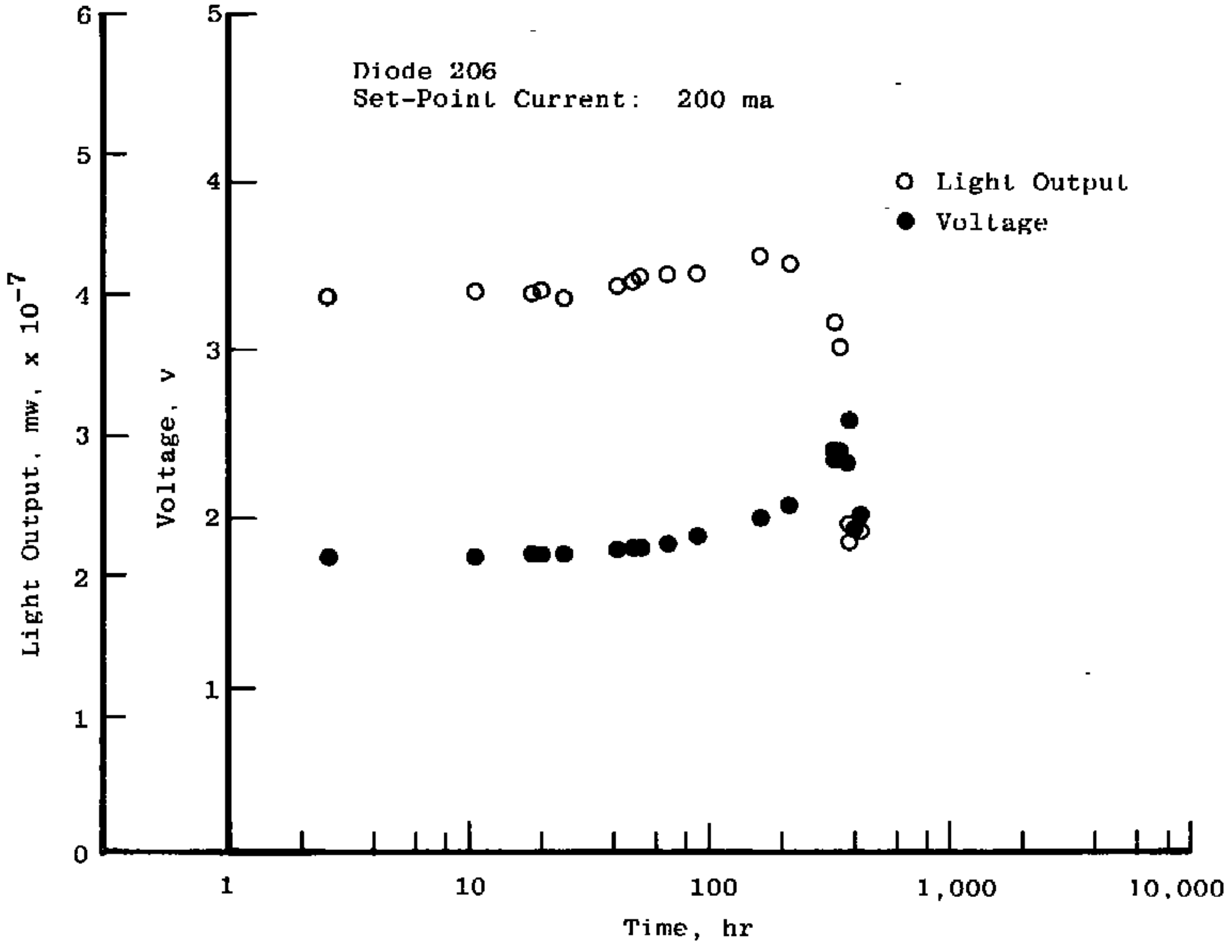

b. Light output and voltage vs time
Figure 5. Concluded.

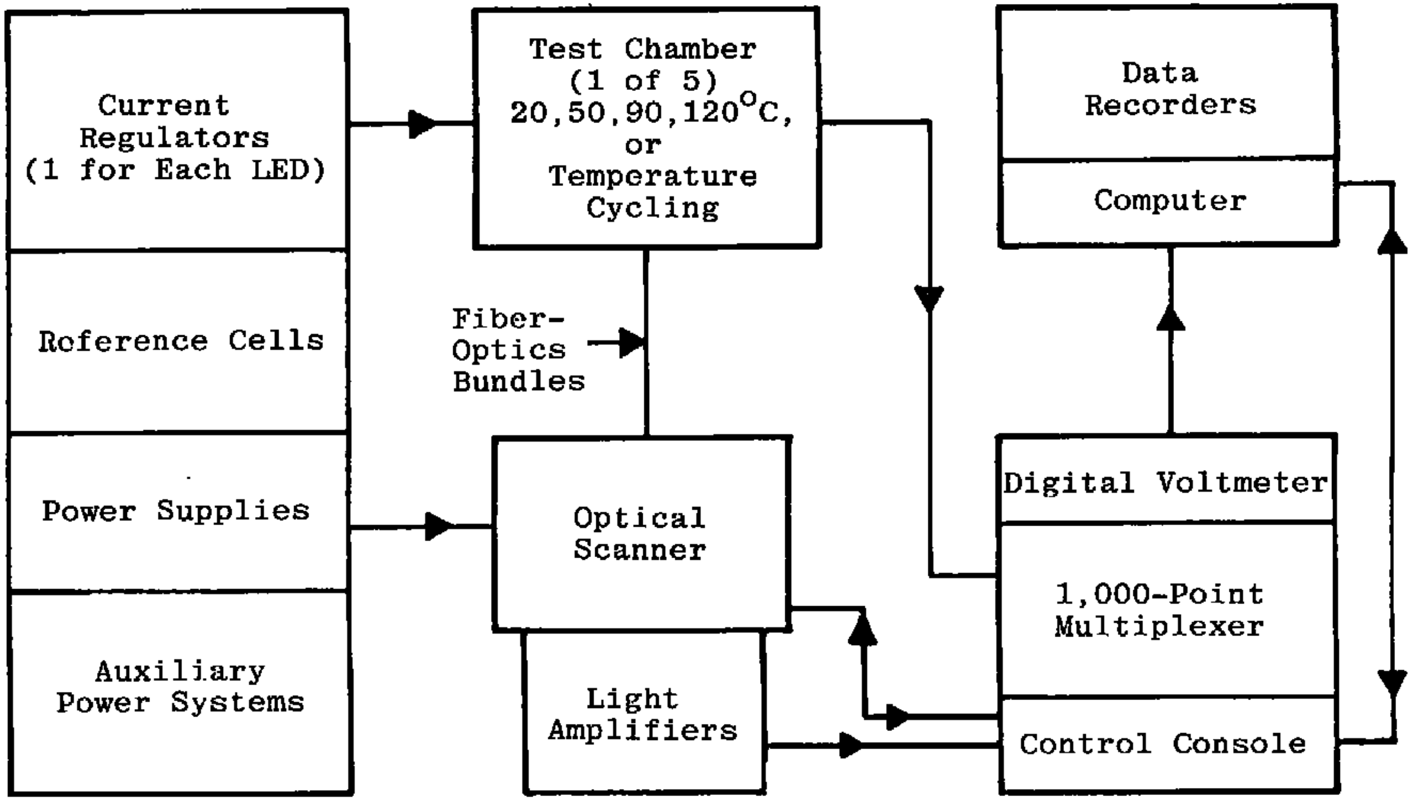

Figure 6. Block diagram of LED test complex.

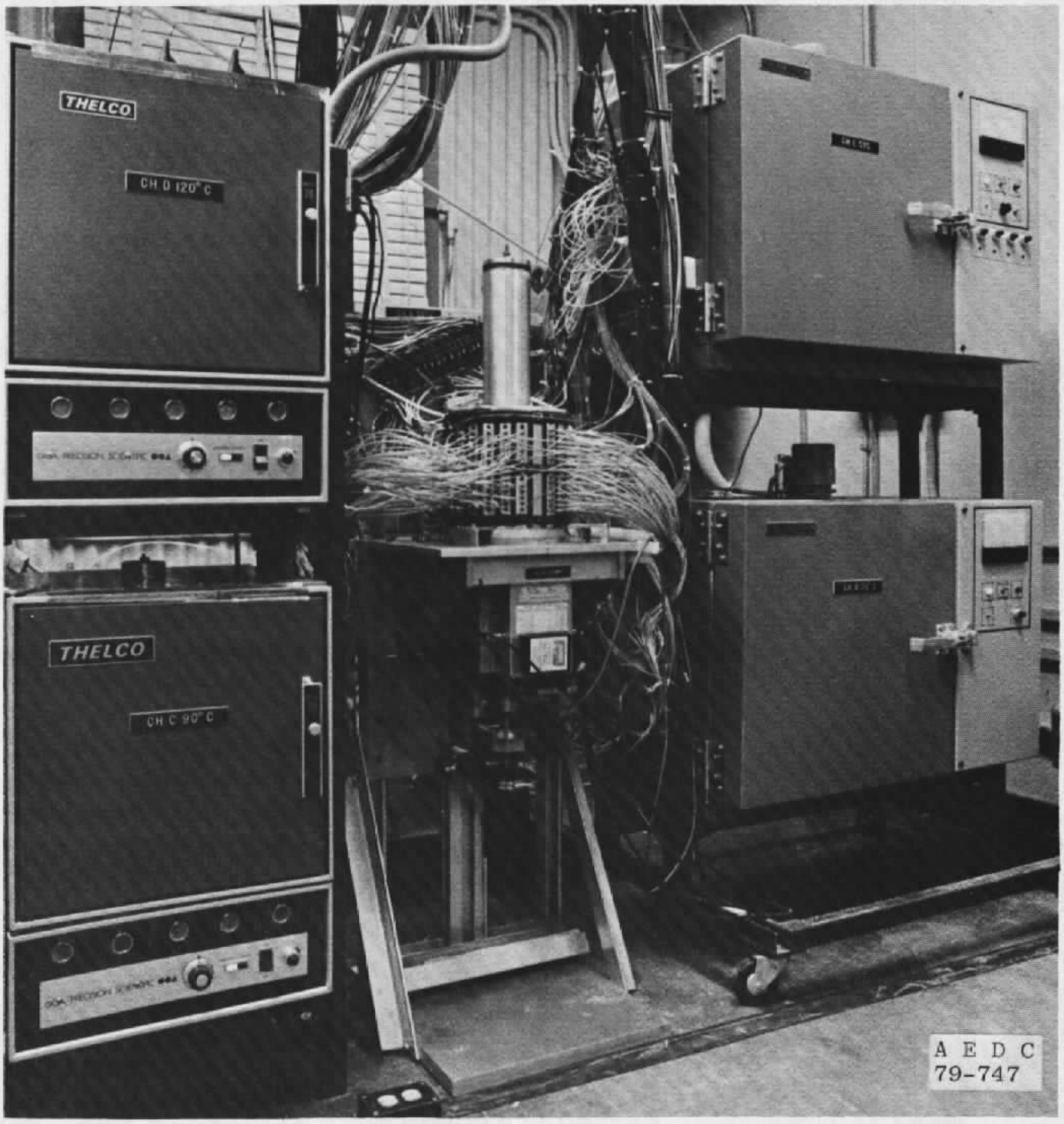

Figure 7. Experimental arrangement.

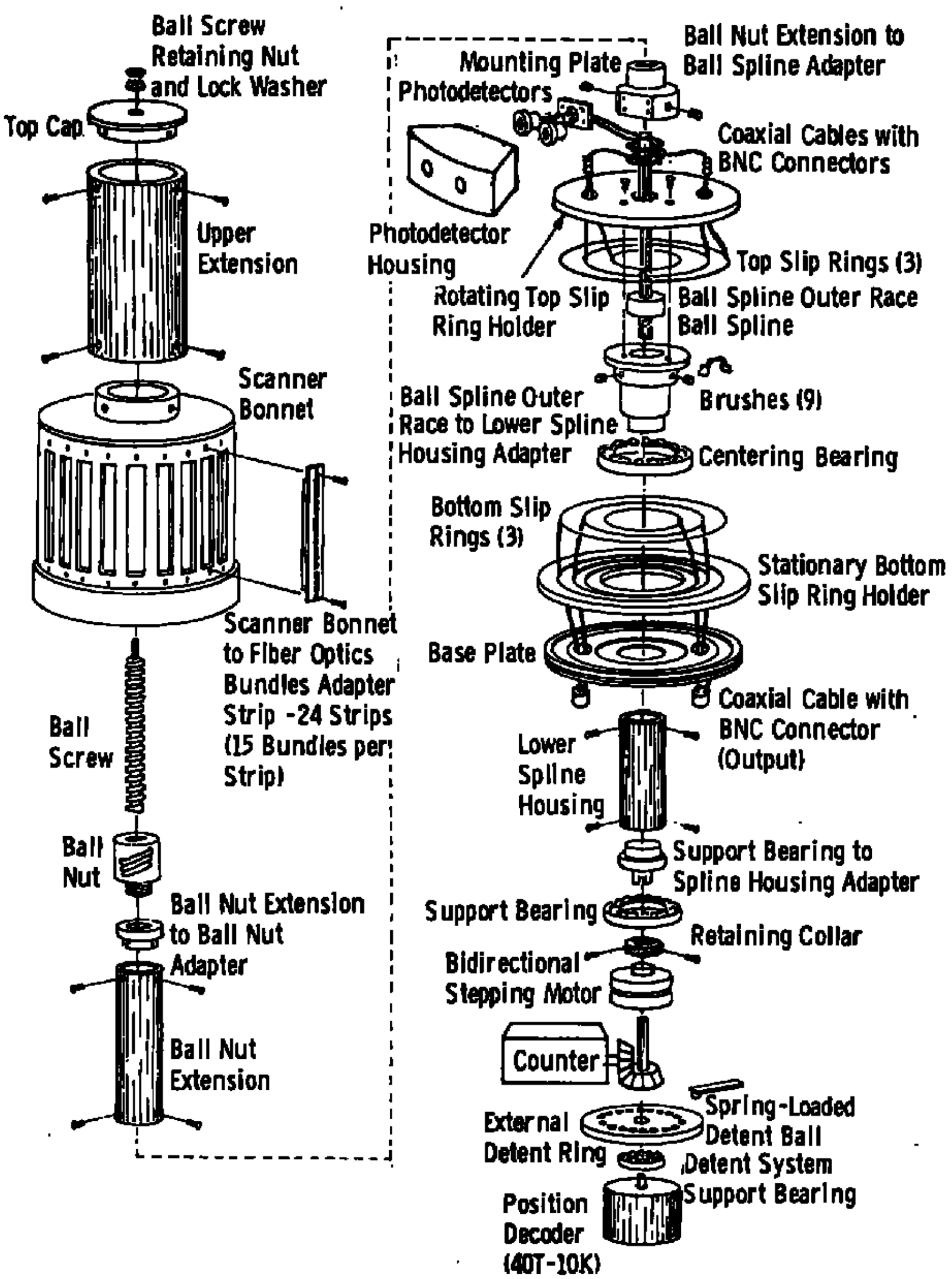

Figure 8. Exploded view of LED test complex.

Figure 9. Instrument rack.

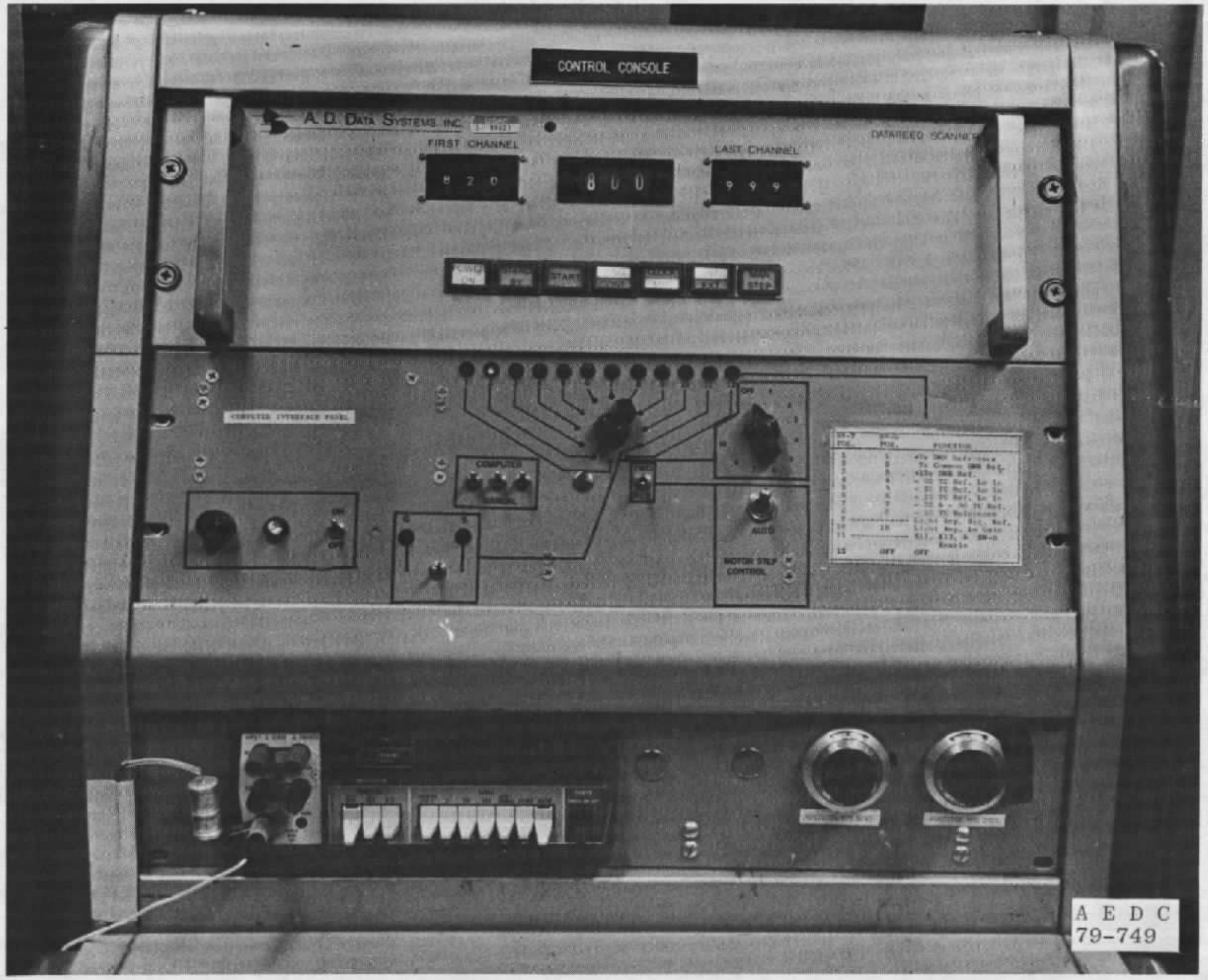

Figure 10. Computer/manual console.

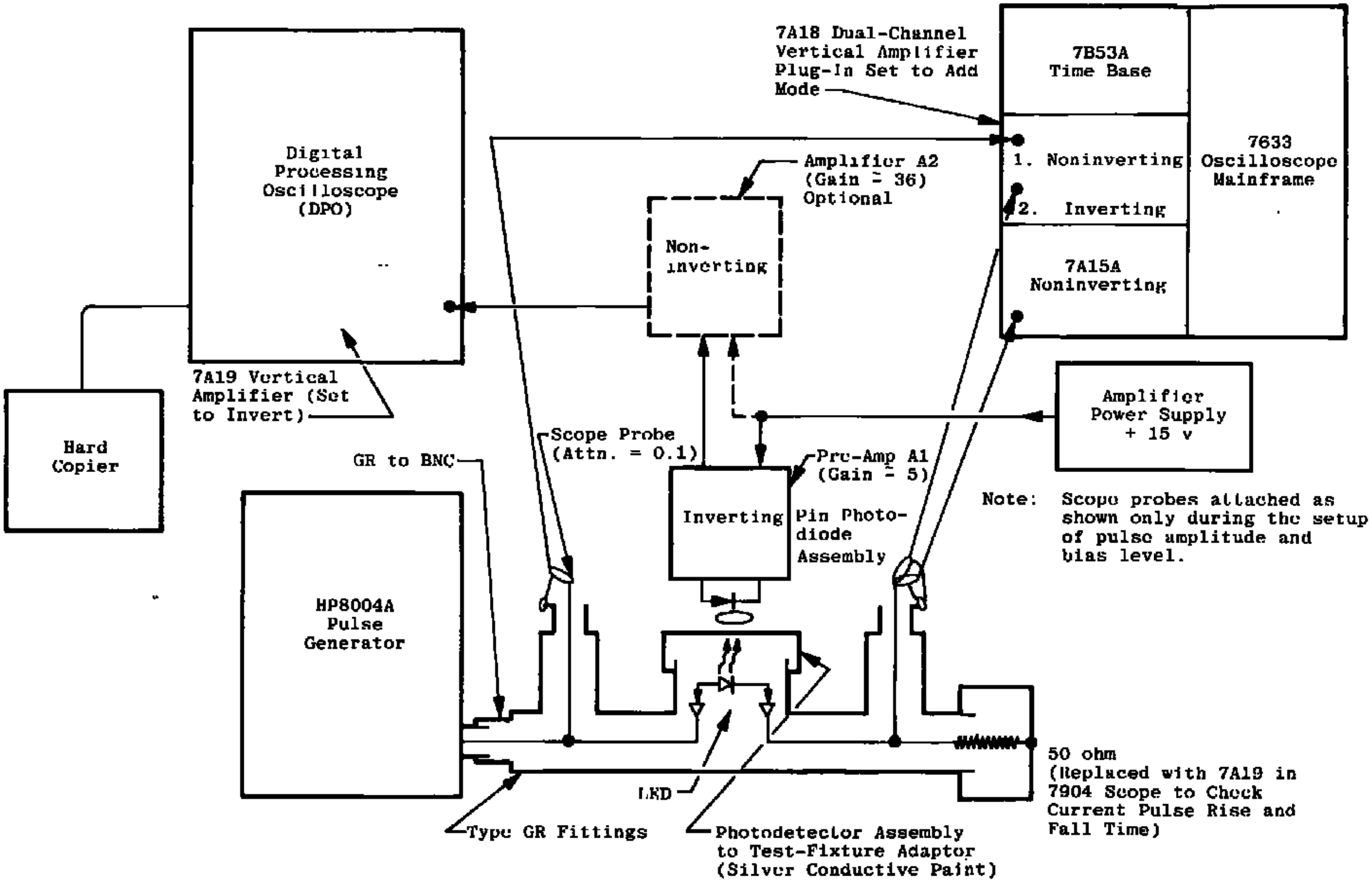

Figure 11. Block diagram of rise and fall time experiment.

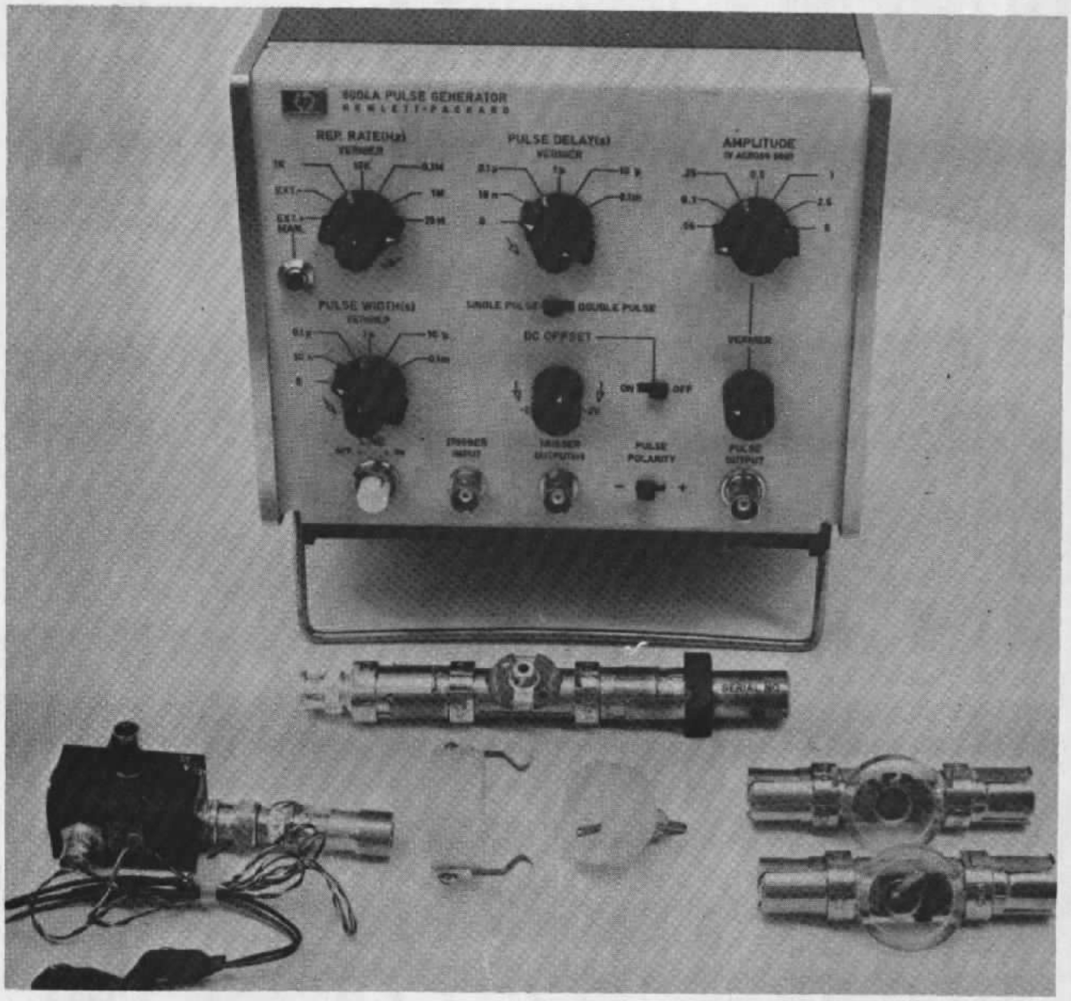

Figure 12. Rise and fall time hardware.

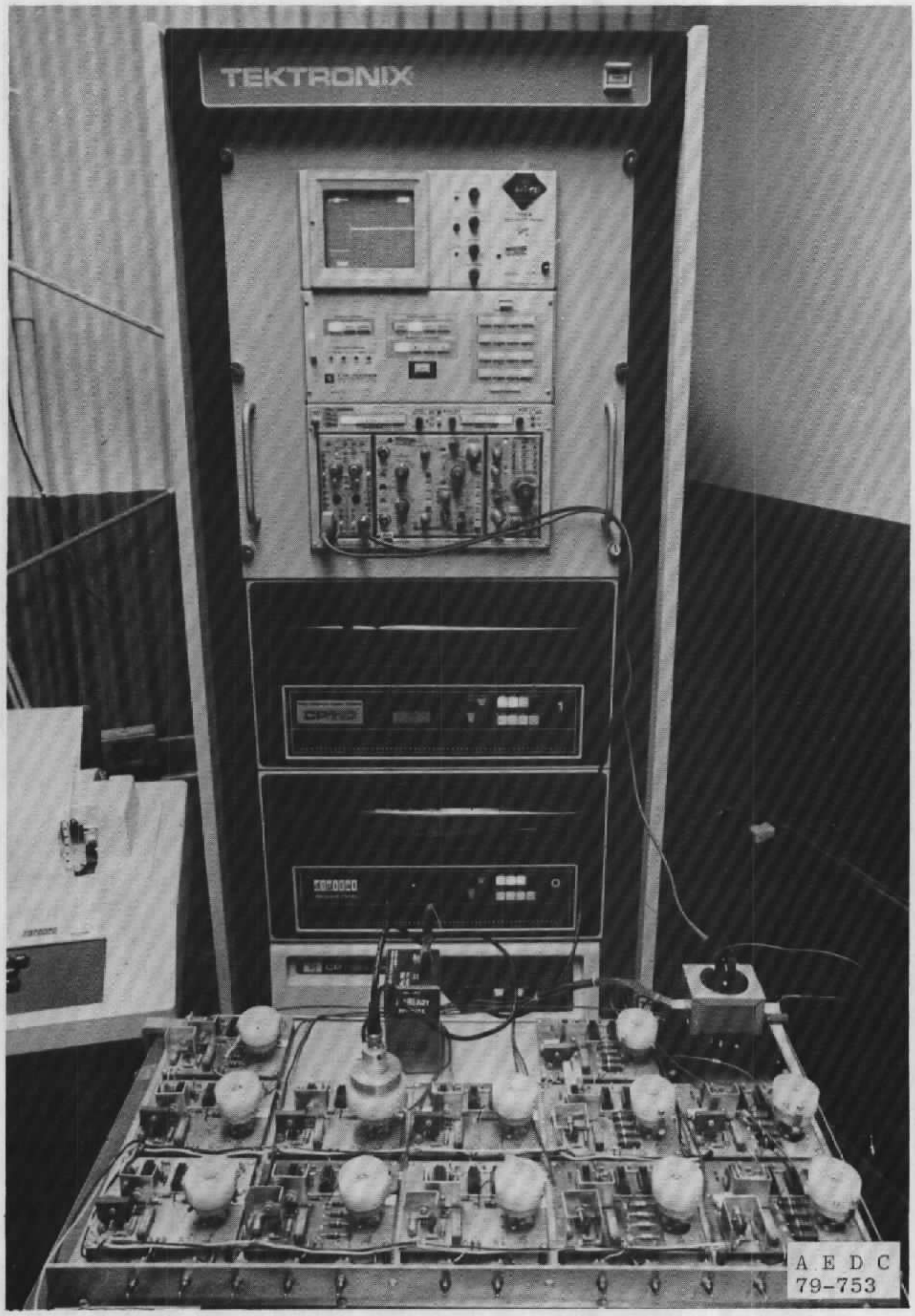

Figure 13. Pulse-test setup.

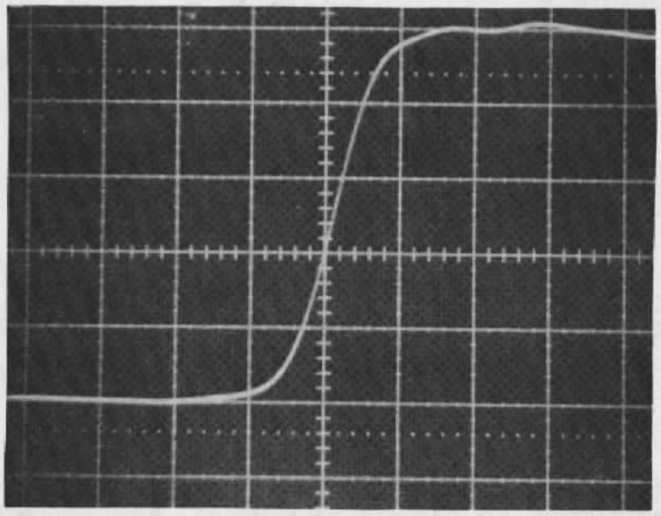

1 nsec/cm

a. Rise time

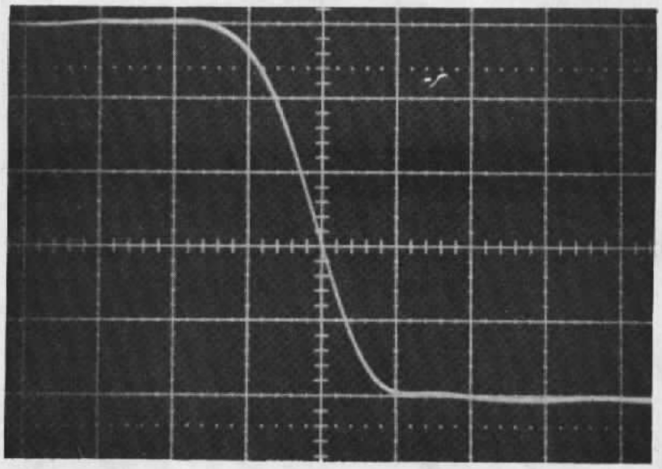

1 nsec/cm

b. Fall time

Figure 14. Pulse generator rise and fall time.

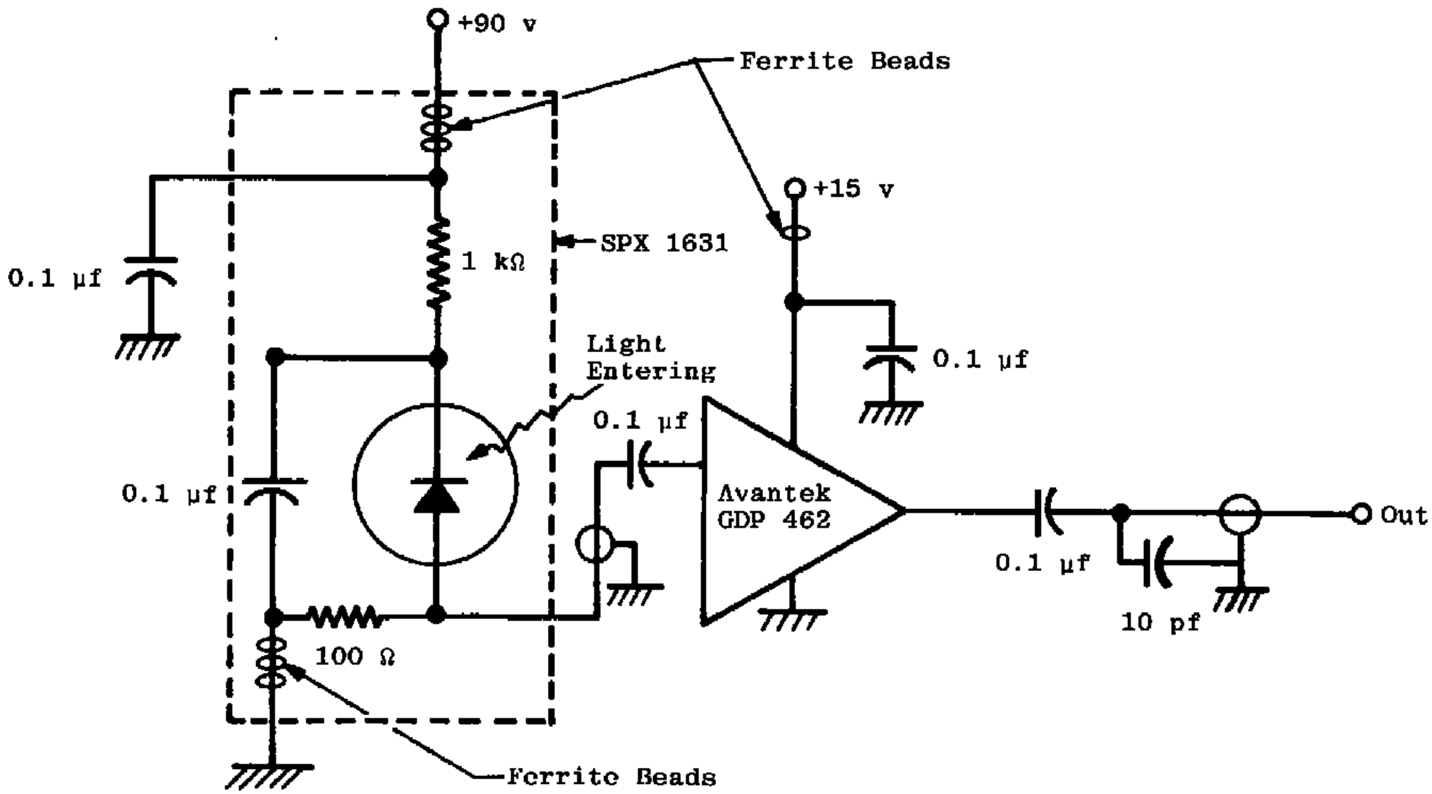

Figure 15. Photodiode amplifier circuit.

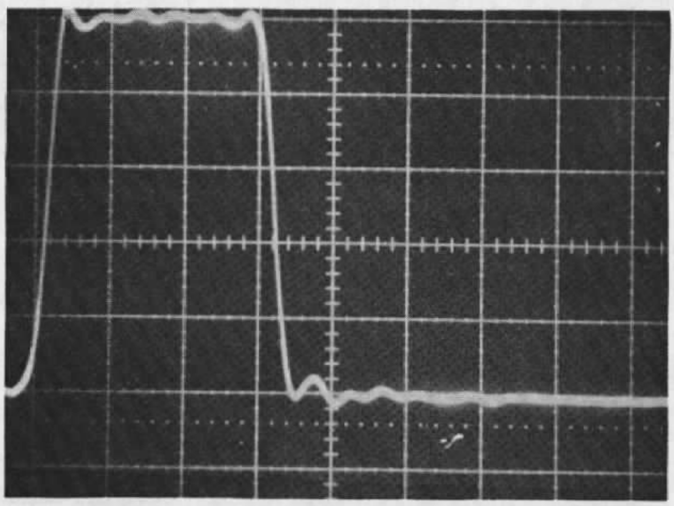

5 nsec/cm

Figure 16. Pulse amplifier response.

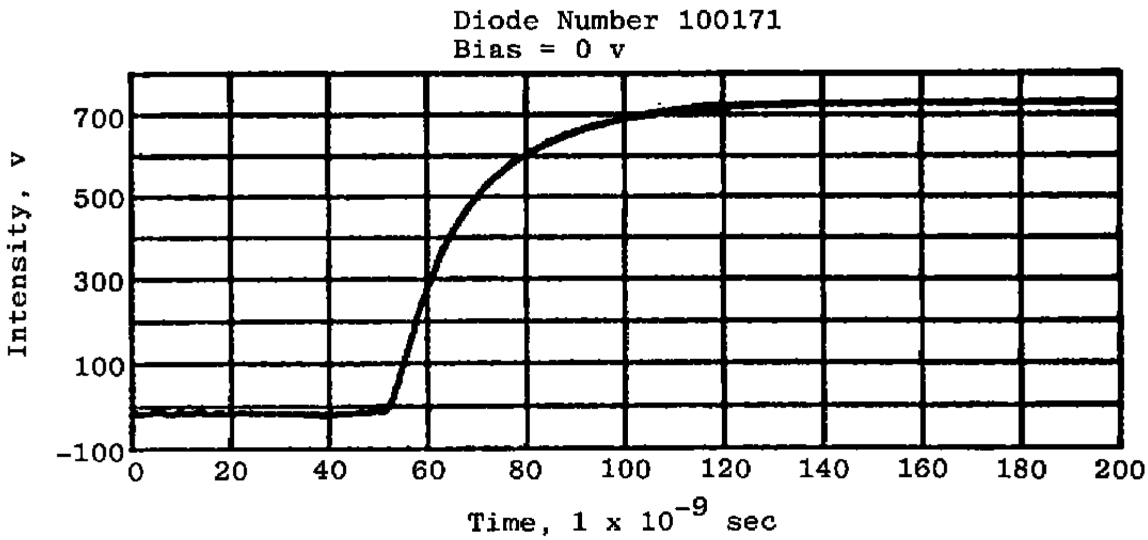

a. Rise time = 3.46932 x 10^{-9} sec

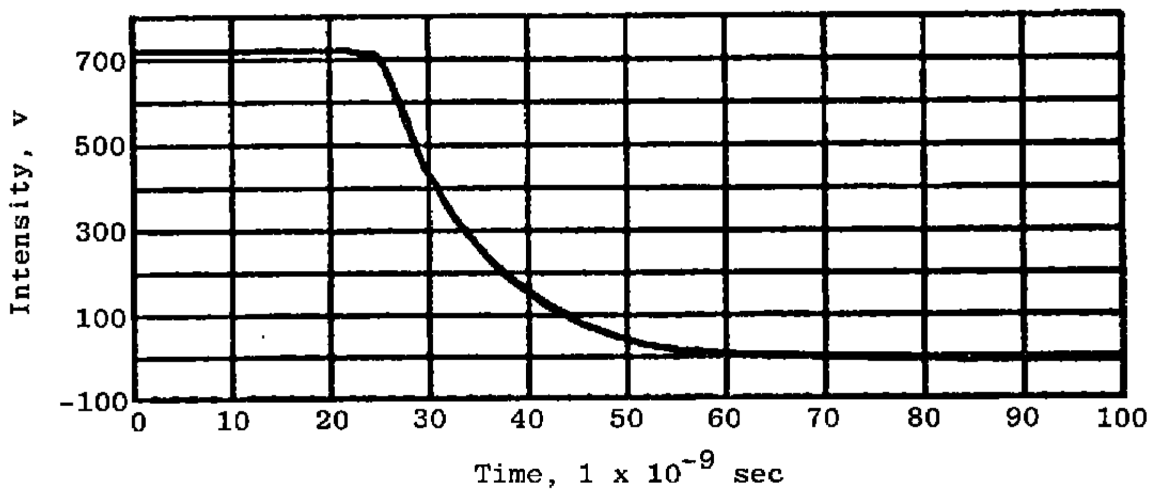

b. Fall time = 2.08696 x 10^{-8} sec

Figure 17. Typical rise and fall time printouts – SPX 2231.

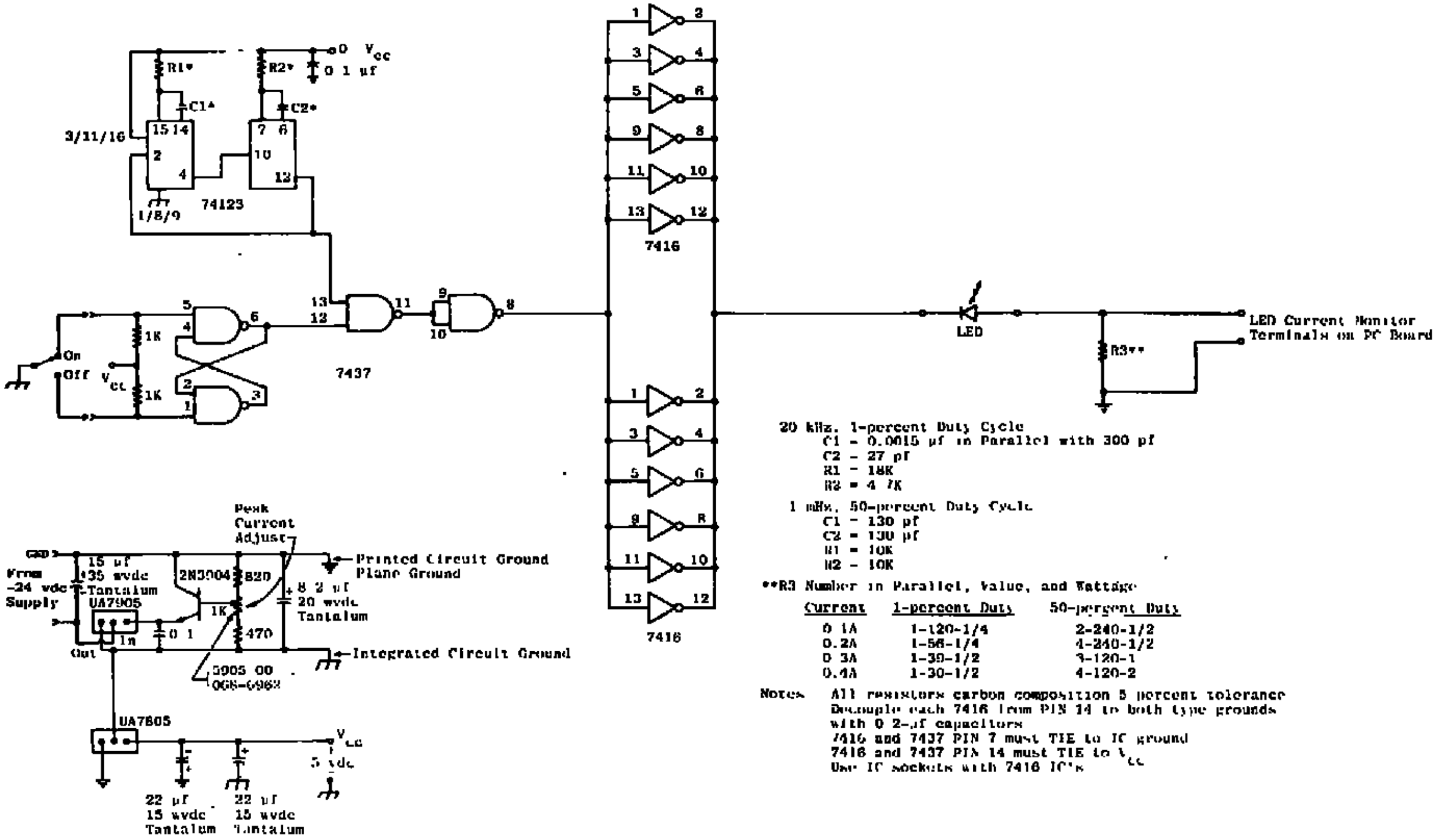

Figure 18. Pulse mode circuitry.

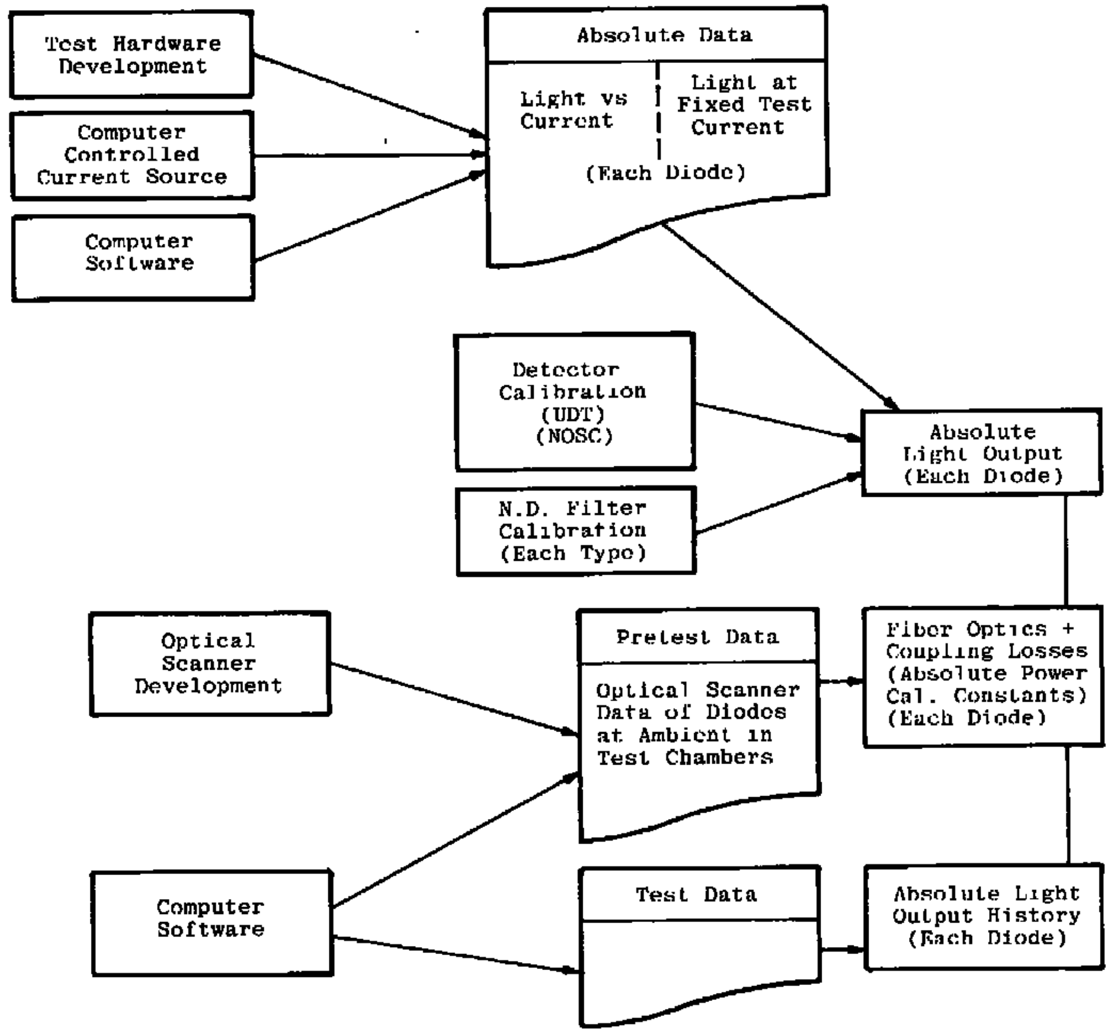

Figure 19. Philosophy of LED light output measurements.

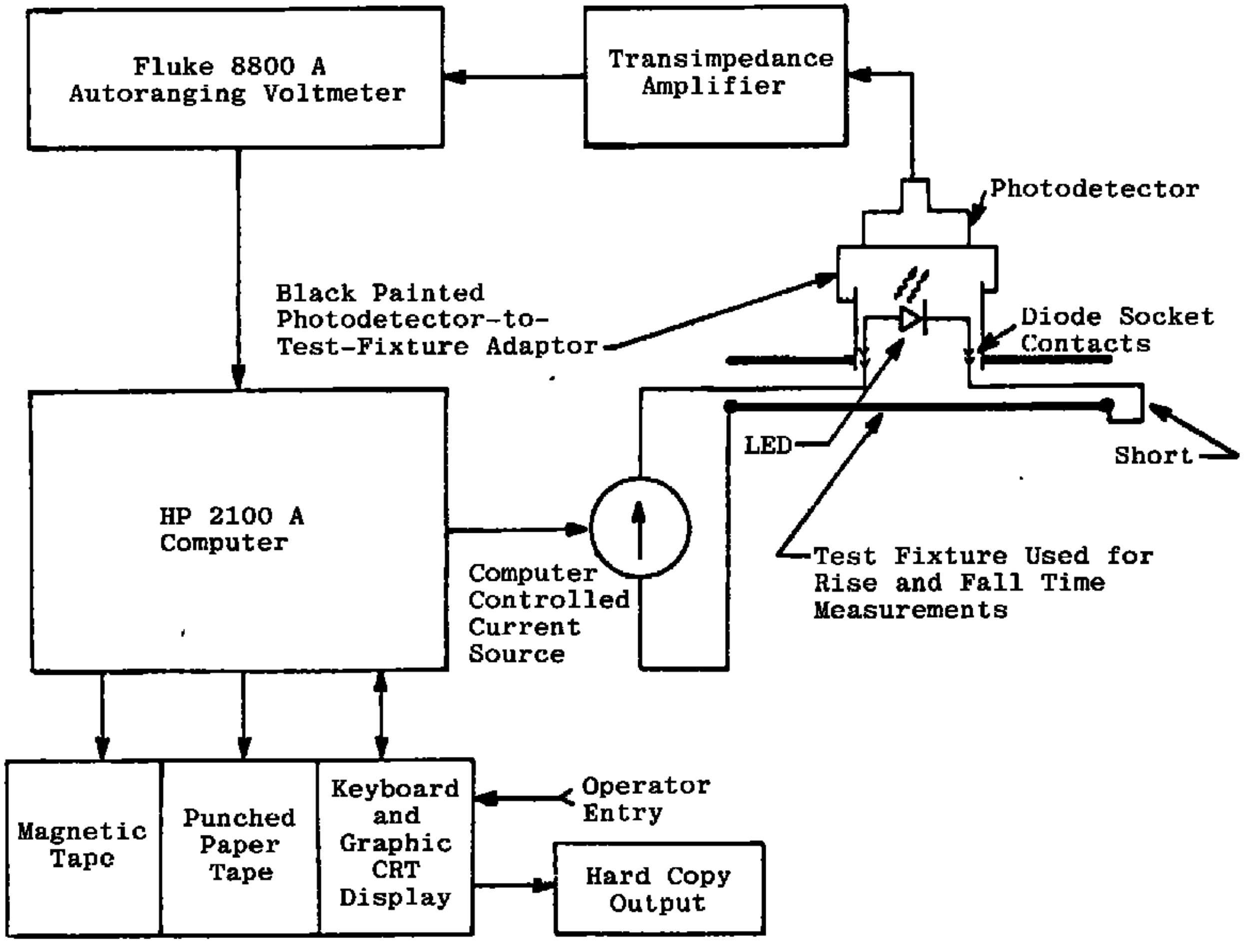

Figure 20. Block diagram for pretest light output measurements.

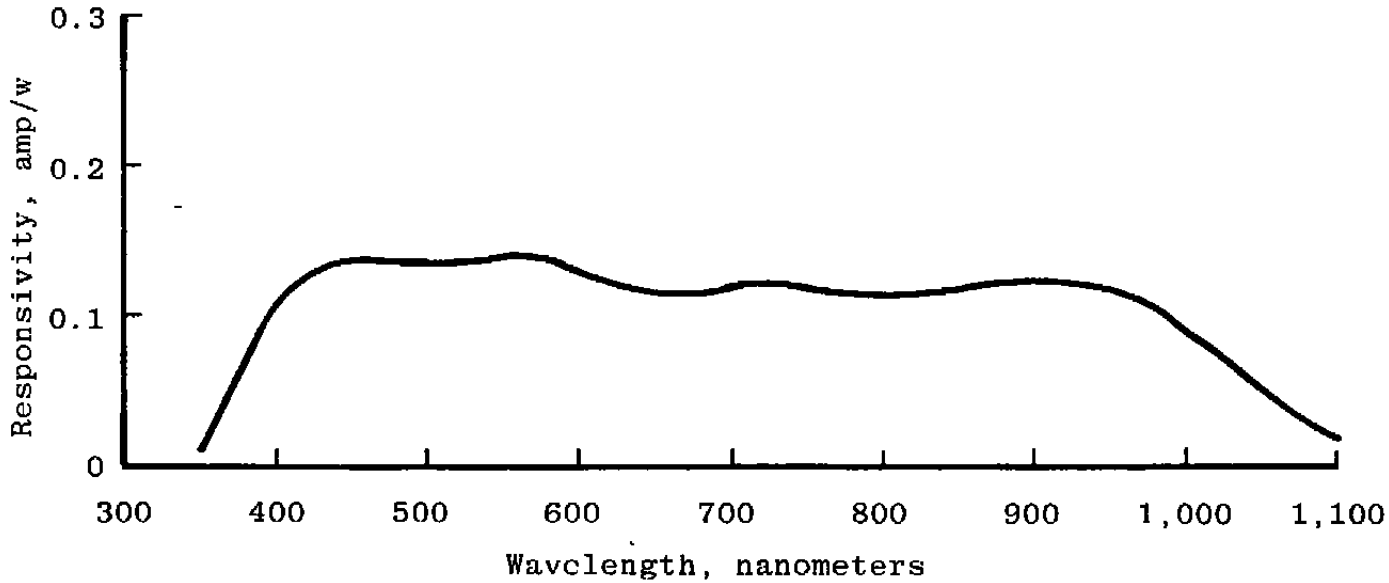

Figure 21. Photodetector spectral response.

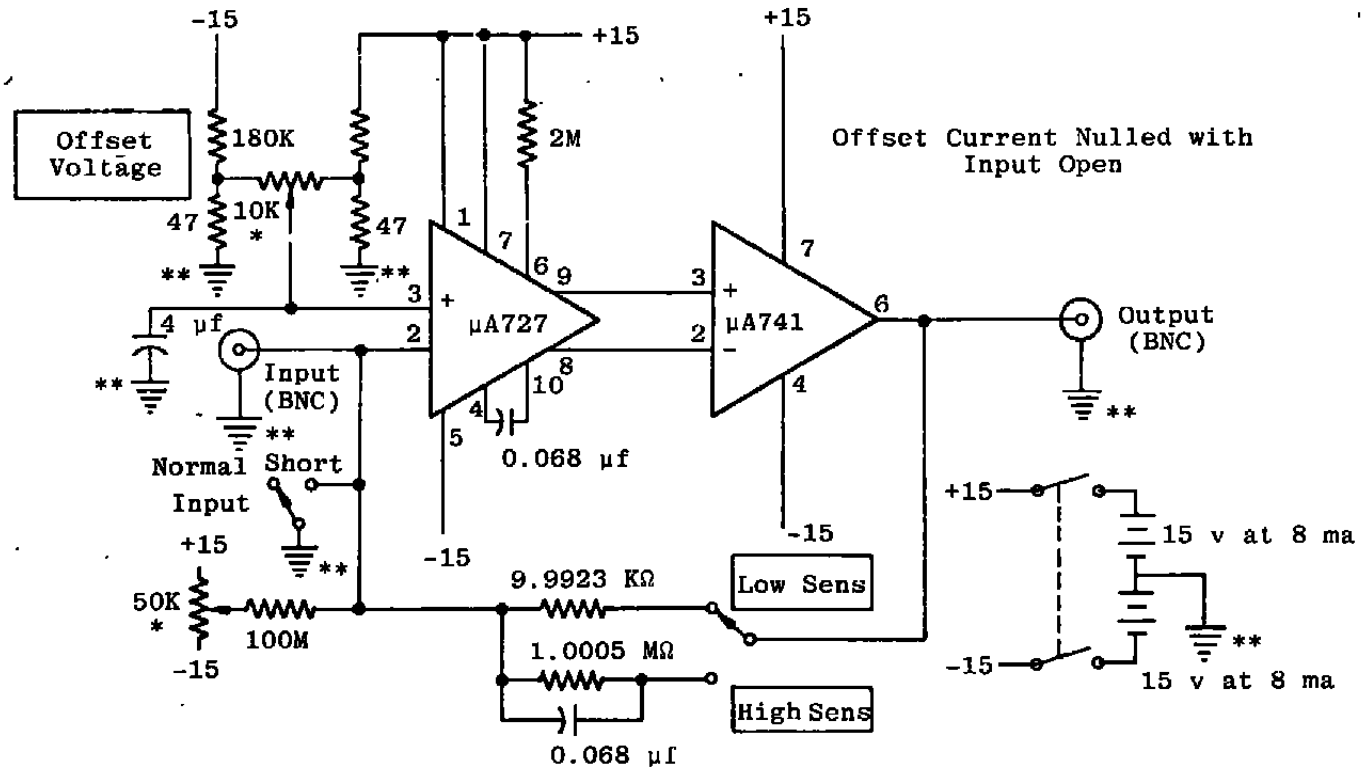

* 10-Turn Pot
** Power Supply Common (Not Founded)

Figure 22. Schematic diagram transimpedance amplifiers.

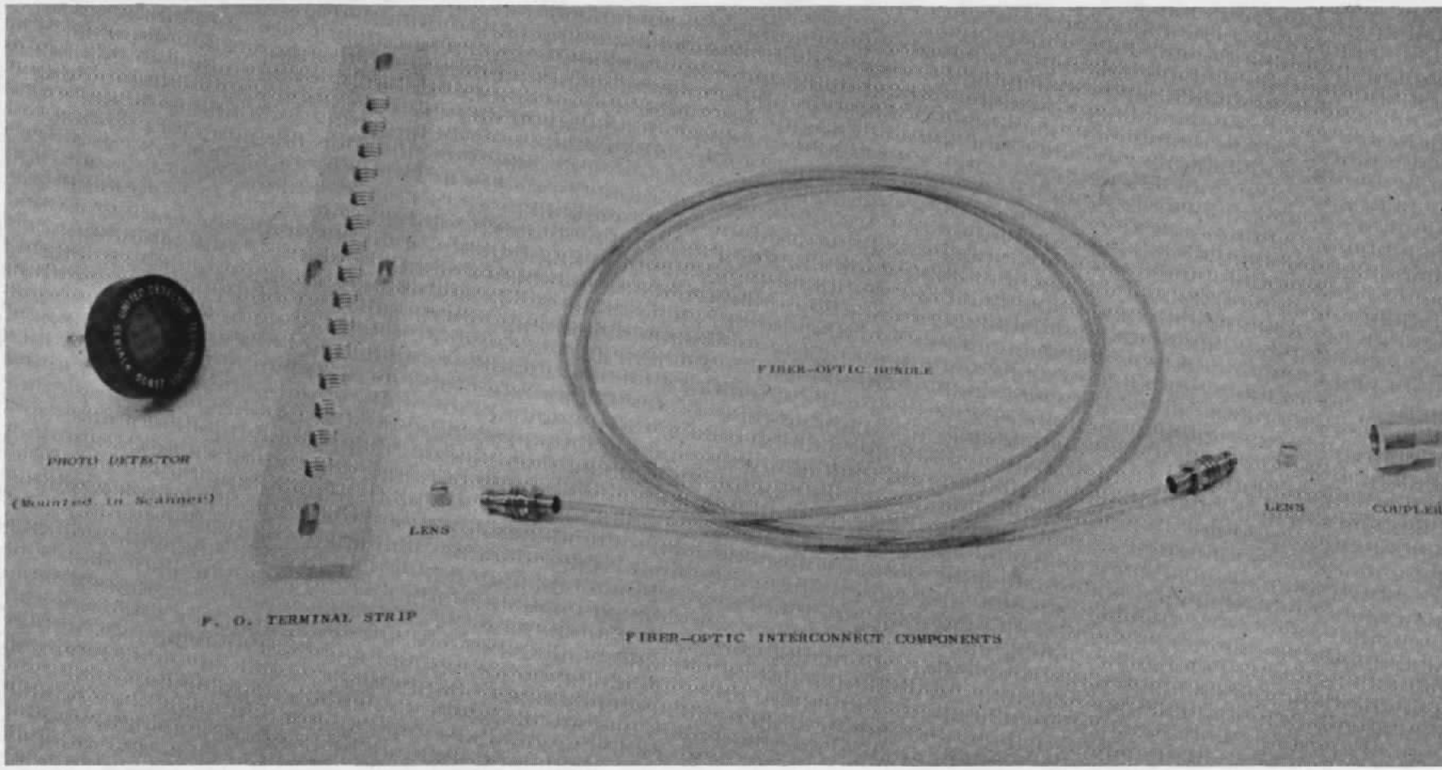

Figure 23. Optical coupling components.

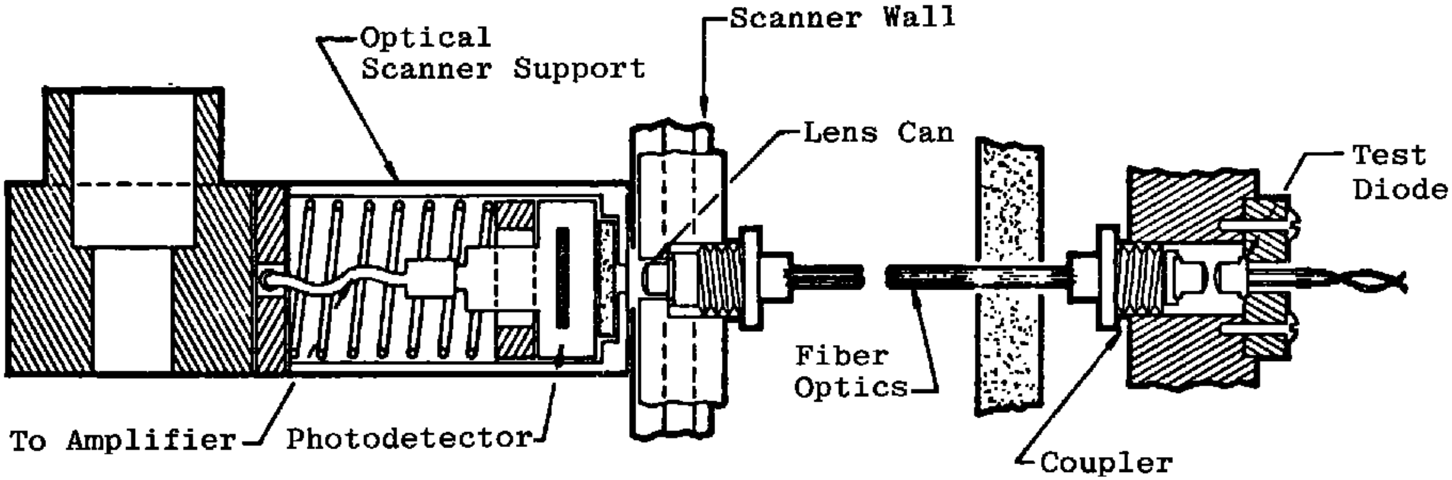

Figure 24. Internal optical scanner components.

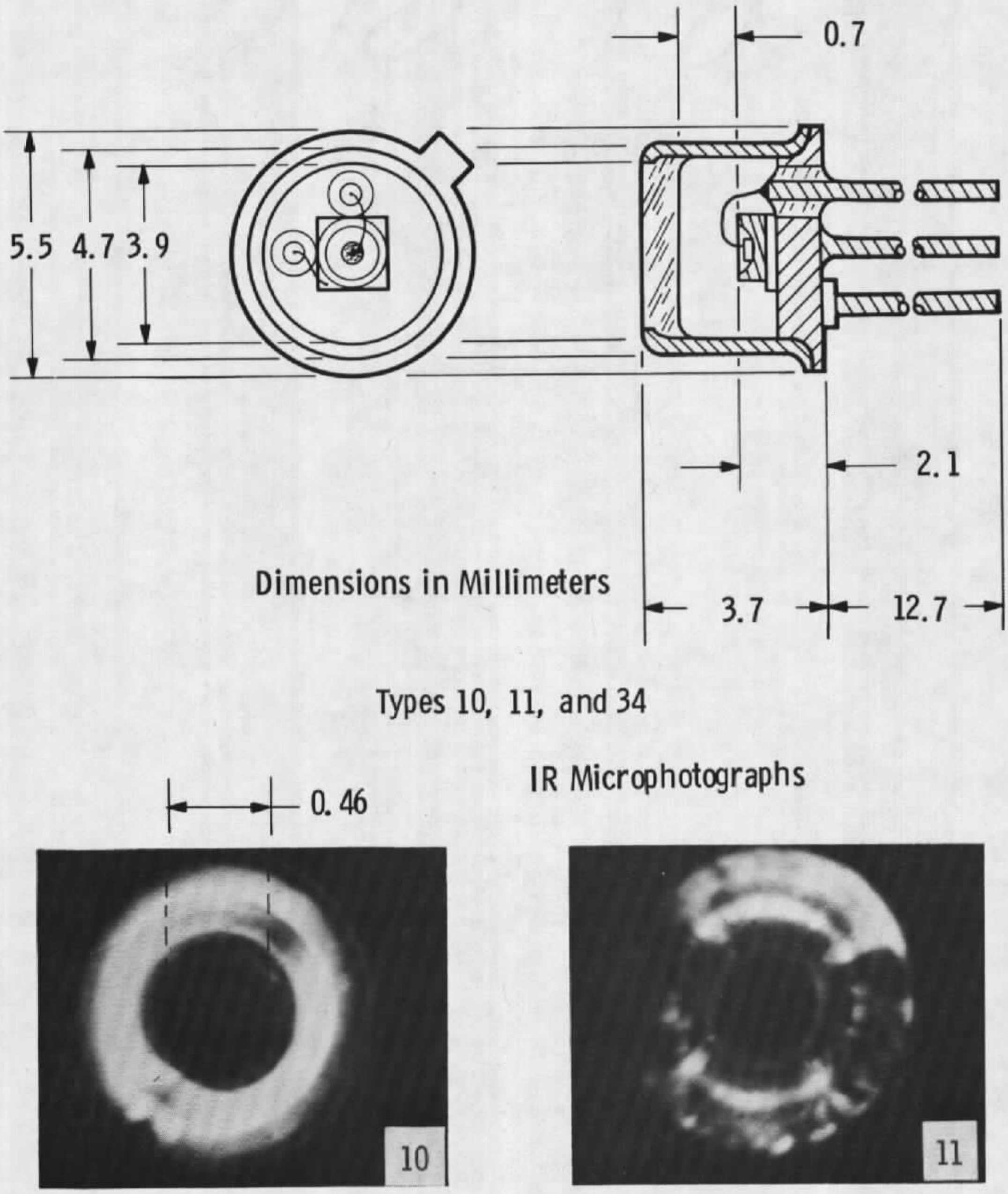

Figure 25. Schematic diagrams of SPX 2231, 2231F, and 2234 LED's including IR microphotographs of light output.

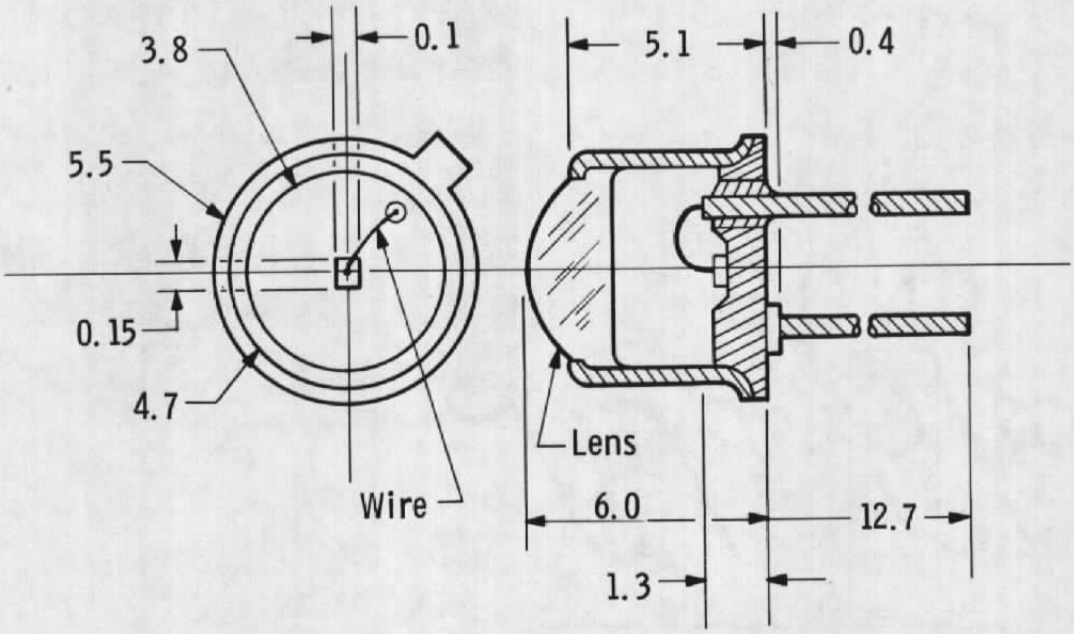

Dimensions in Millimeters

Types 40 and 41

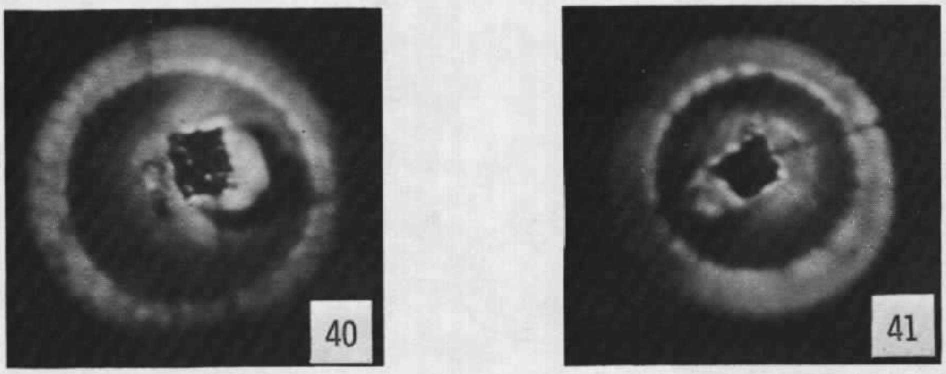

IR Microphotographs

Figure 26. Schematic diagram and IR microphotograph of SPX 2354 and 2354F LED's.

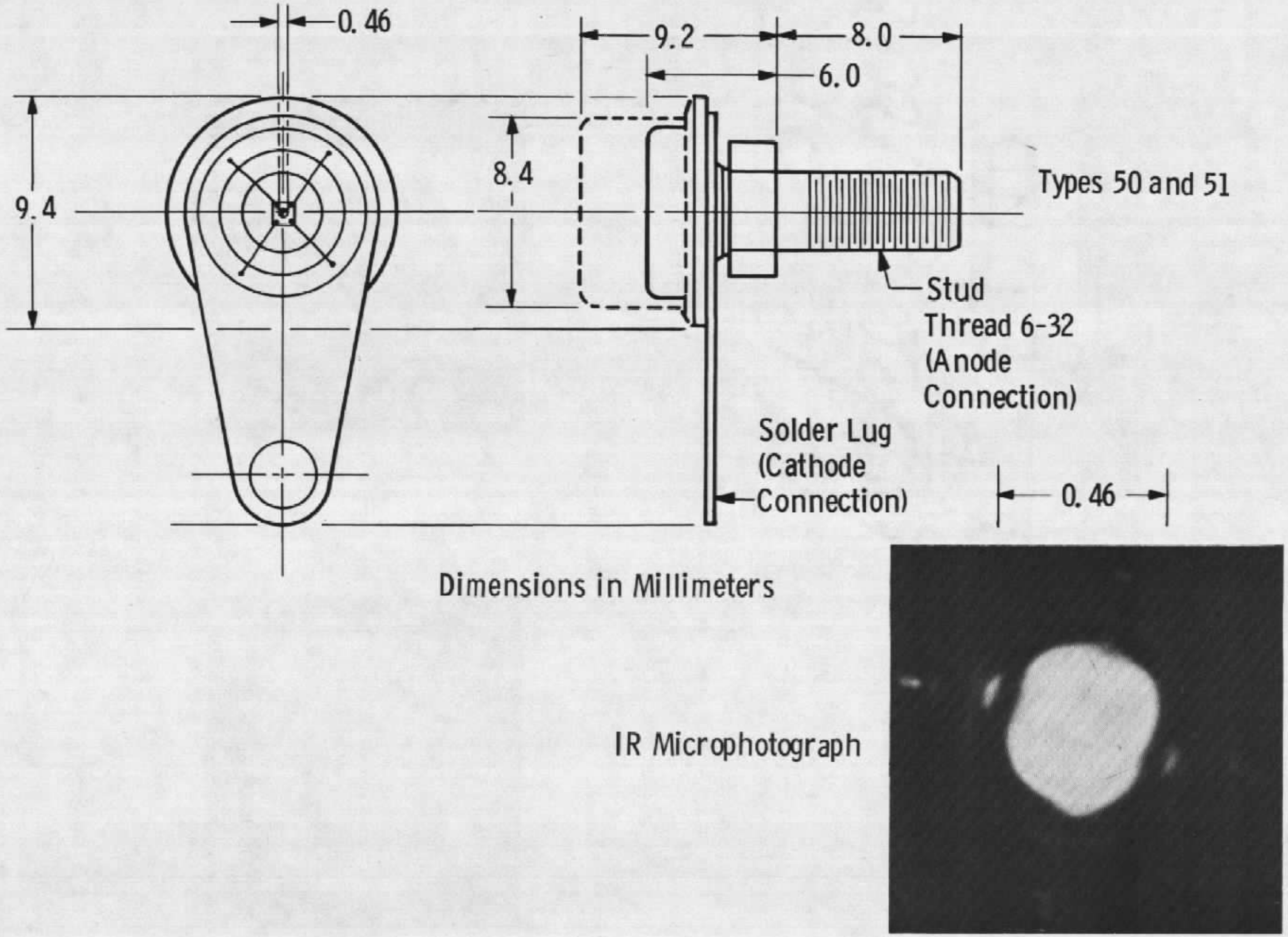

Figure 27. Schematic diagram and IR microphotograph of TIES 35 and TIXL 35 LED's.

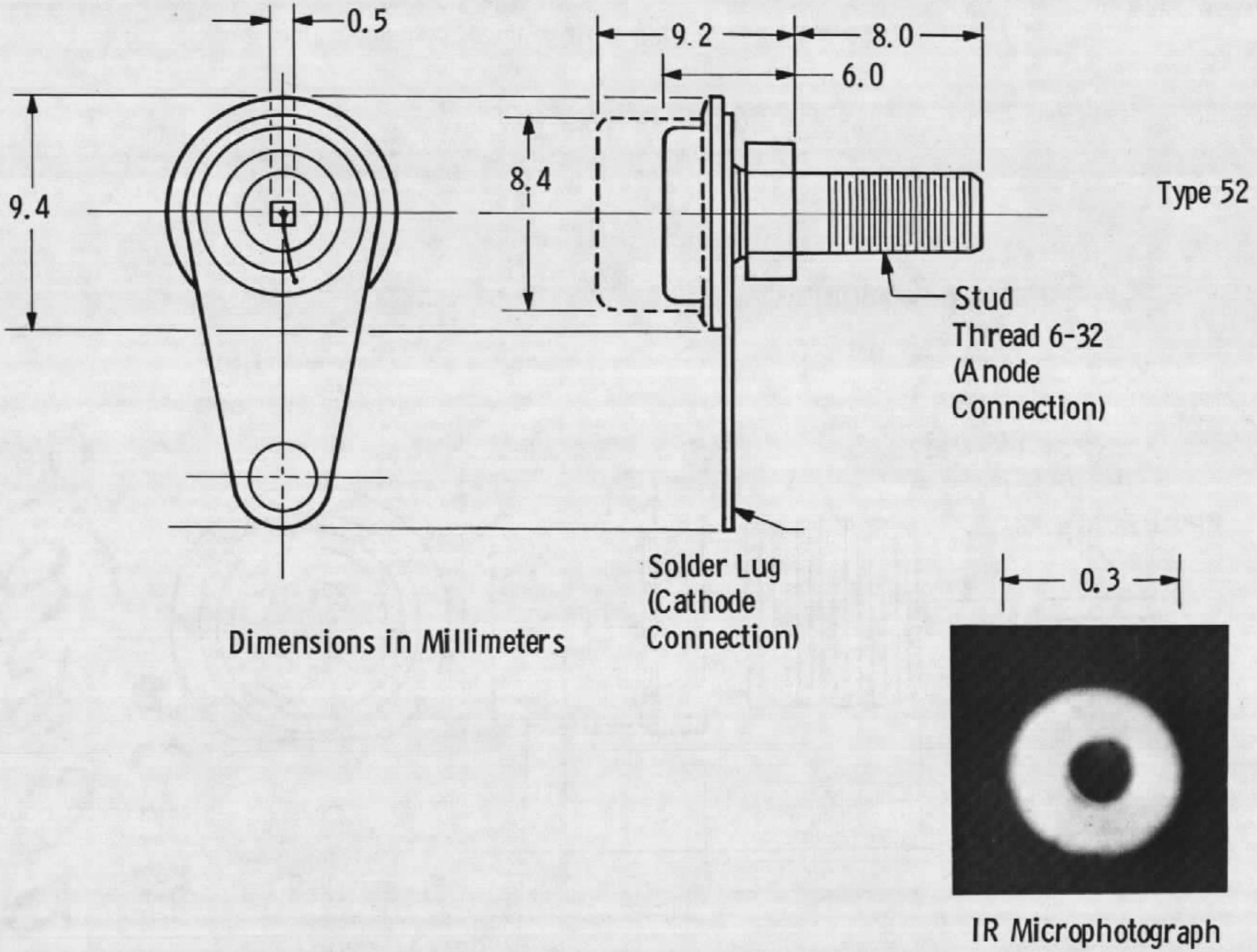

Figure 28. Schematic diagram and IR microphotograph of TI Special LED.

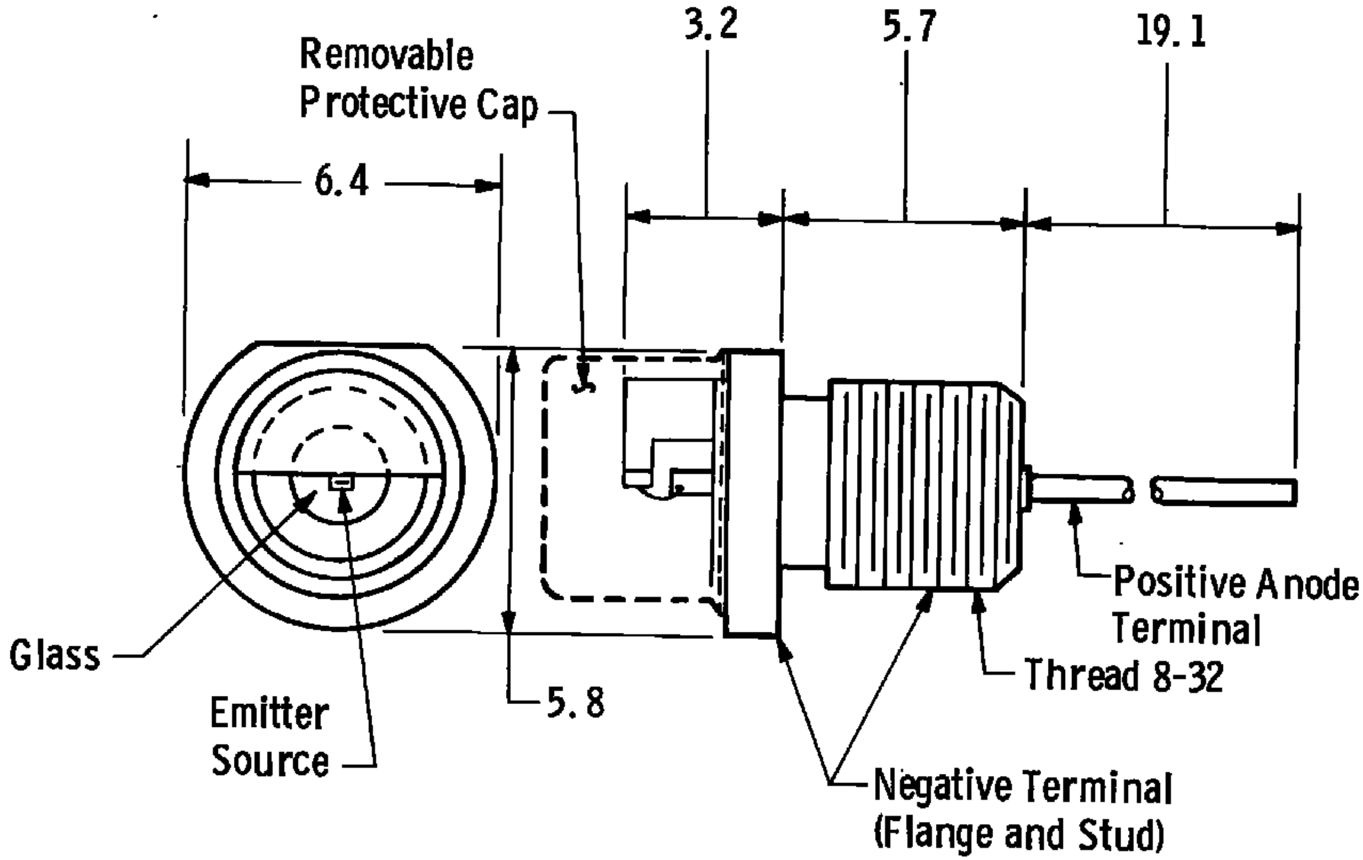

Types 30 and 90

Figure 29. Schematic diagram of RCA C30119 and RCA C30123 LED's.

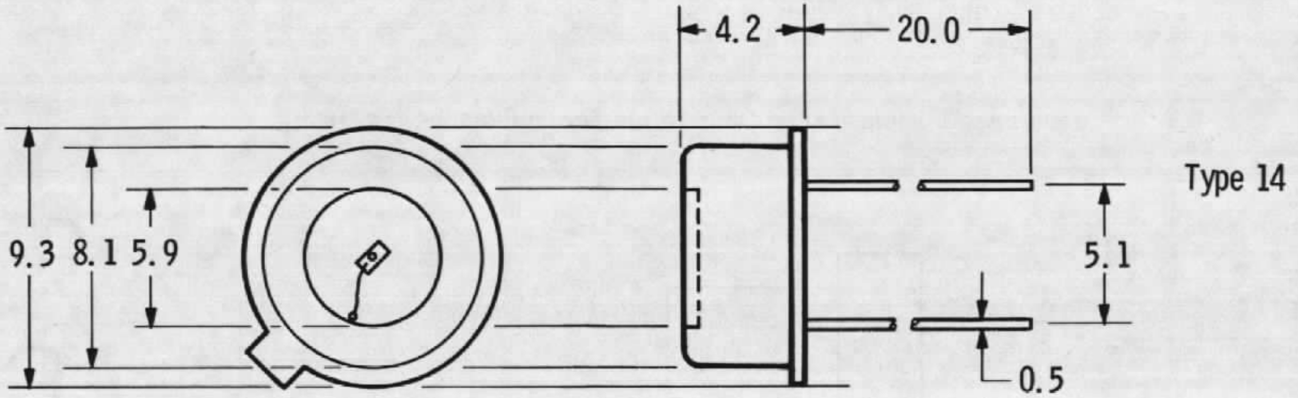

Dimensions in Millimeters

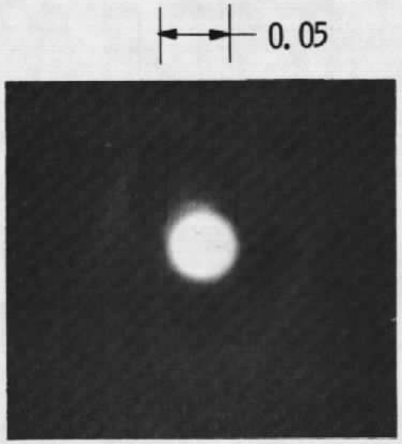

IR Microphotograph

Figure 30. Schematic diagram and IR microphotograph of MED 104 LED.

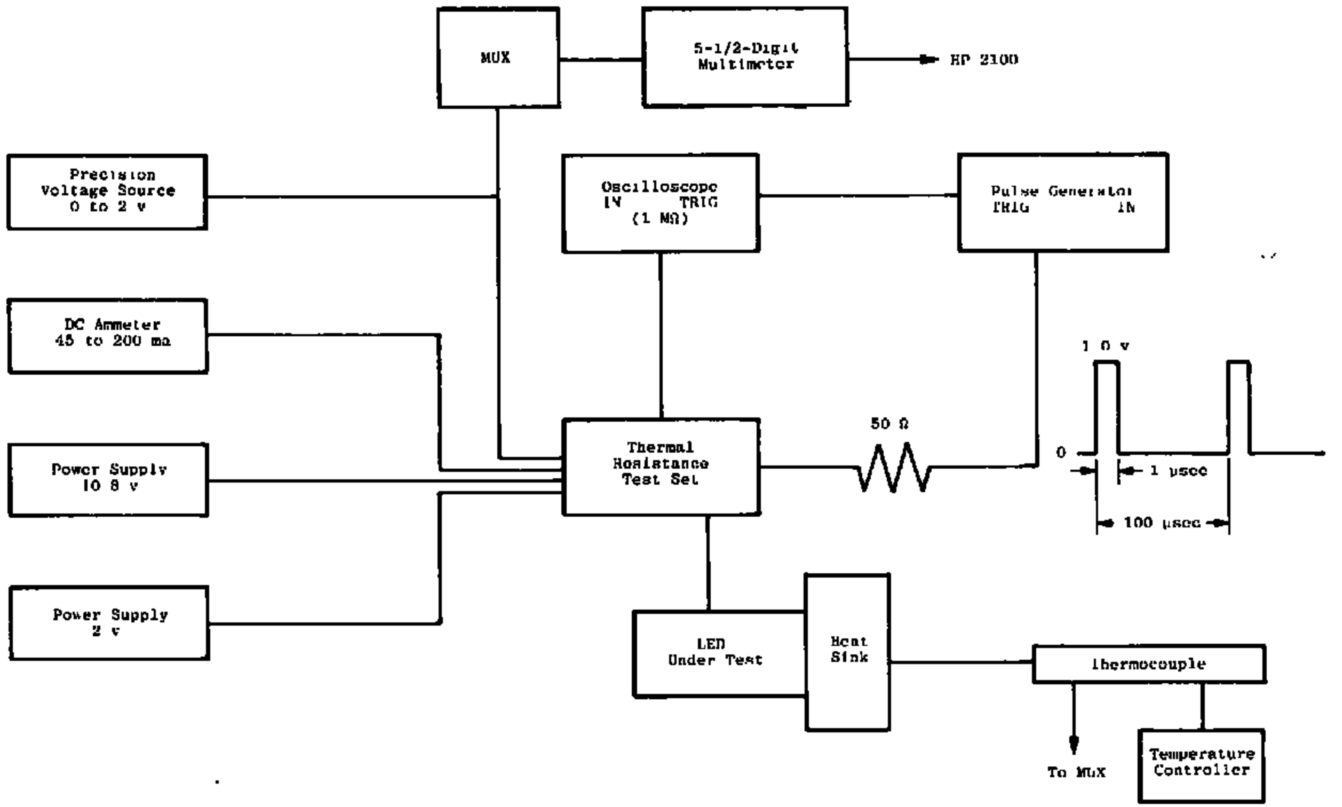

Figure 31. Schematic diagram of thermal resistance measurement.

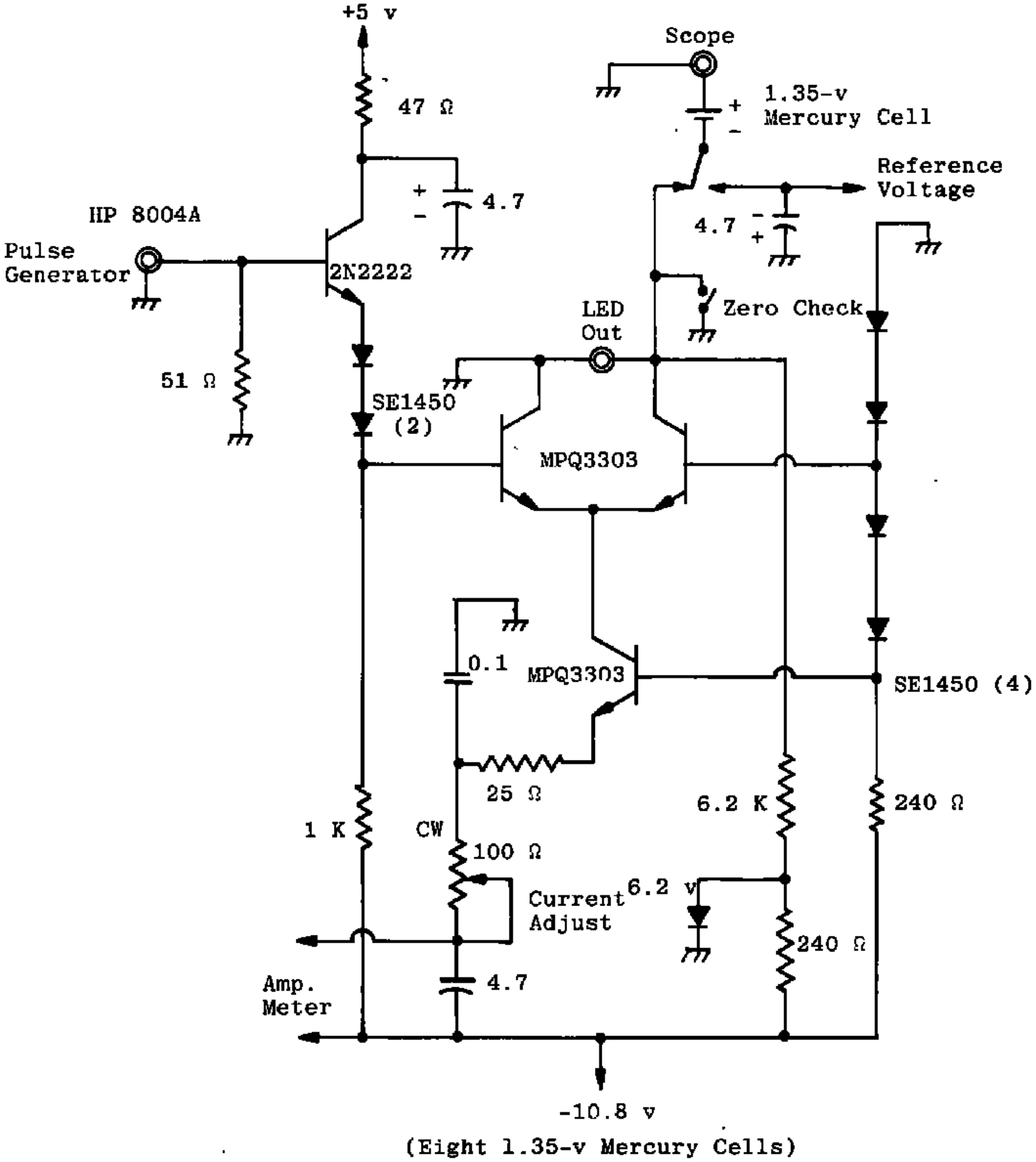

Figure 32. Thermal resistance test set.

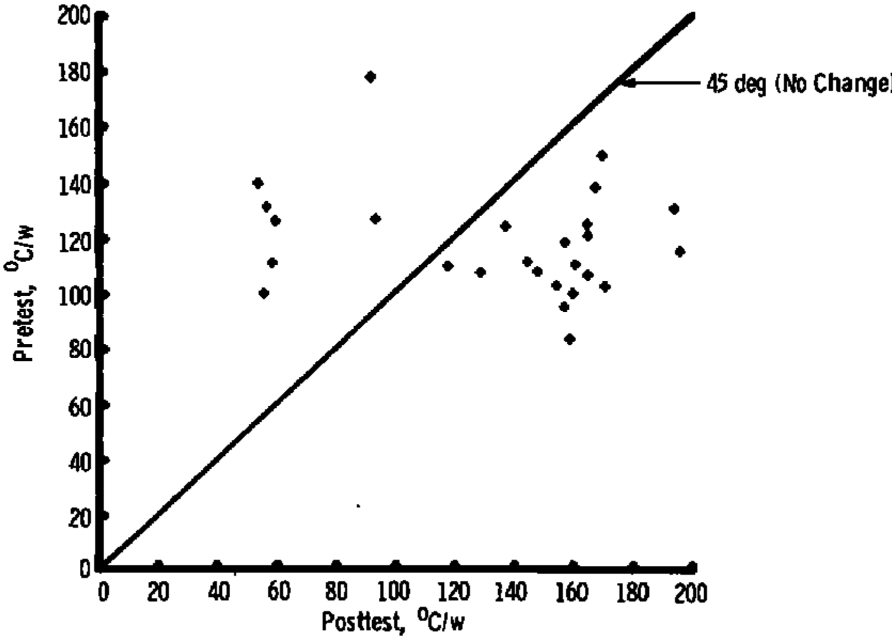

a. RCA C30119

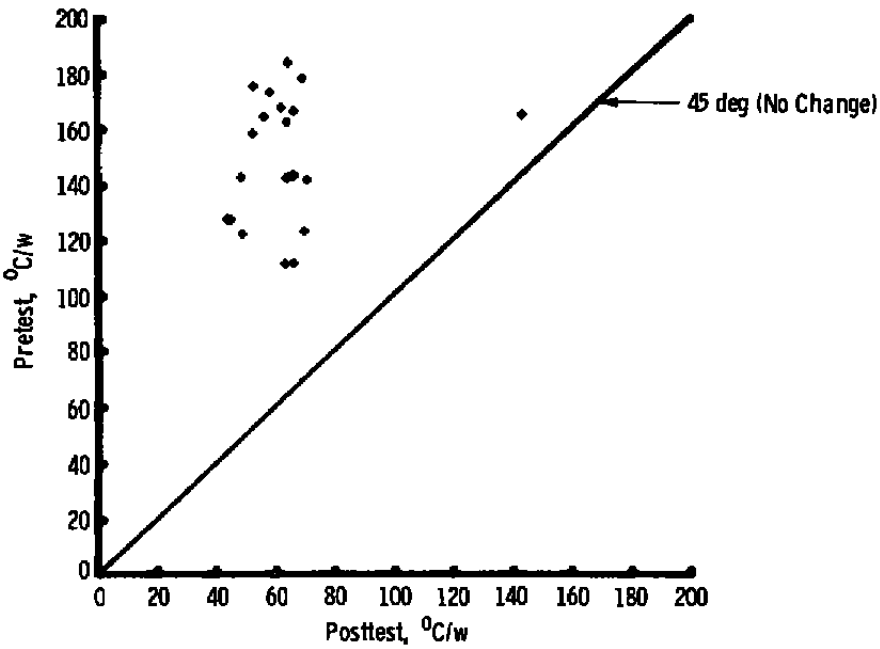

b. RCA C30123

Figure 33. Pretest vs posttest thermal resistance.

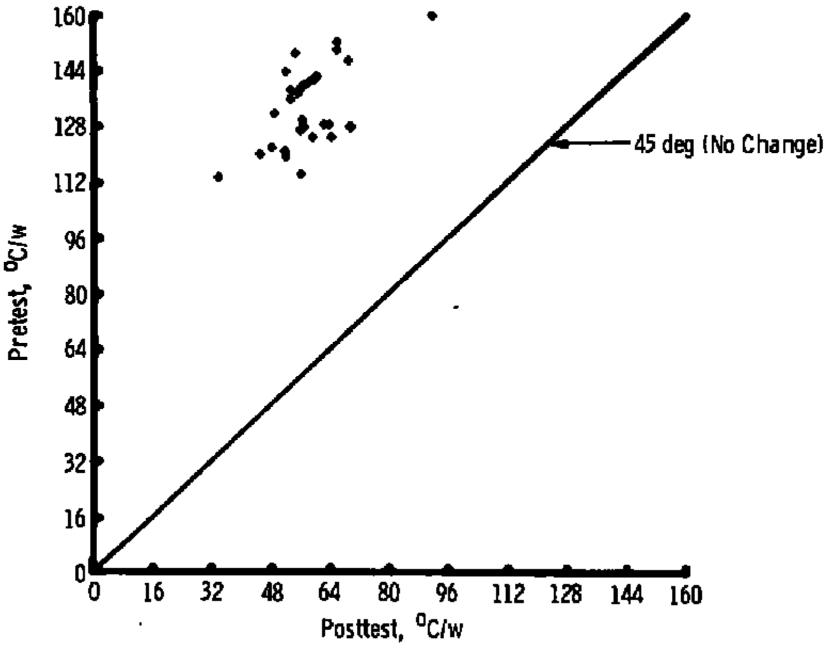

c. MEK 104

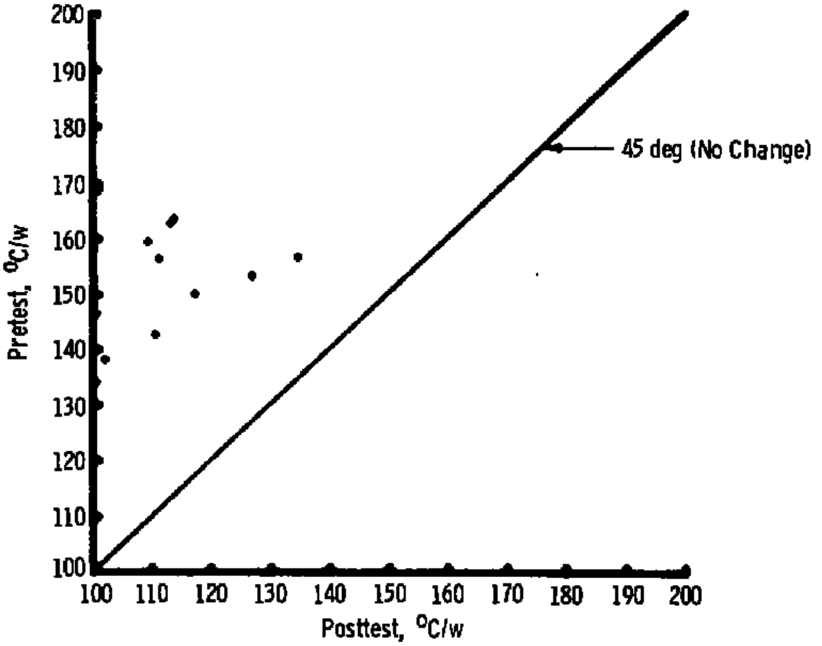

d. SPX 2231

Figure 33. Continued.

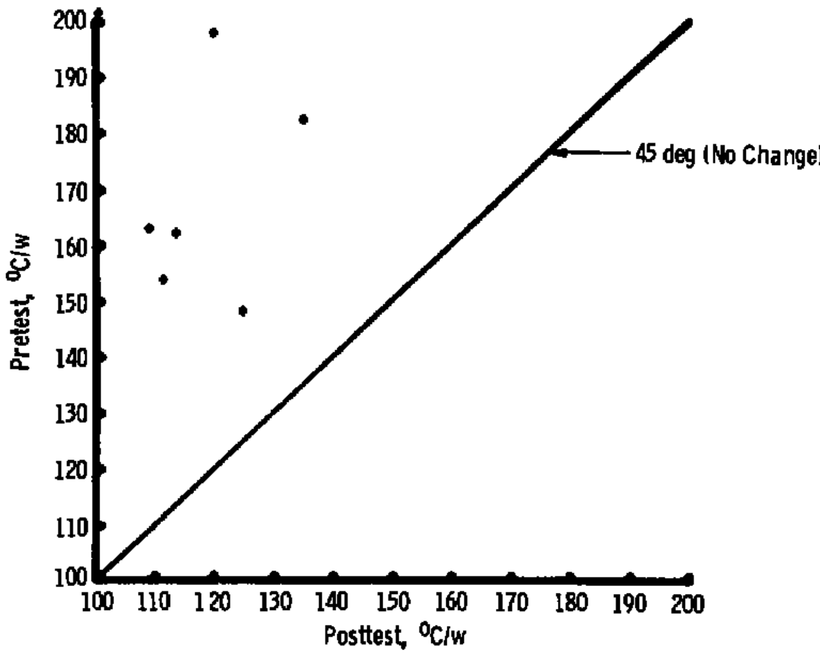

e. SPX 2231F

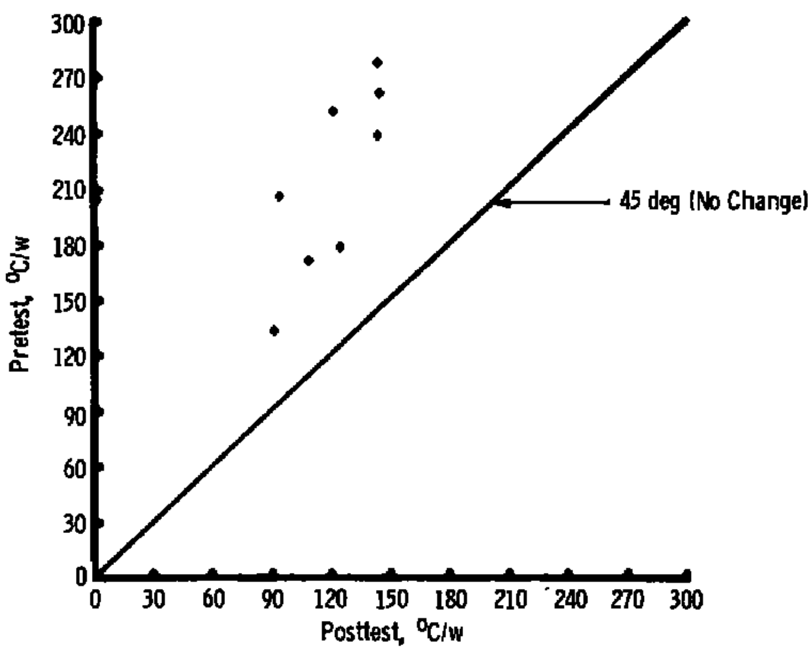

f. SPX 2234

Figure 33. Continued.

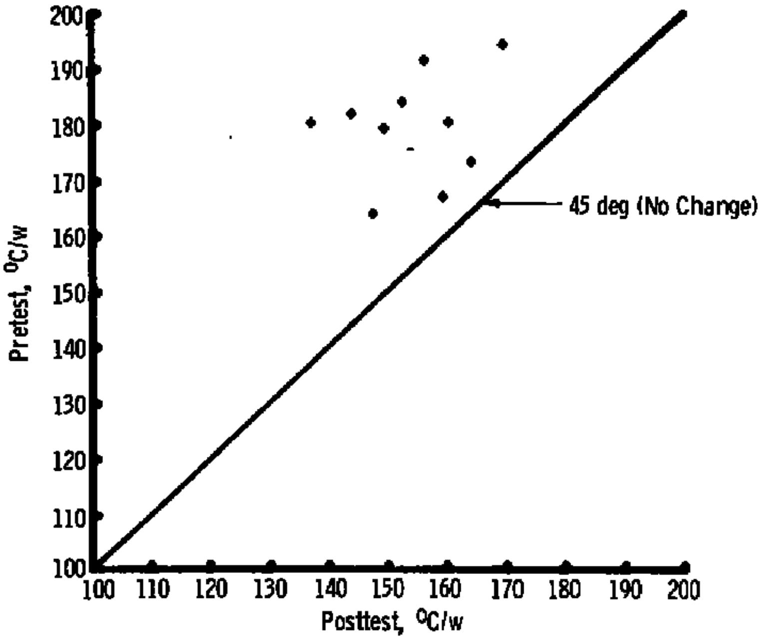

g. SPX 2354

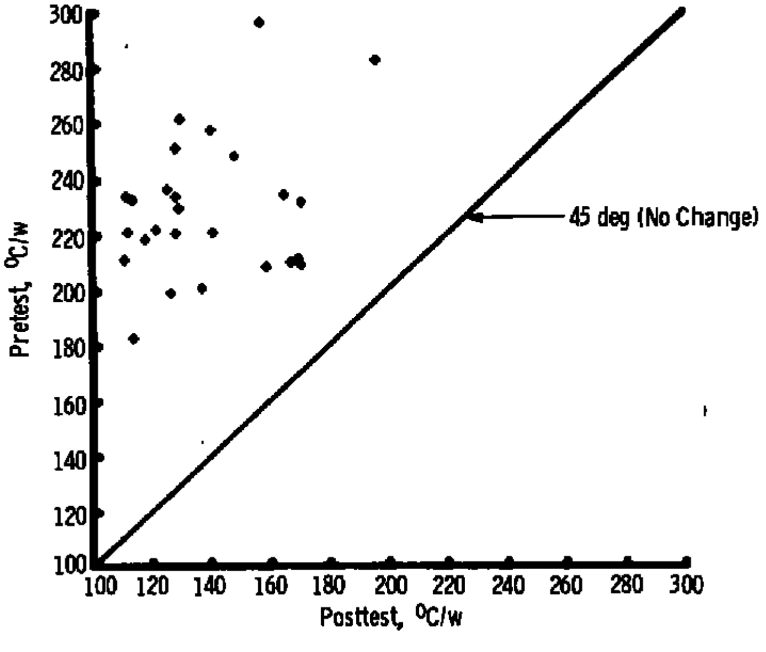

h. SPX 2354F

Figure 33. Continued.

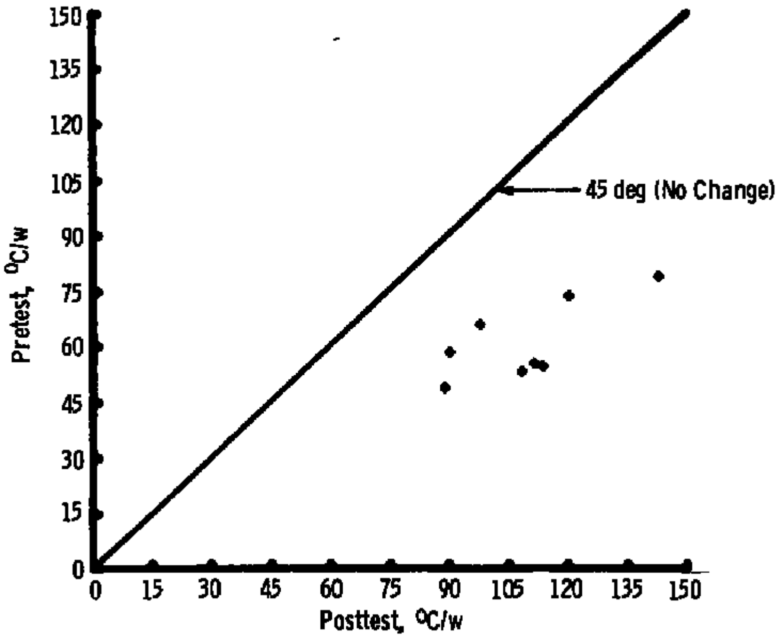

i. TIES 35

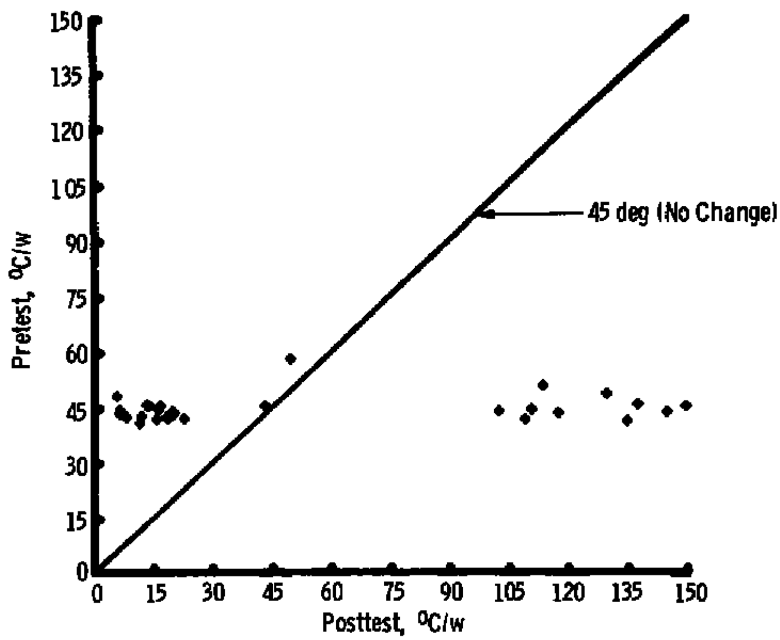

j. TI special

Figure 33. Concluded.

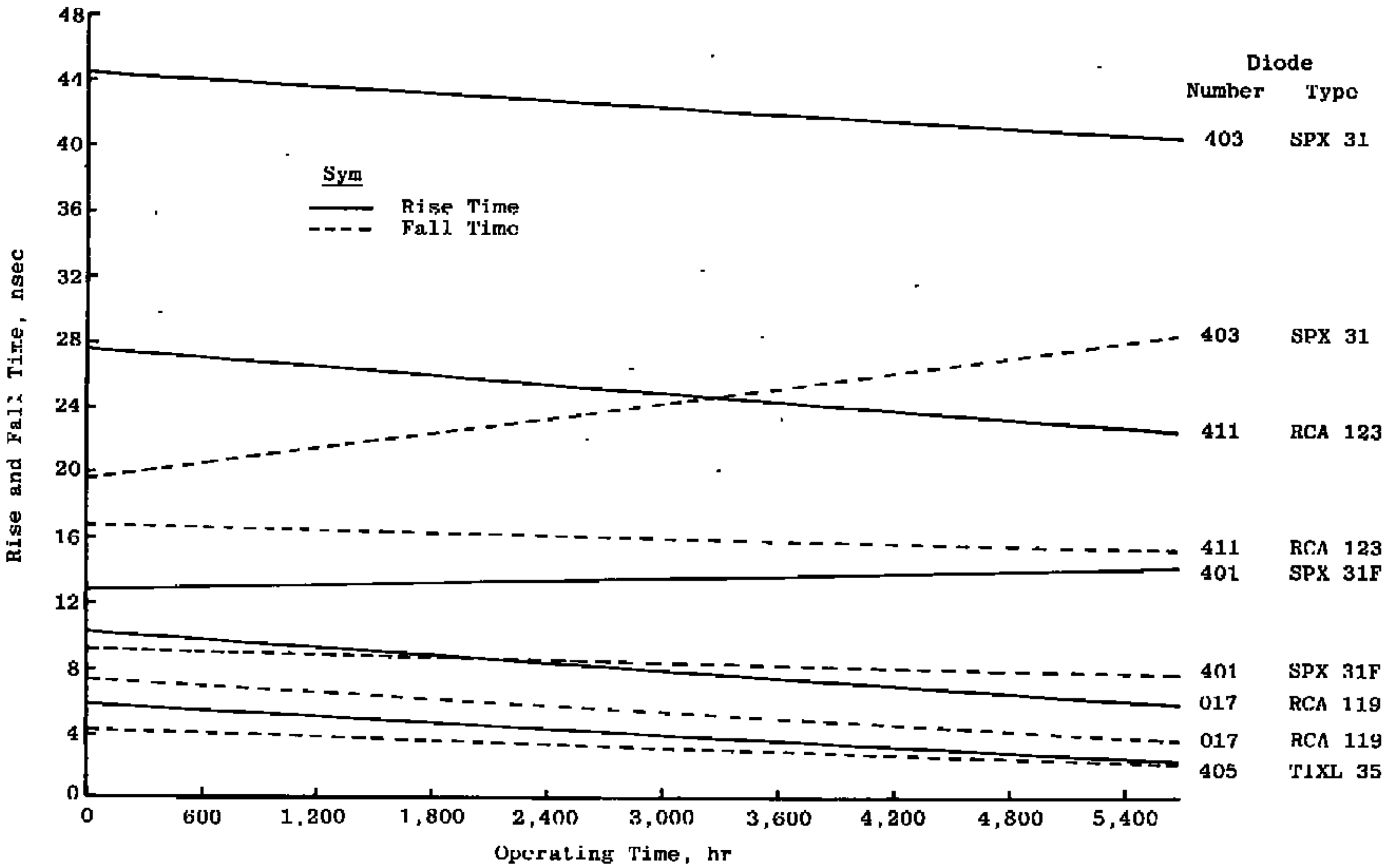

Figure 34. Rise and fall time vs operating time.

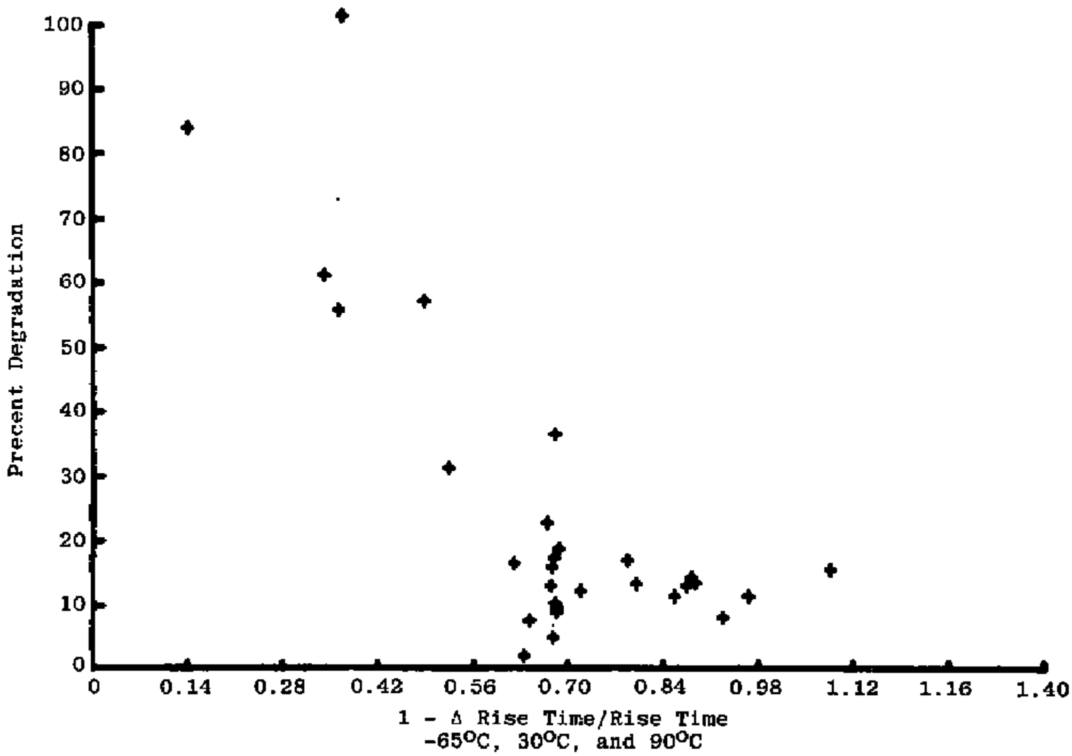

a. Percent degradation vs 1 – Δ rise time/rise time

Statistical Analysis for Data

Mean of 1 - Δ Rise Time/Rise Time Array = 0.679

Mean of Percent Degradation Array = 22.393

Standard Deviation of 1 - Δ Rise Time/Rise Time = 0.199

Standard Deviation of Percent Degradation = 23.657

Correlation Coefficient = -0.768

Slope = -91.346

Intercept = 84.417

b. Summary of analysis

Figure 35. Percent degradation vs change in rise time – RCA C30123.

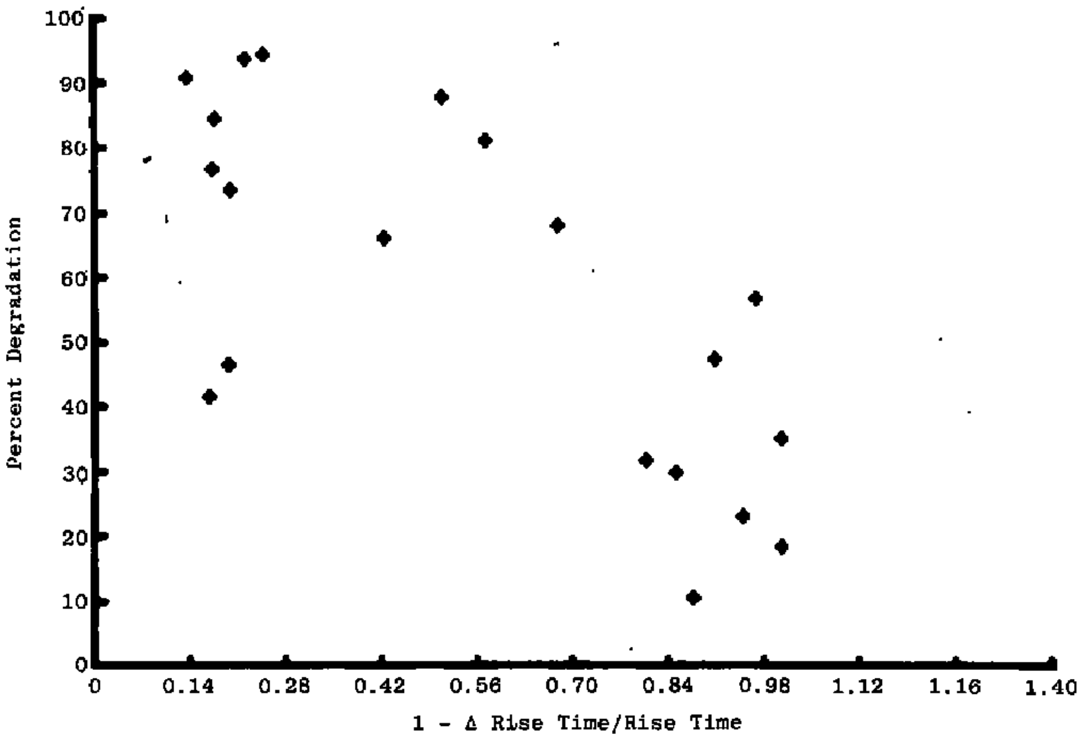

a. Percent degradation vs 1 – Δ rise time/rise time

Statistical Analysis for Data

Mean of 1 - Δ Rise Time/Rise Time Array = 0.547

Mean of Percent Degradation Array = 56.39

Standard Deviation of 1 - Δ Rise Time/Rise Time = 0.333

Standard Deviation of Percent Degradation = 26.548

Correlation Coefficient = -0.712

Slope = -56.719

Intercept = 87.455

b. Summary of analysis

Figure 36. Percent degradation vs change in rise time – SPX 2231F.

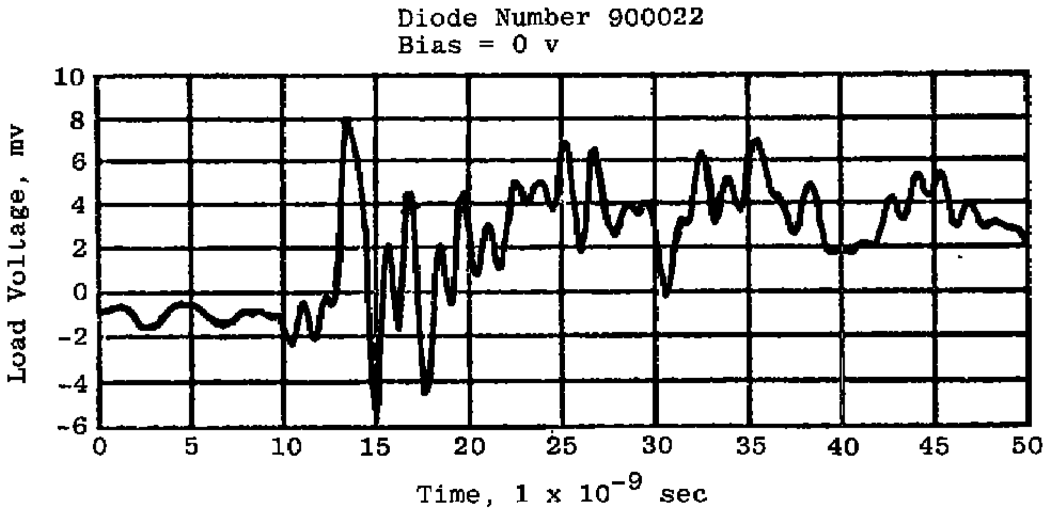

a. Rise time = 5.07119 x 10^{-9} sec

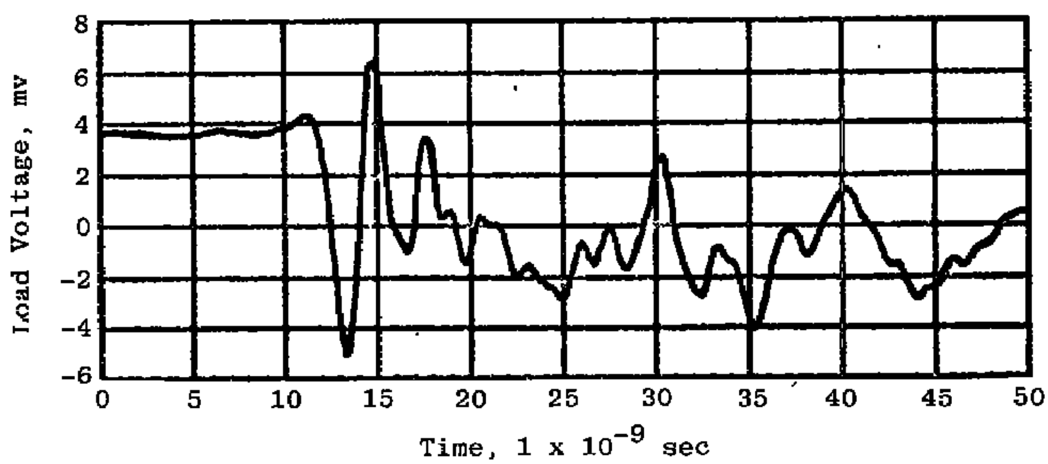

b. Fall time = 5.20822 x 10^{-8} sec

Figure 37. Pretest rise and fall time – RCA C30119.

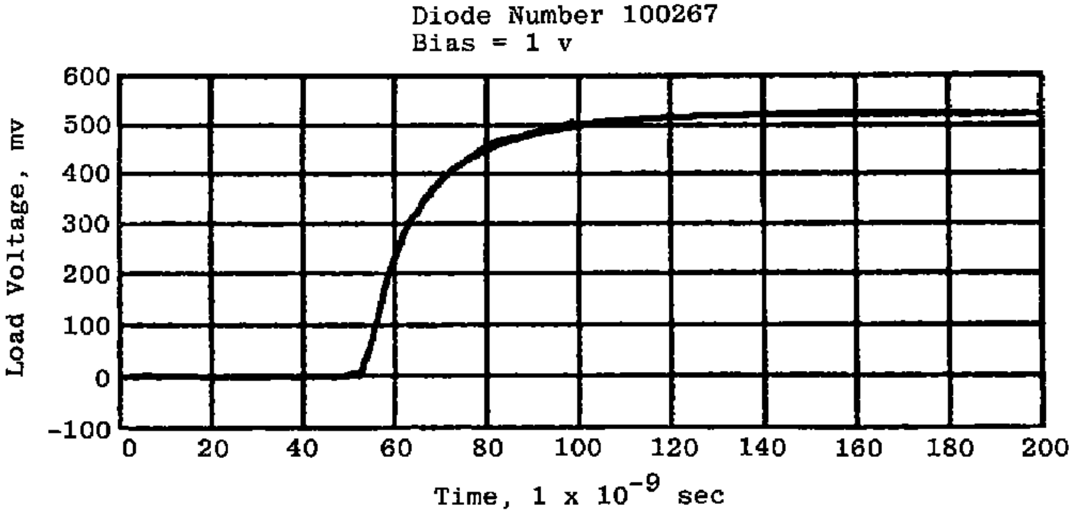

a. Rise time = 3.09331×10^{-8} sec

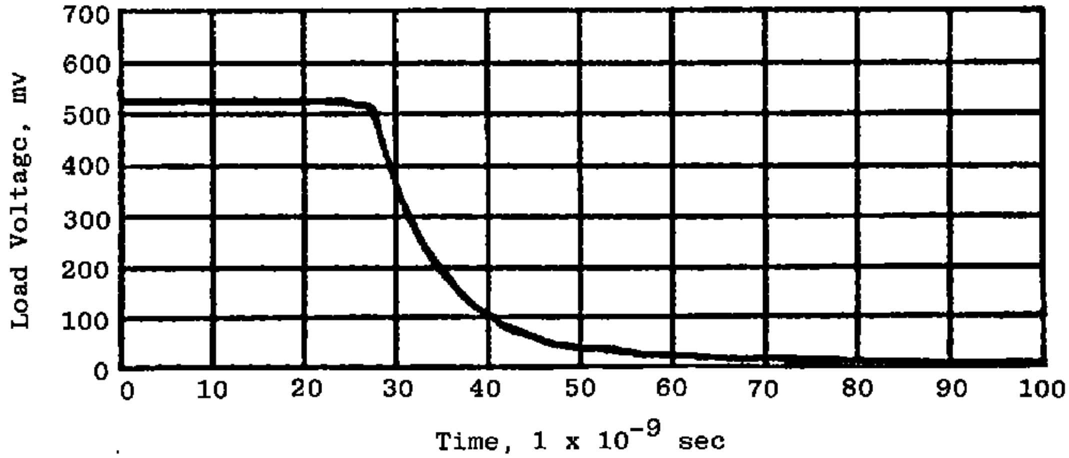

b. Fall time = 1.72741×10^{-8} sec

Figure 38. Pretest rise and fall time – SPX 2231.

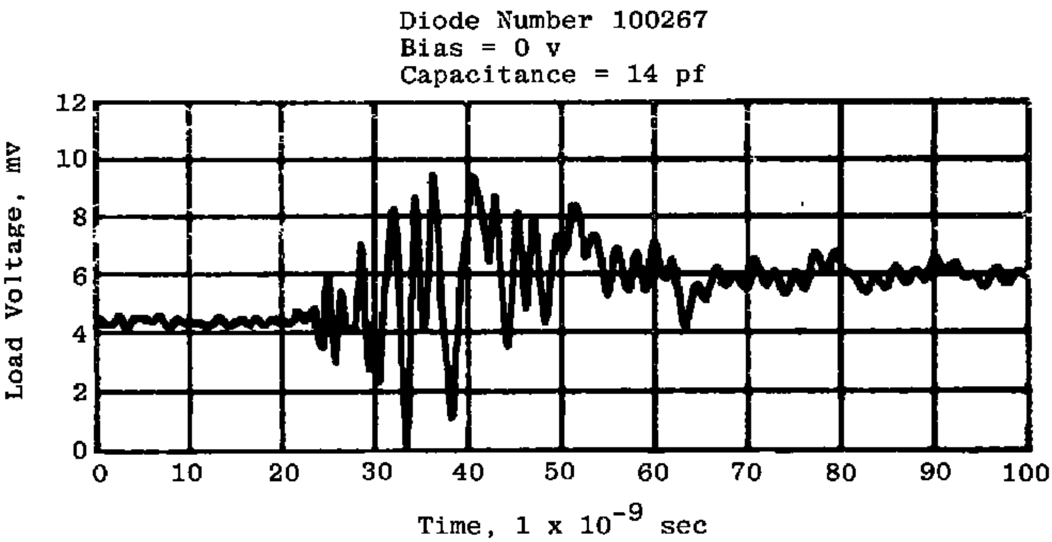

a. Rise time = 0.87078 x 10^{-8} sec

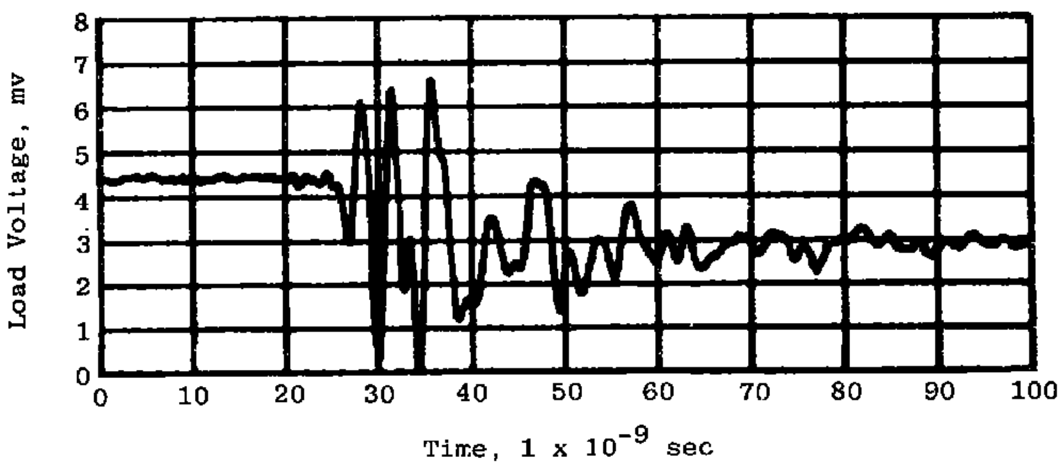

b. Fall time = 0.08380 x 10^{-8} sec

Figure 39. Posttest rise and fall time – SPX 2231.

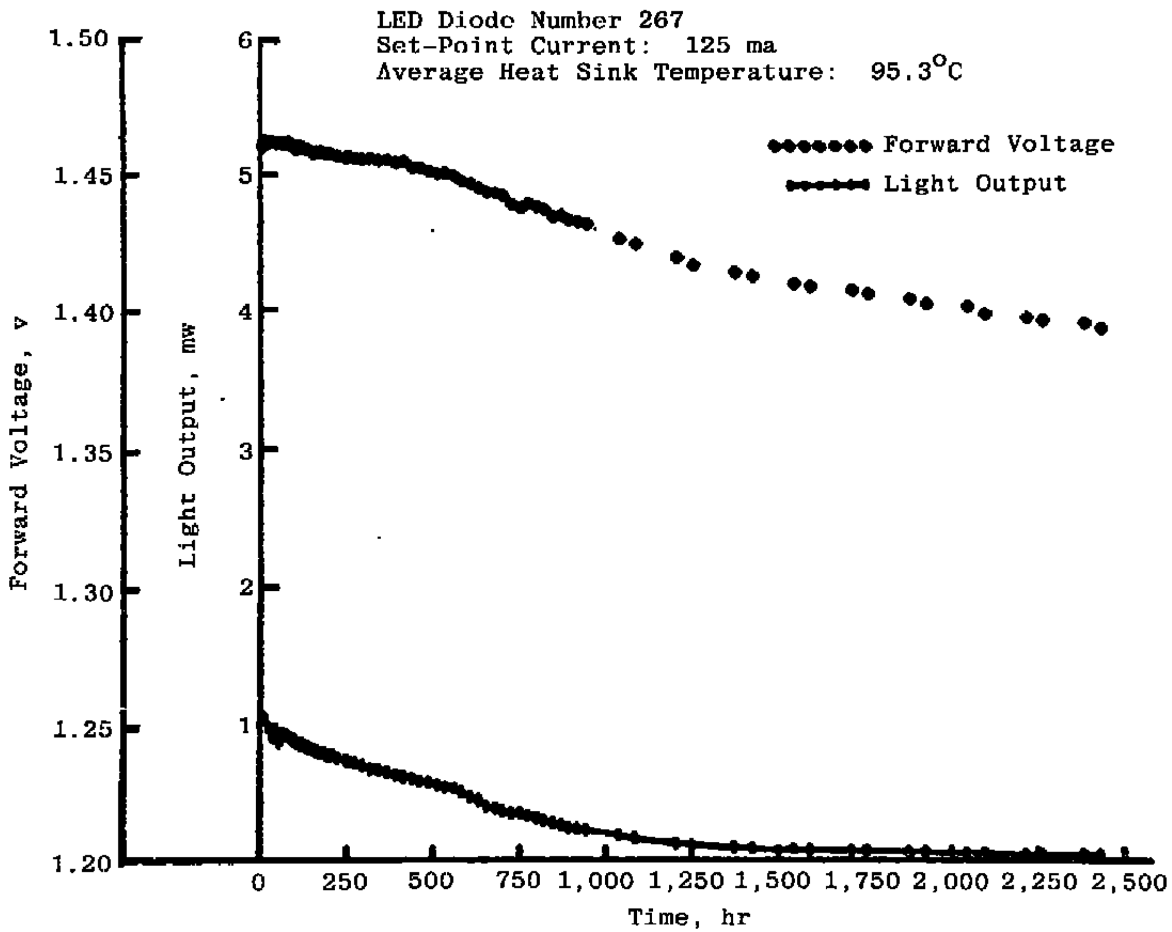

a. Light output power vs time – SPX 2231
Figure 40. Pottest rise and falls time and light output power vs time – SPX 2231.

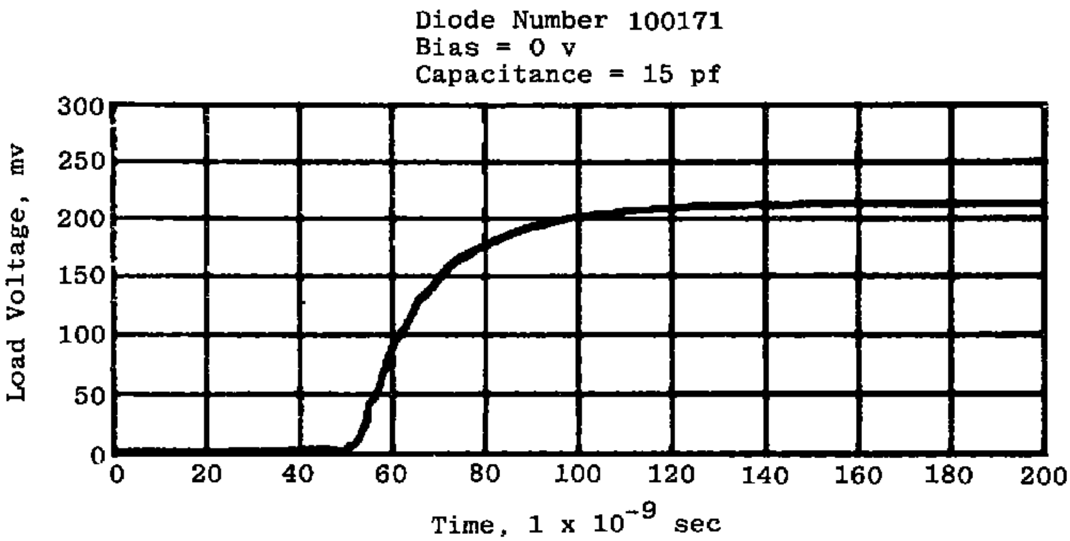

b. Rise time = 3.58652 x 10^{-8} sec

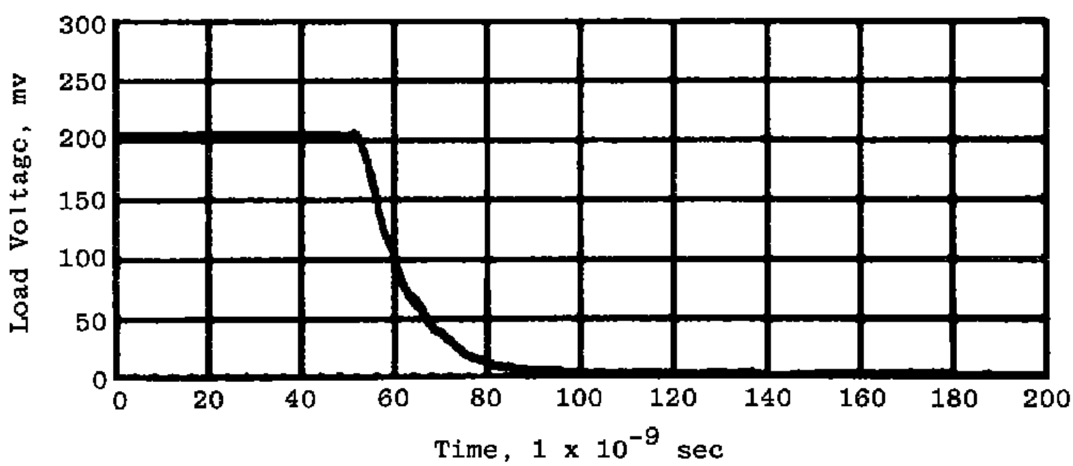

c. Fall time = 2.04850 x 10^{-8} sec

Figure 40. Concluded.

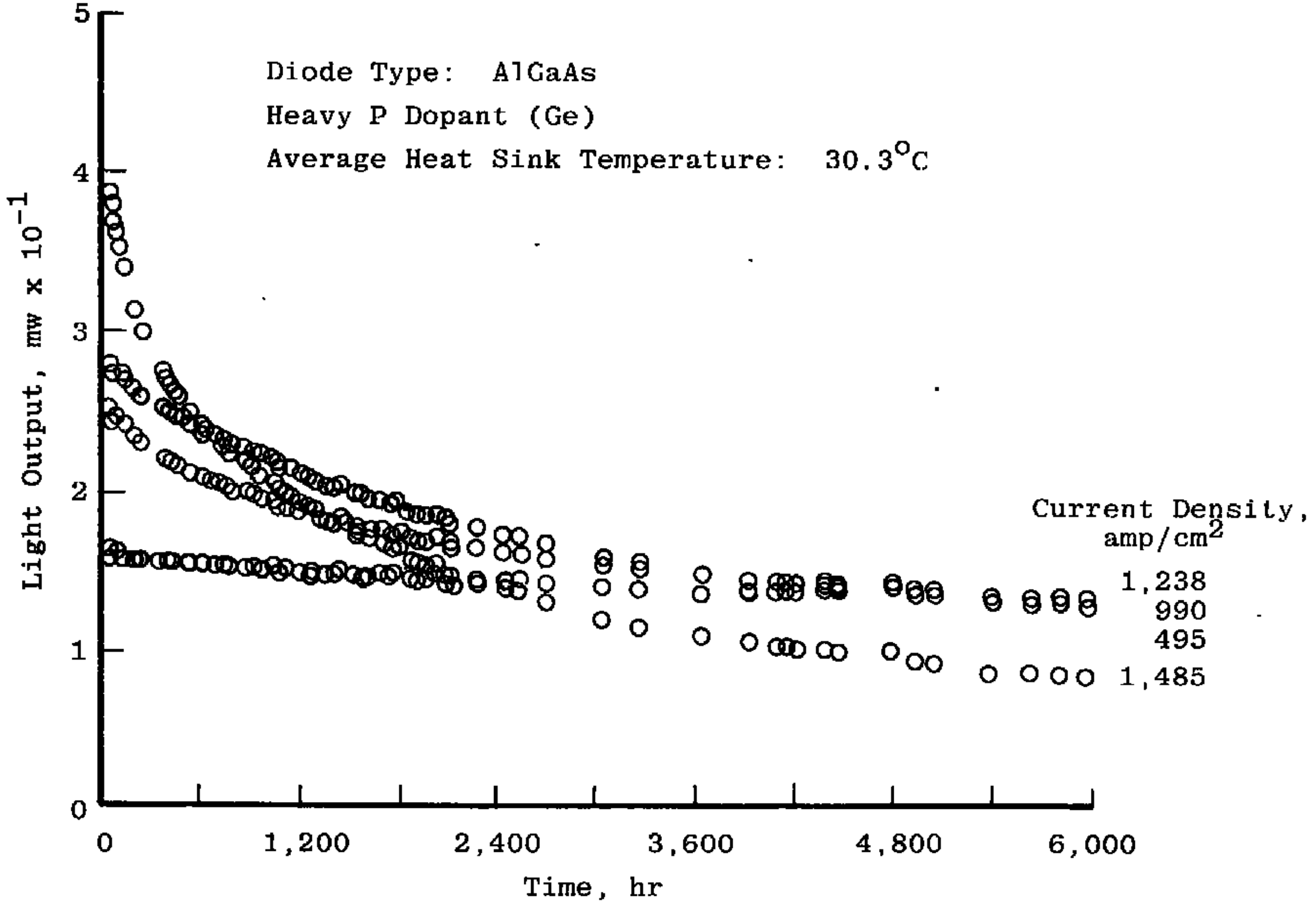

Figure 41. Light output vs time (30°C environment) – RCA C30119.

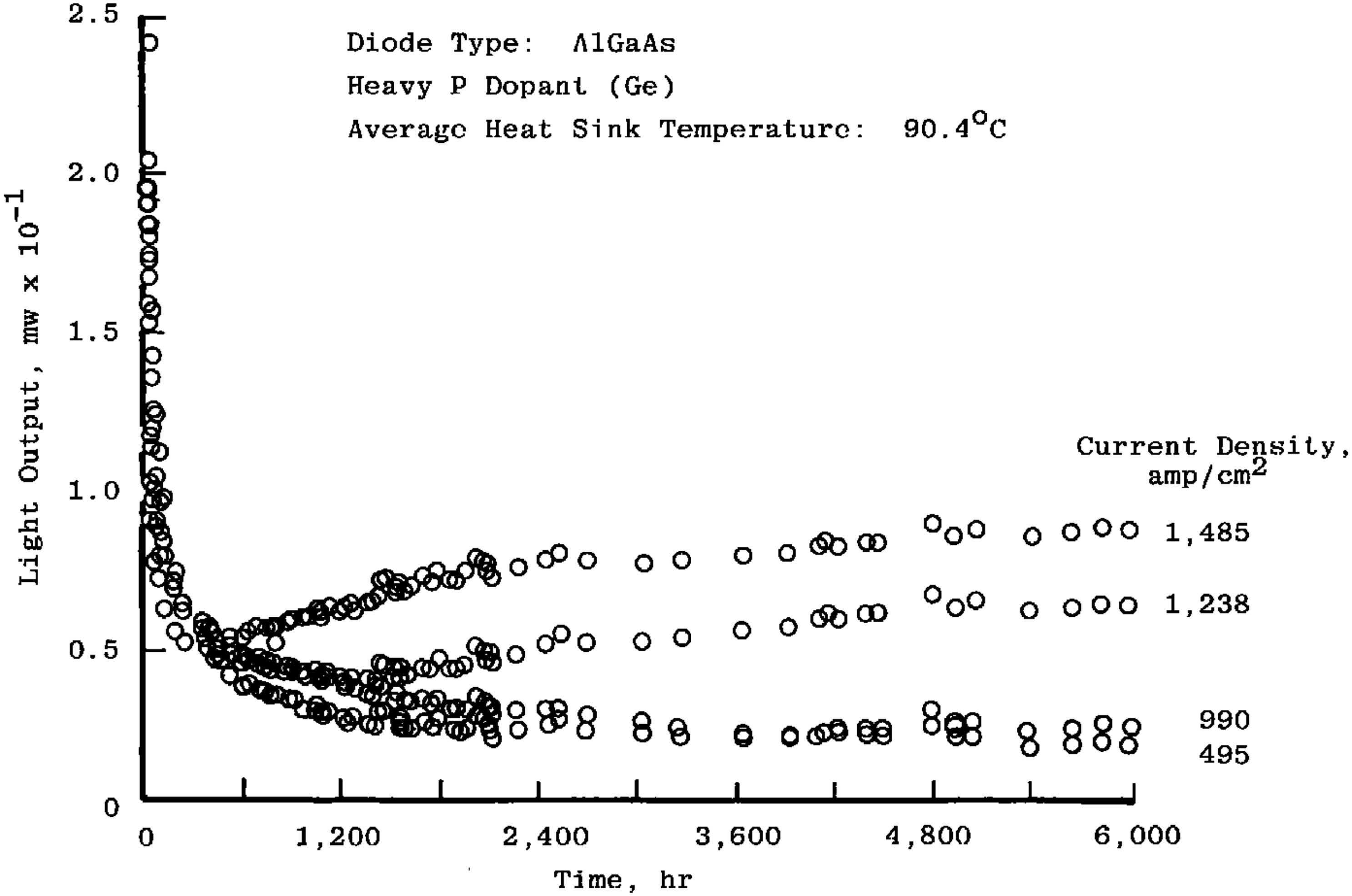

Figure 42. Light output vs time (90°C environment) – RCA C30119.

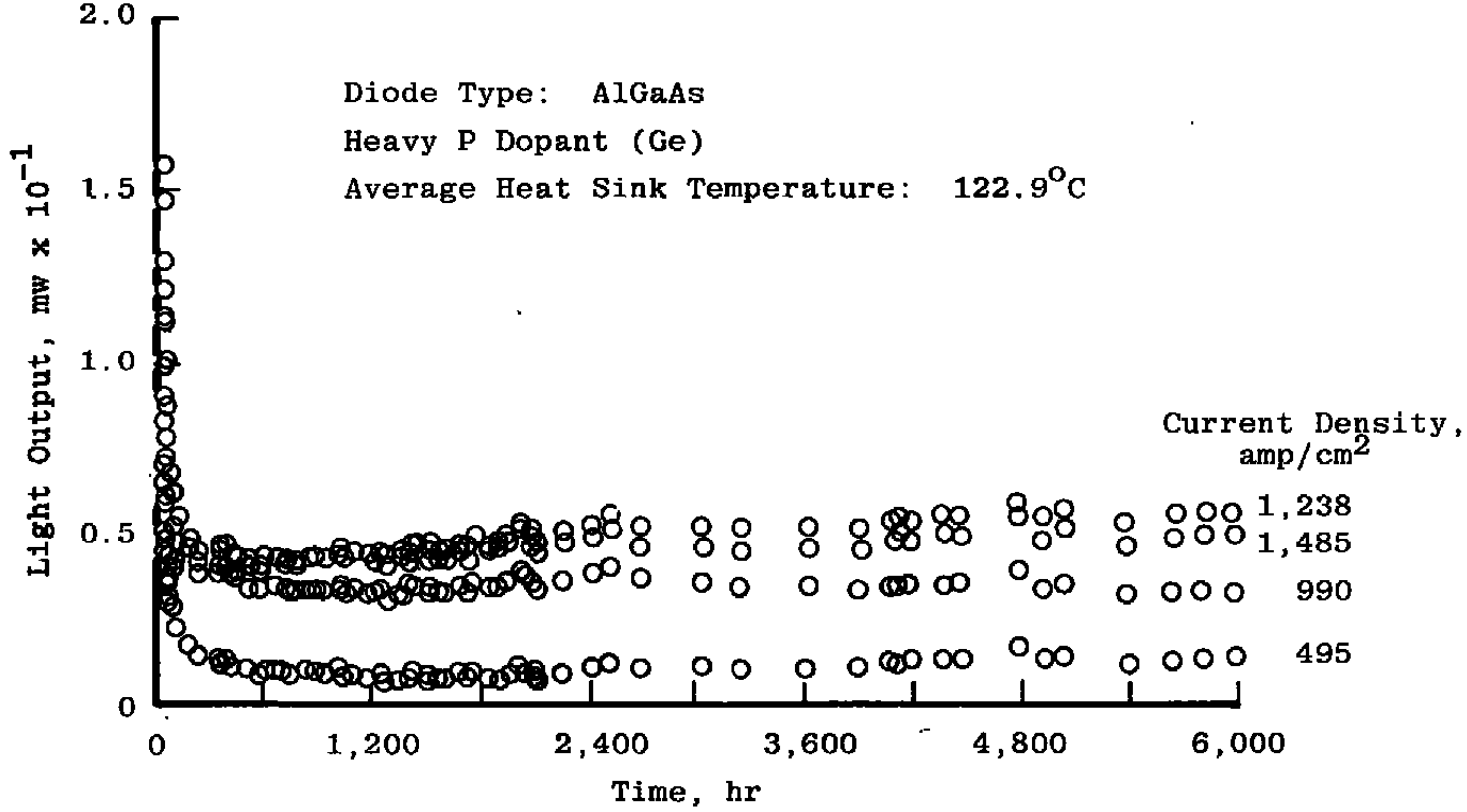

Figure 43. Light output vs time (120°C environment) – RCA C30119.

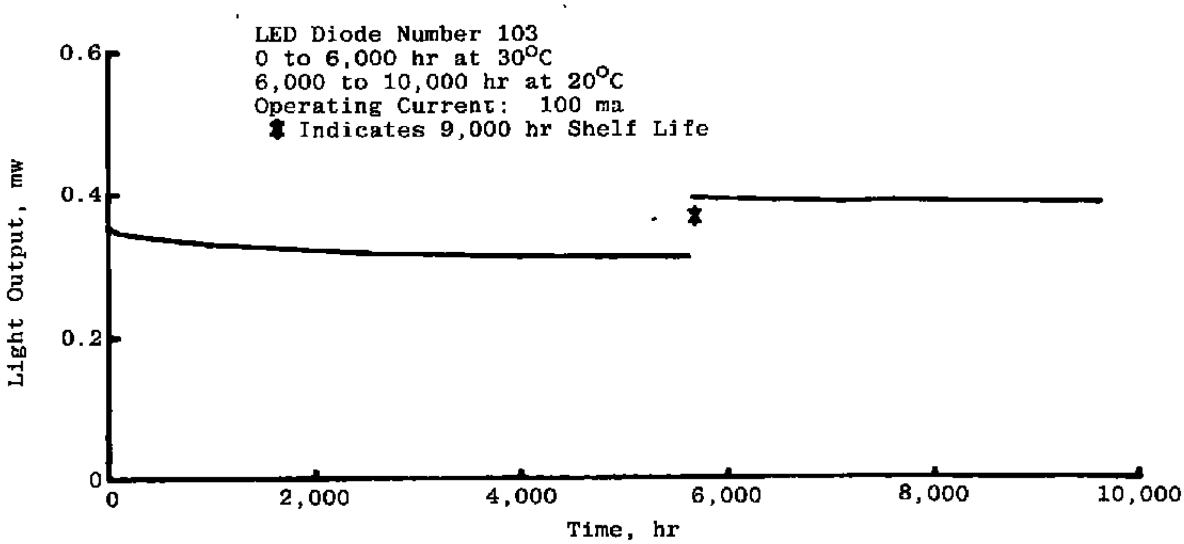

a. 20°C RCA C30123

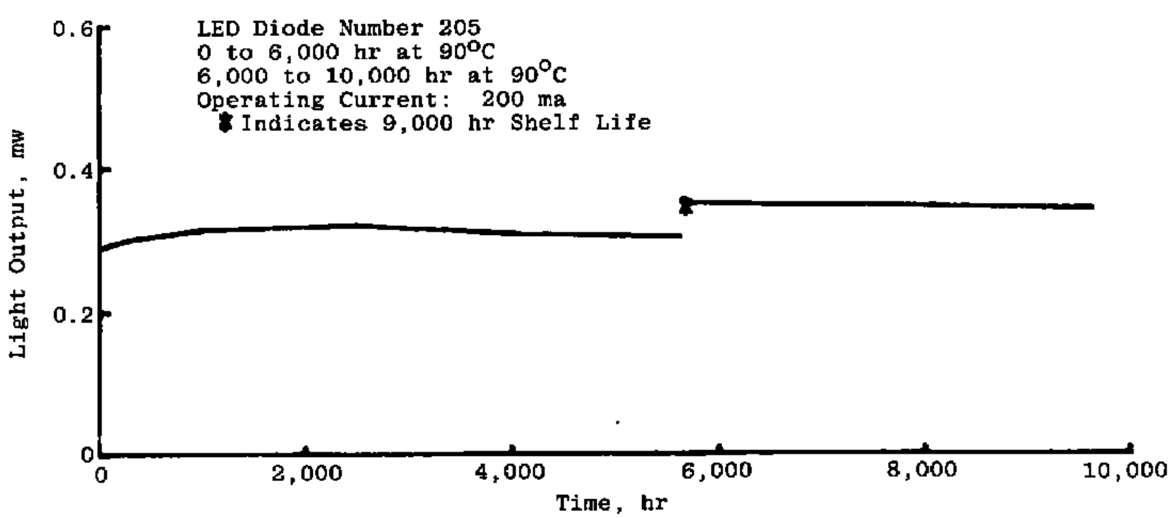

b. 90°C RCA C30123

Figure 44. Light output power vs time (11,000 hr of operation).

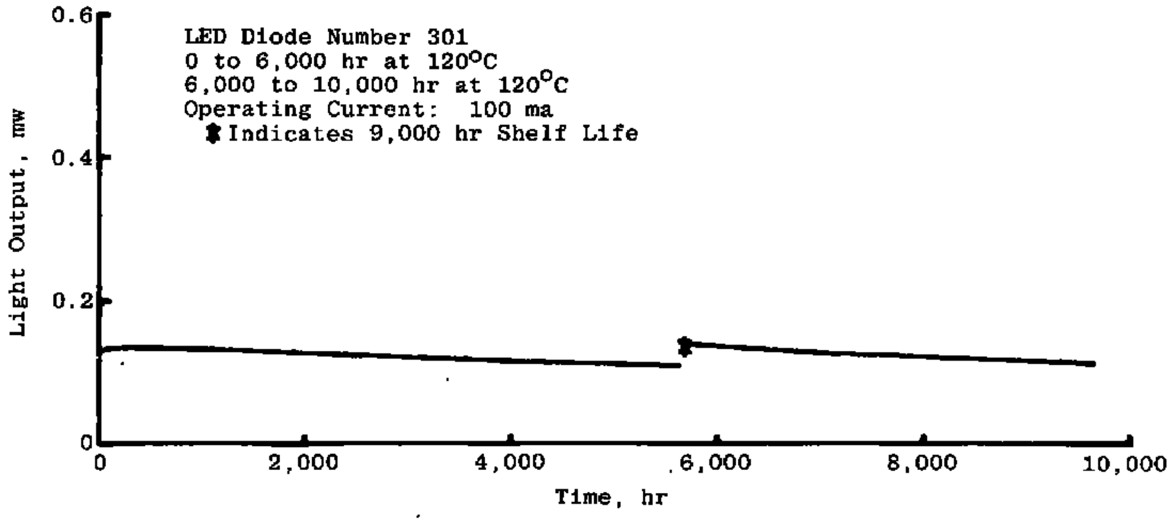

c. 120°C RCA C30123

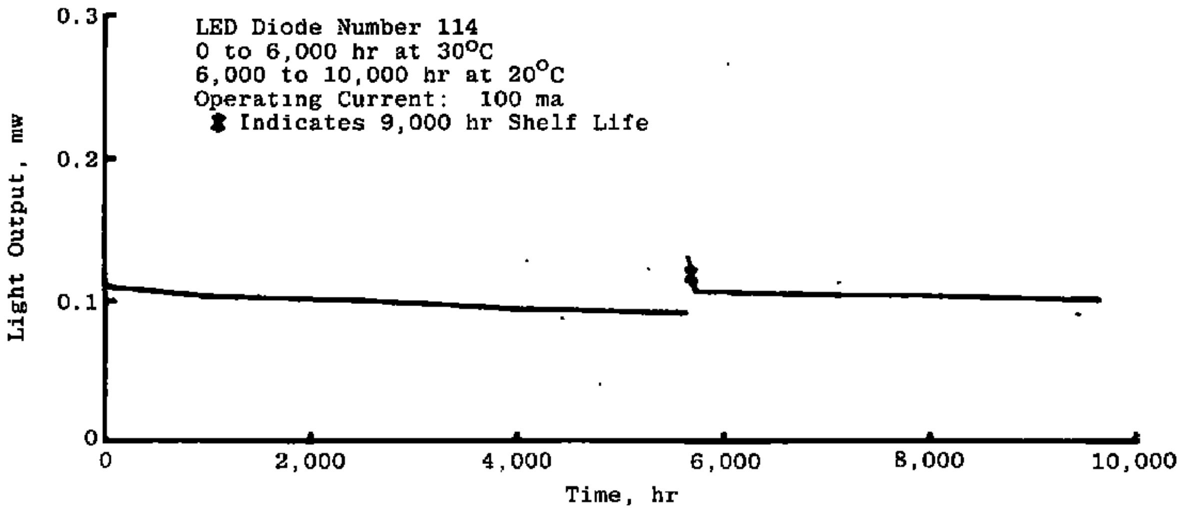

d. 20°C RCA C30119

Figure 44. Continued.

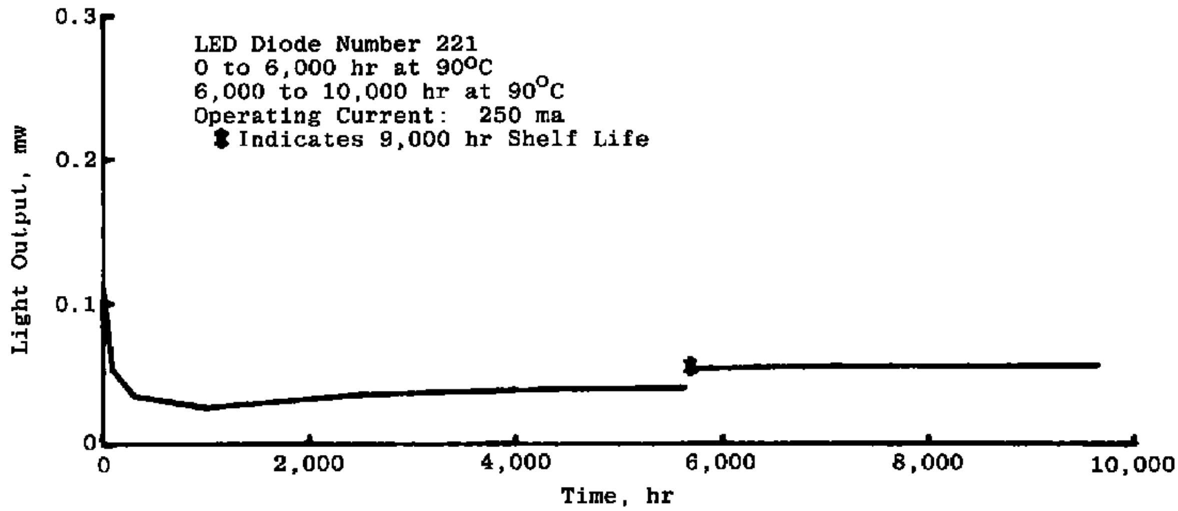

e. 90° C RCA C30119

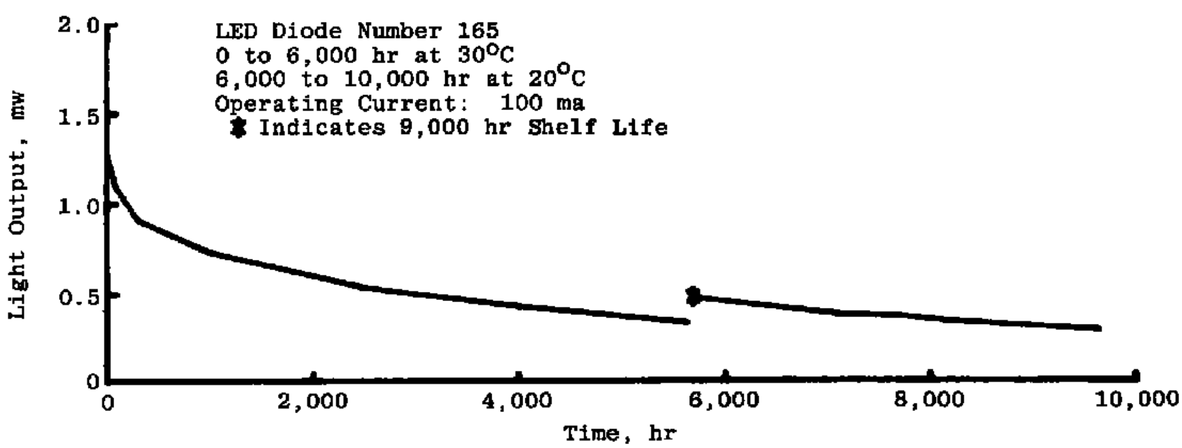

f. 20°C SPX 2231

Figure 44. Continued.

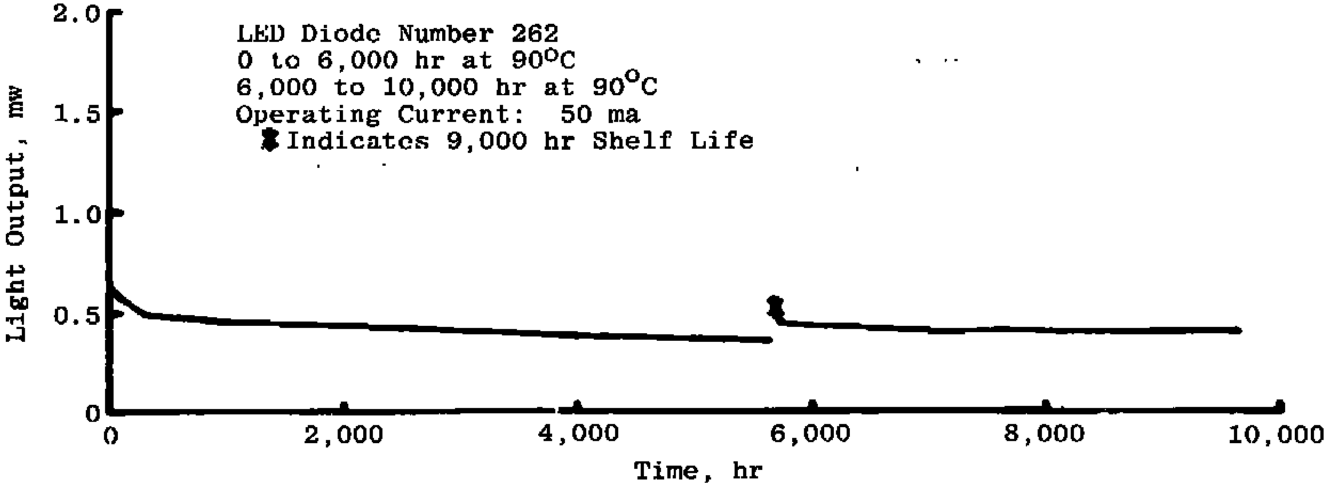

g. 90 °C SPX 2231
Figure 44. Concluded.

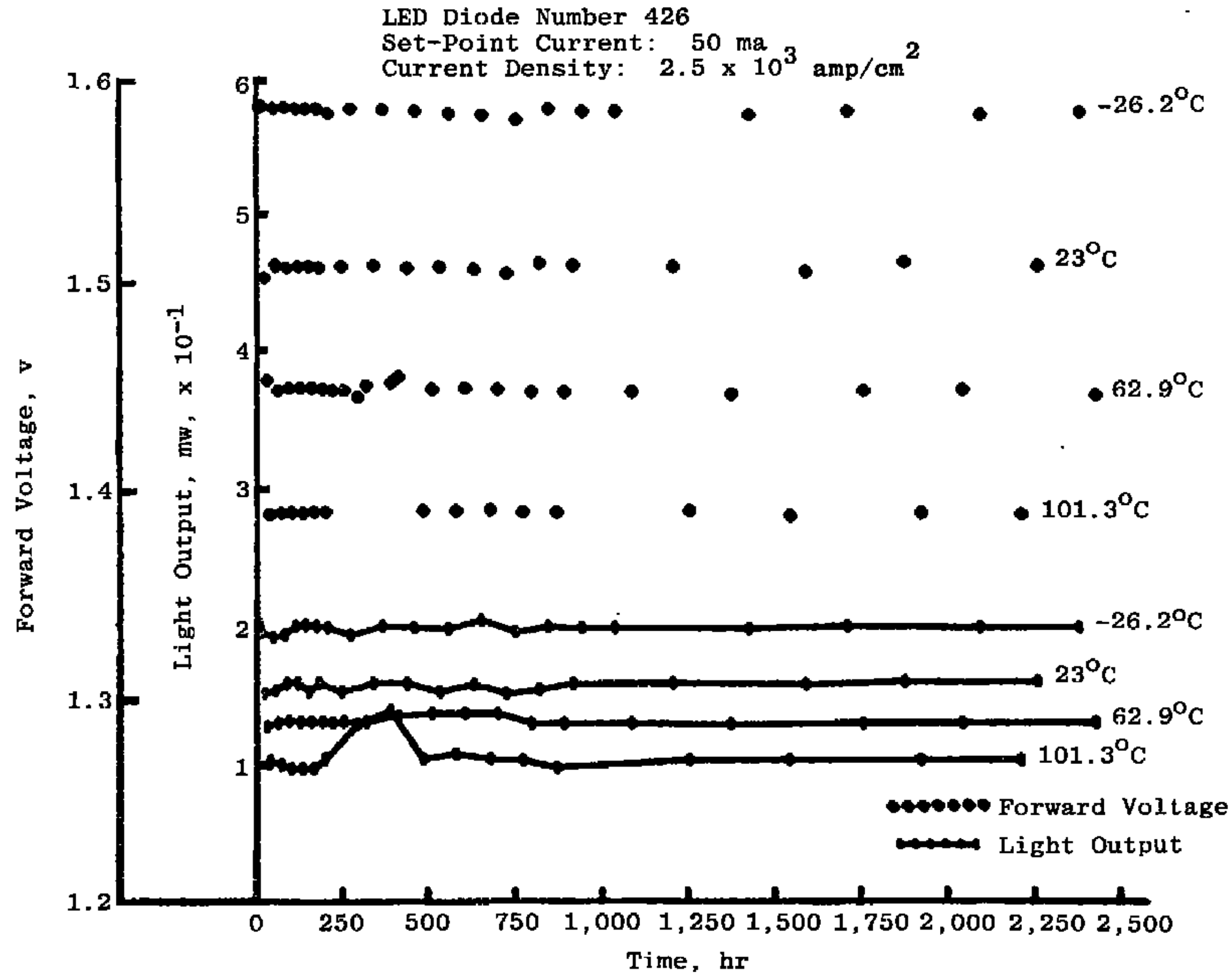

a. Light output vs time, MEK 104 (temperature cycling chamber)

Figure 45. Light output vs time (temperature cycling chamber) — MEK 104.

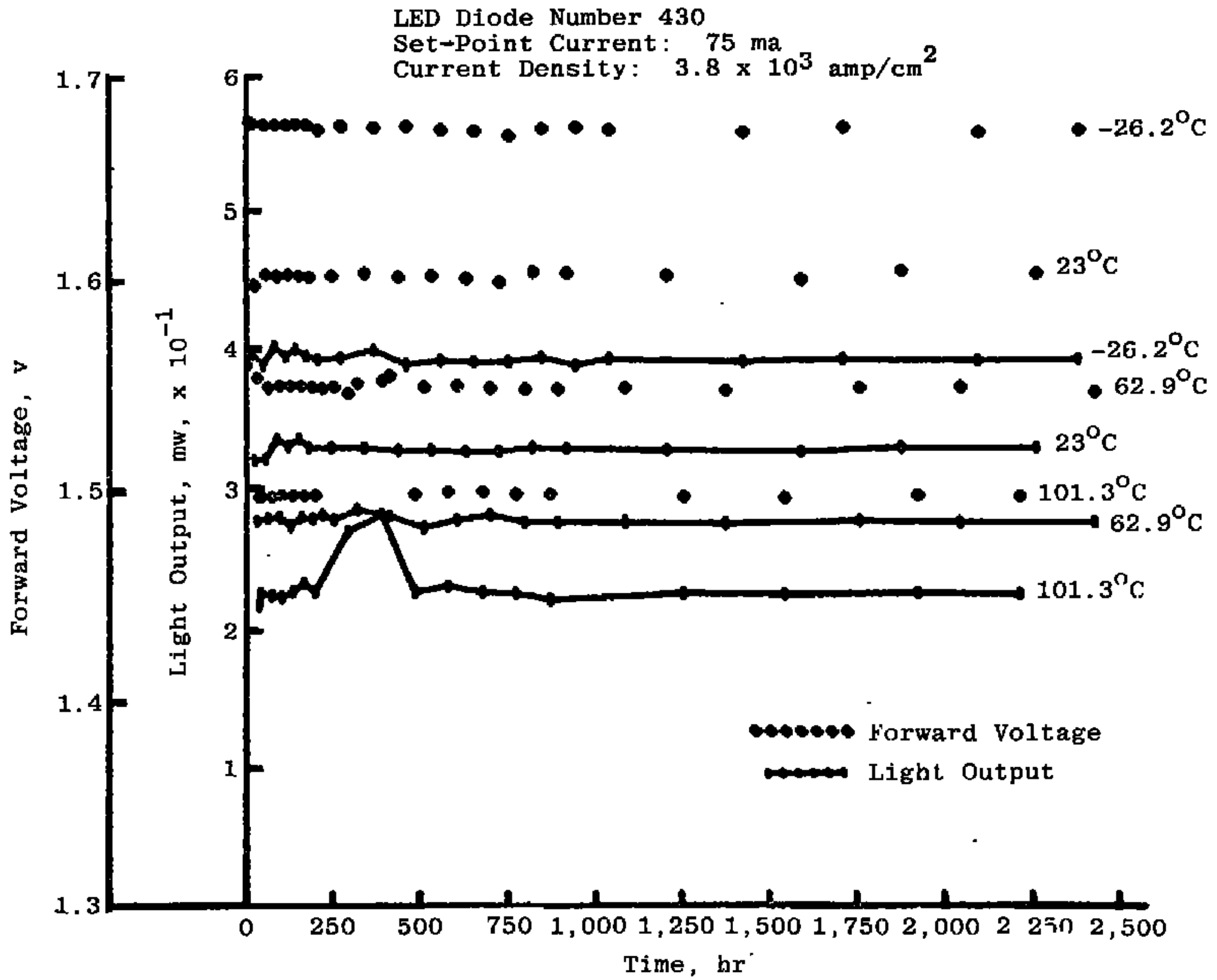

b. Light output vs time, MEK 104 (temperature cycling chamber)

Figure 45. Continued.

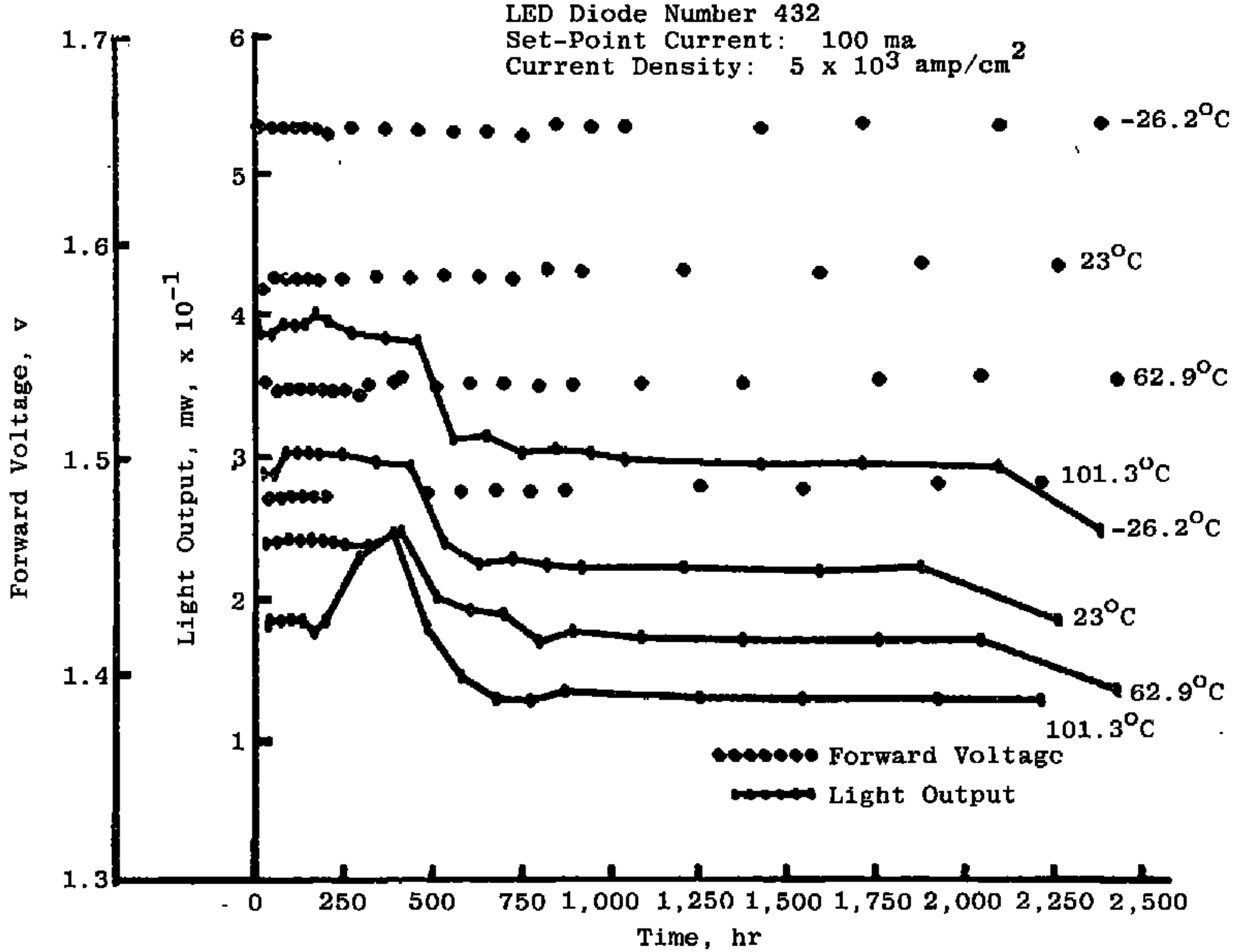

c. Light output vs time, MEK 104 (temperature cycling chamber)

Figure 45. Concluded.

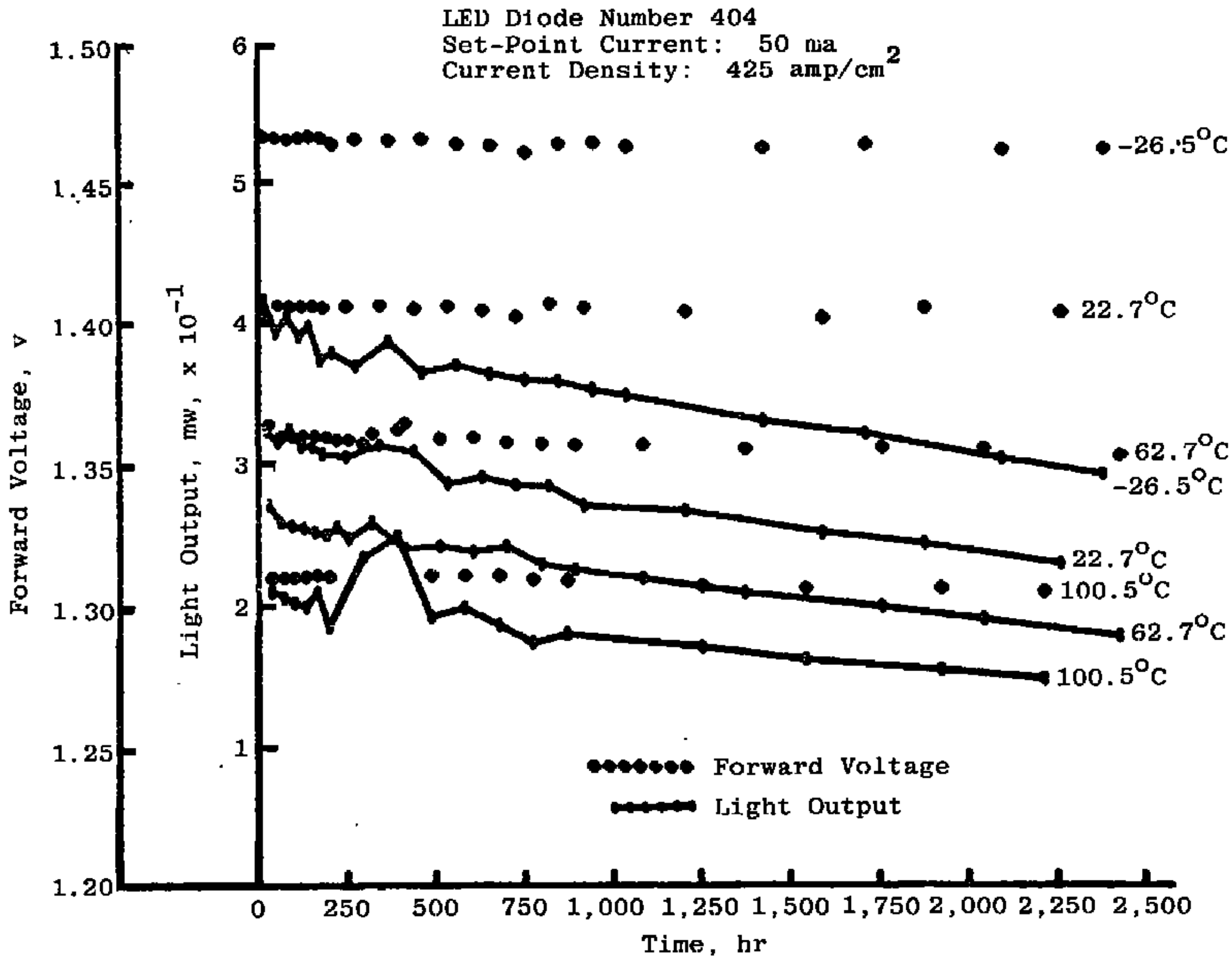

a. Light output vs time, TI Special

Figure 46. Light output vs time (temperature cycling chamber) — TI Special.

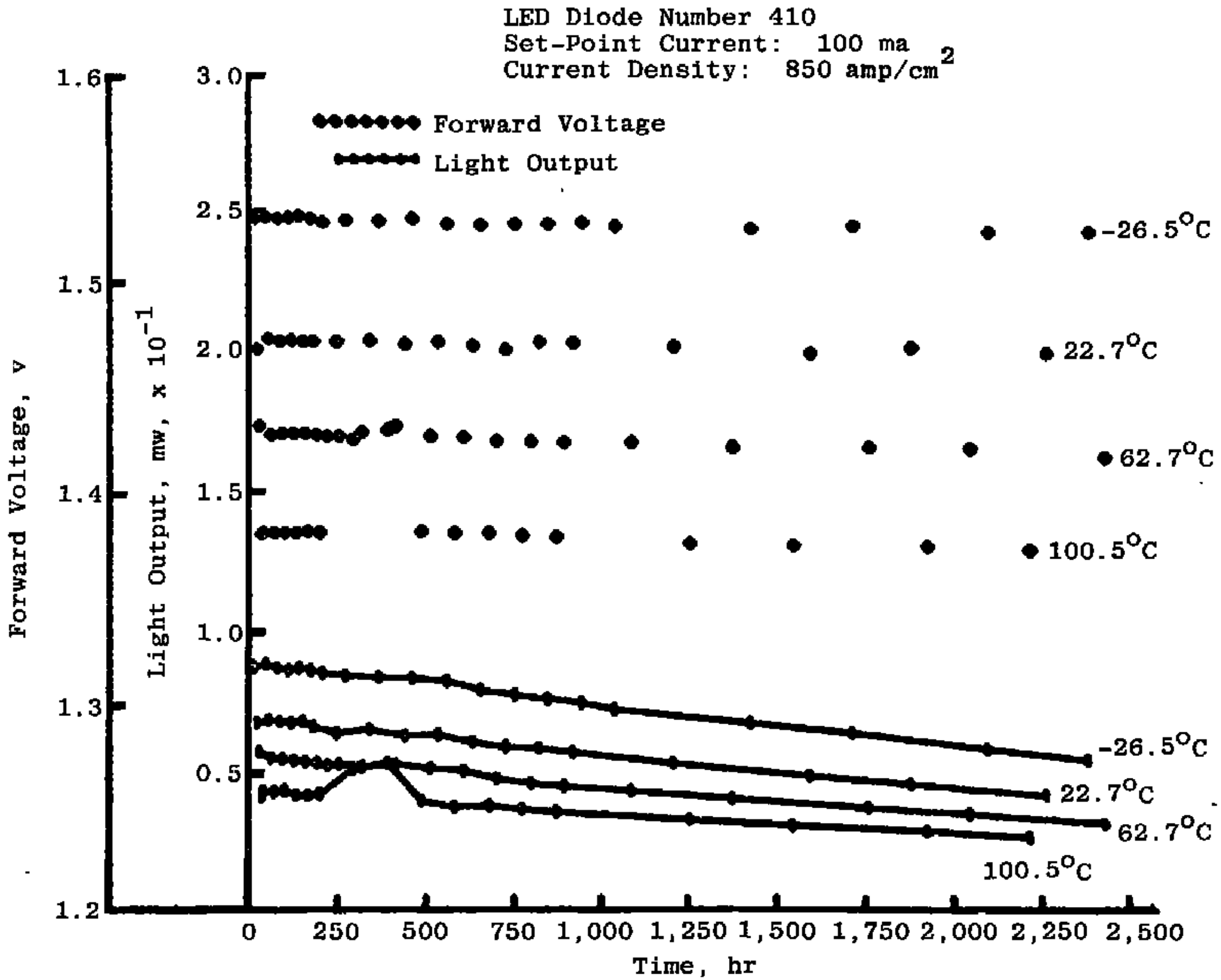

b. Light output vs time, TI Special
Figure 46. Continued.

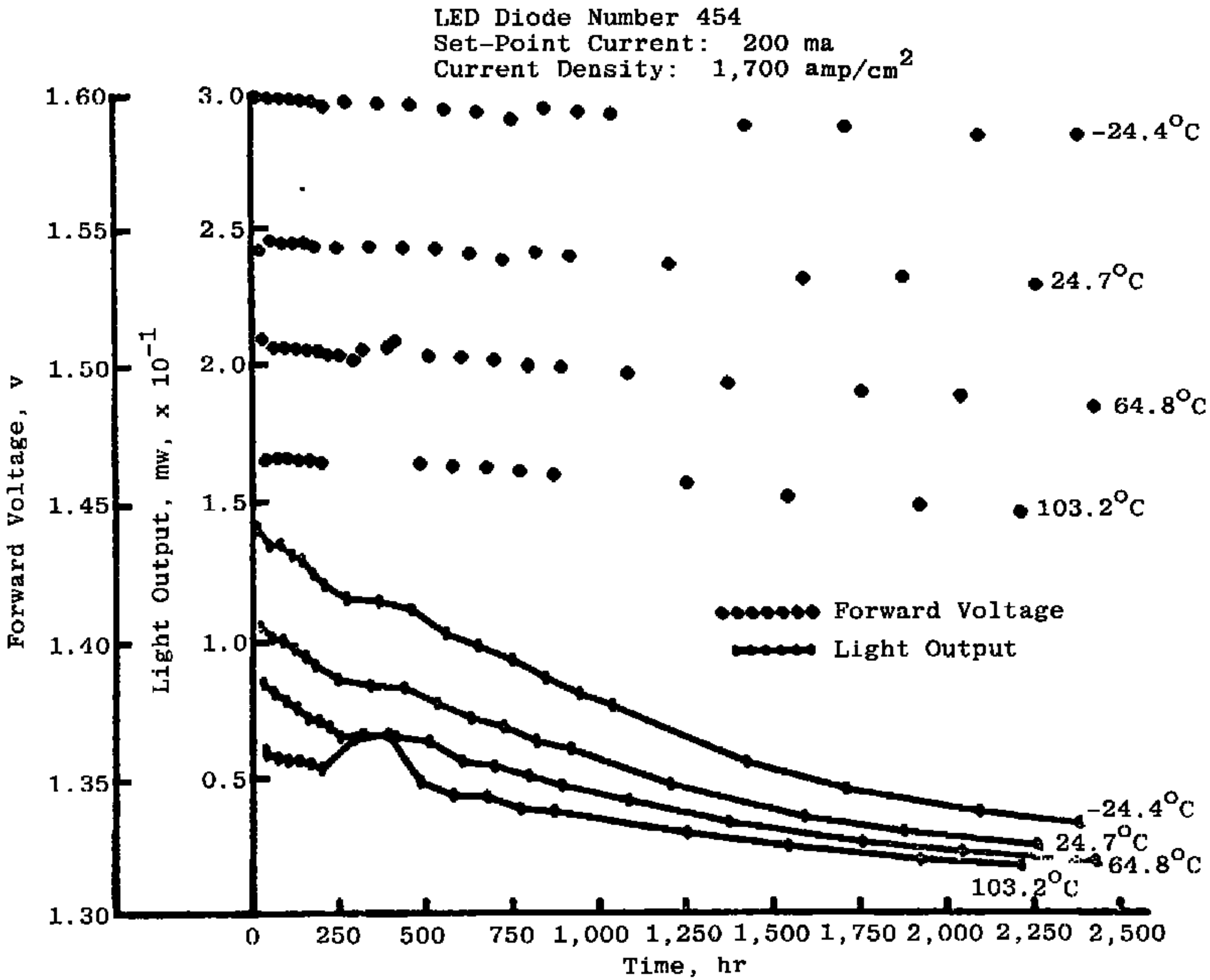

c. Light output vs time, TI Special

Figure 46. Concluded.

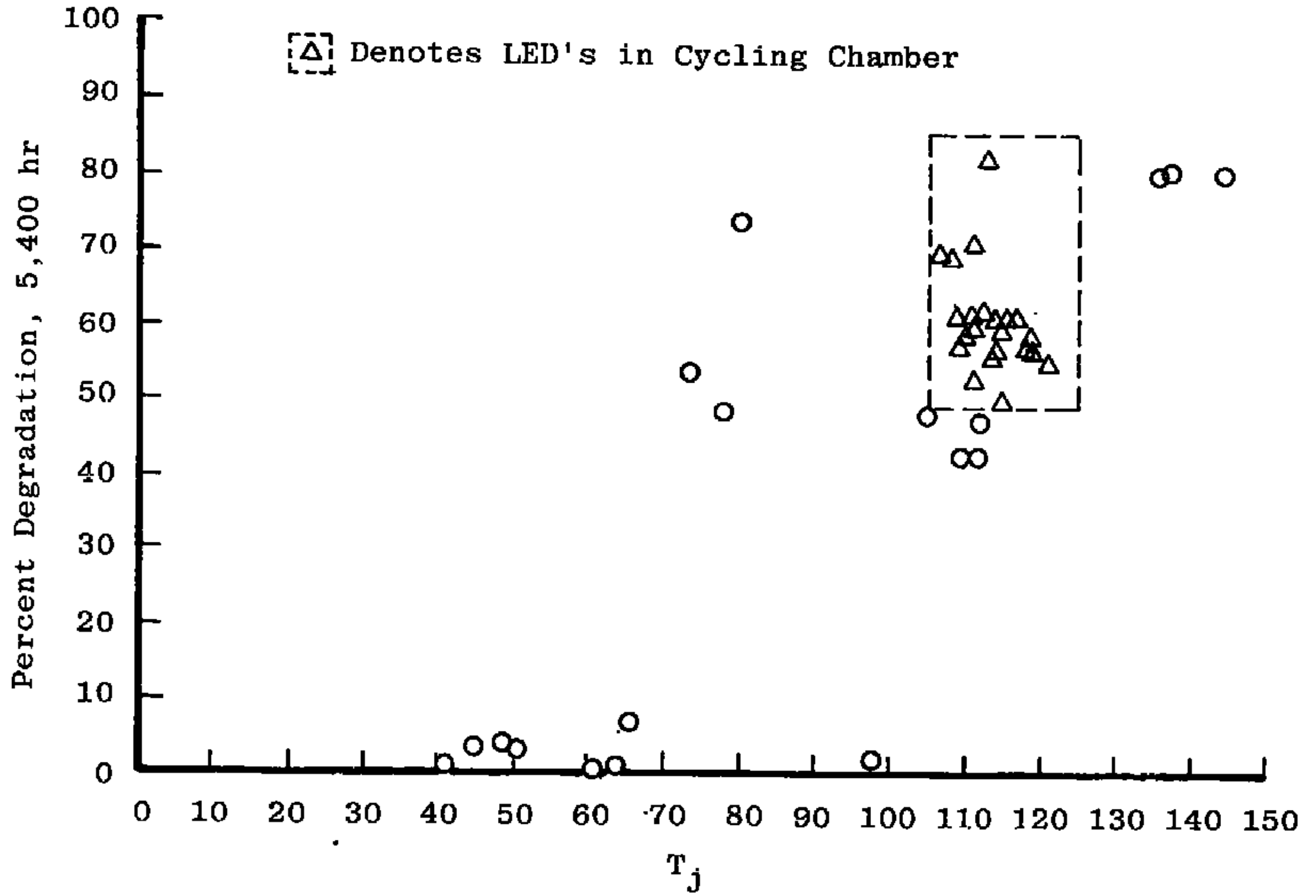

Figure 47. Percent degradation vs junction temperature – TI Special.

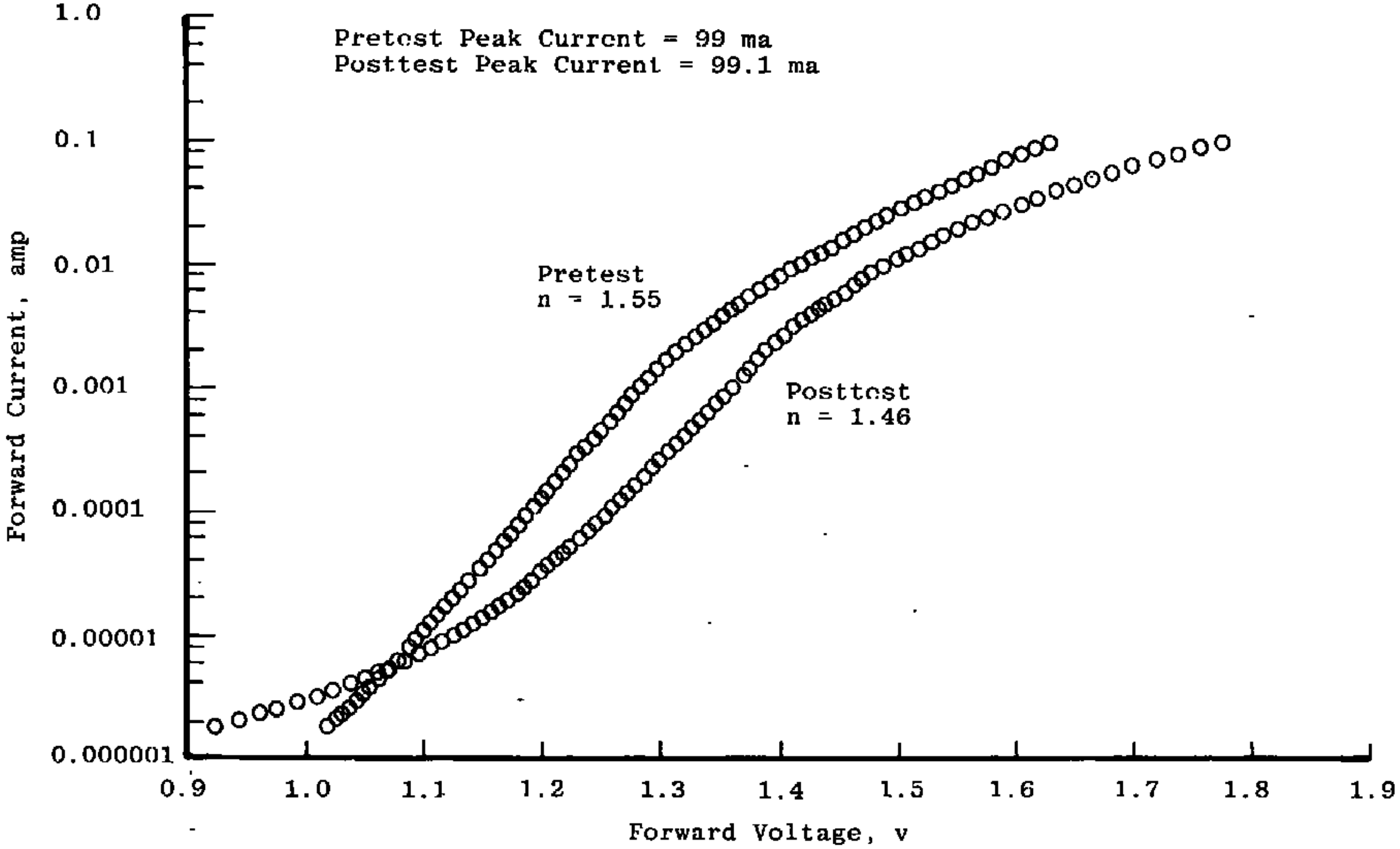

Figure 48. Forward current vs forward voltage, pretest and posttest RCA C30119, Diode No. 315.

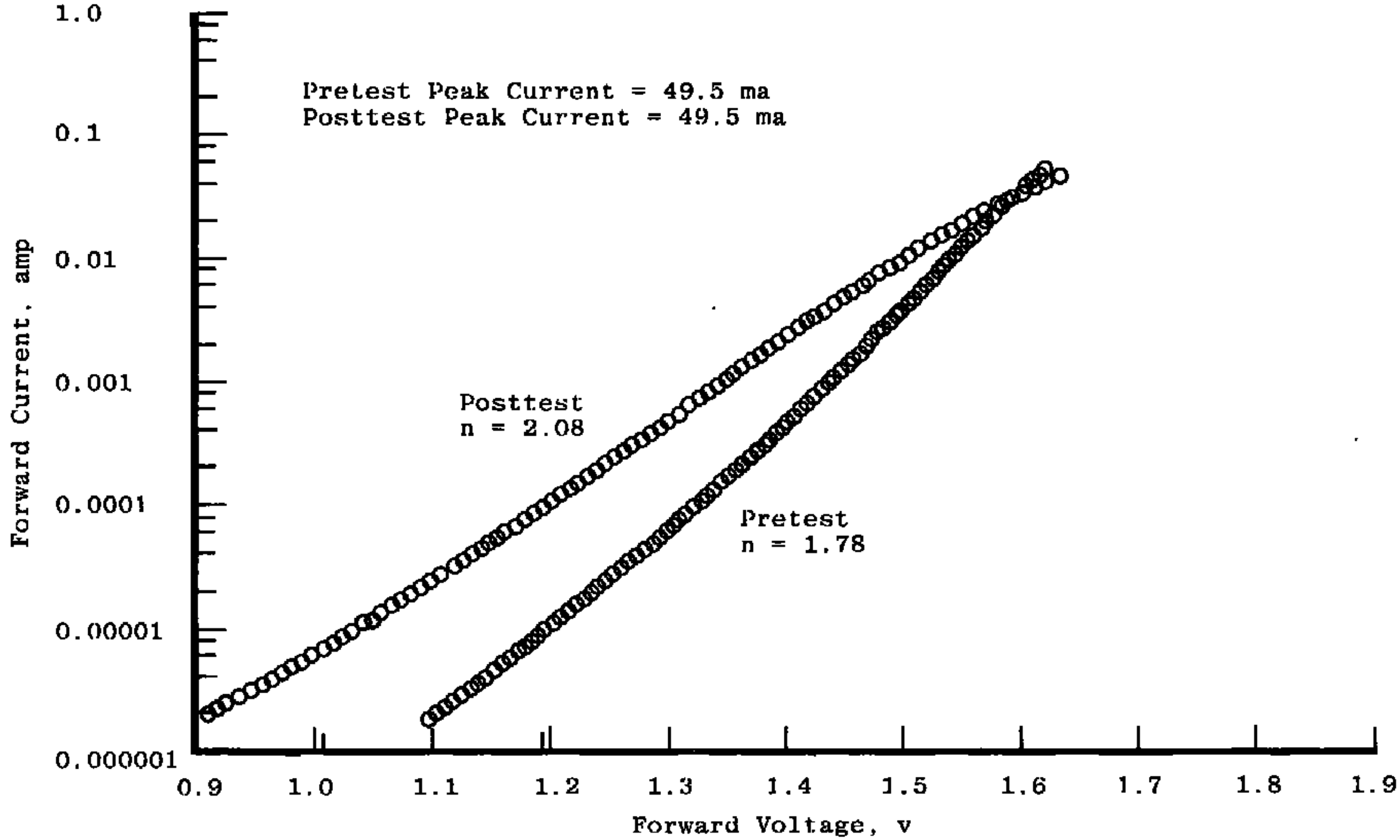

Figure 49. Forward current vs forward voltage, pretest and posttest SPX 2231F, Diode No. 349, (first test).

Operating Current = 100 ma
Run (102)/Run (2) Efficiency Ratio = 0.572877

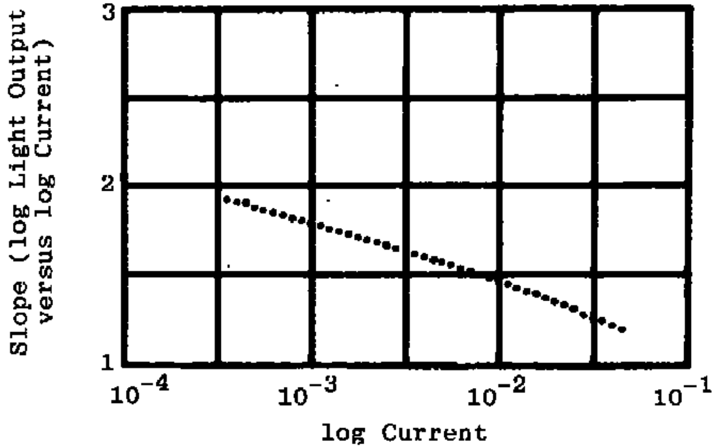

b. Equation (8)

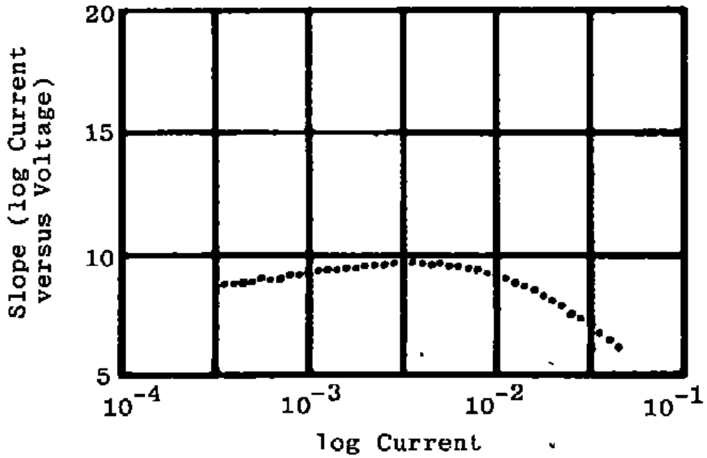

a. Equation (2)

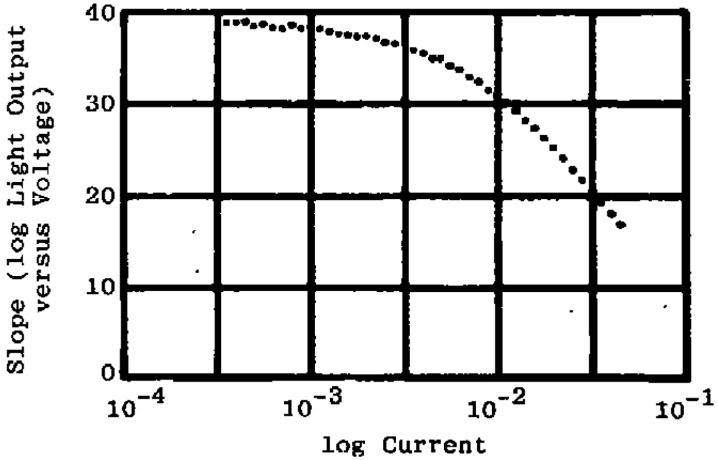

c. Equation (7)

Figure 50. Plots of pretest parameters – SPX 2231.

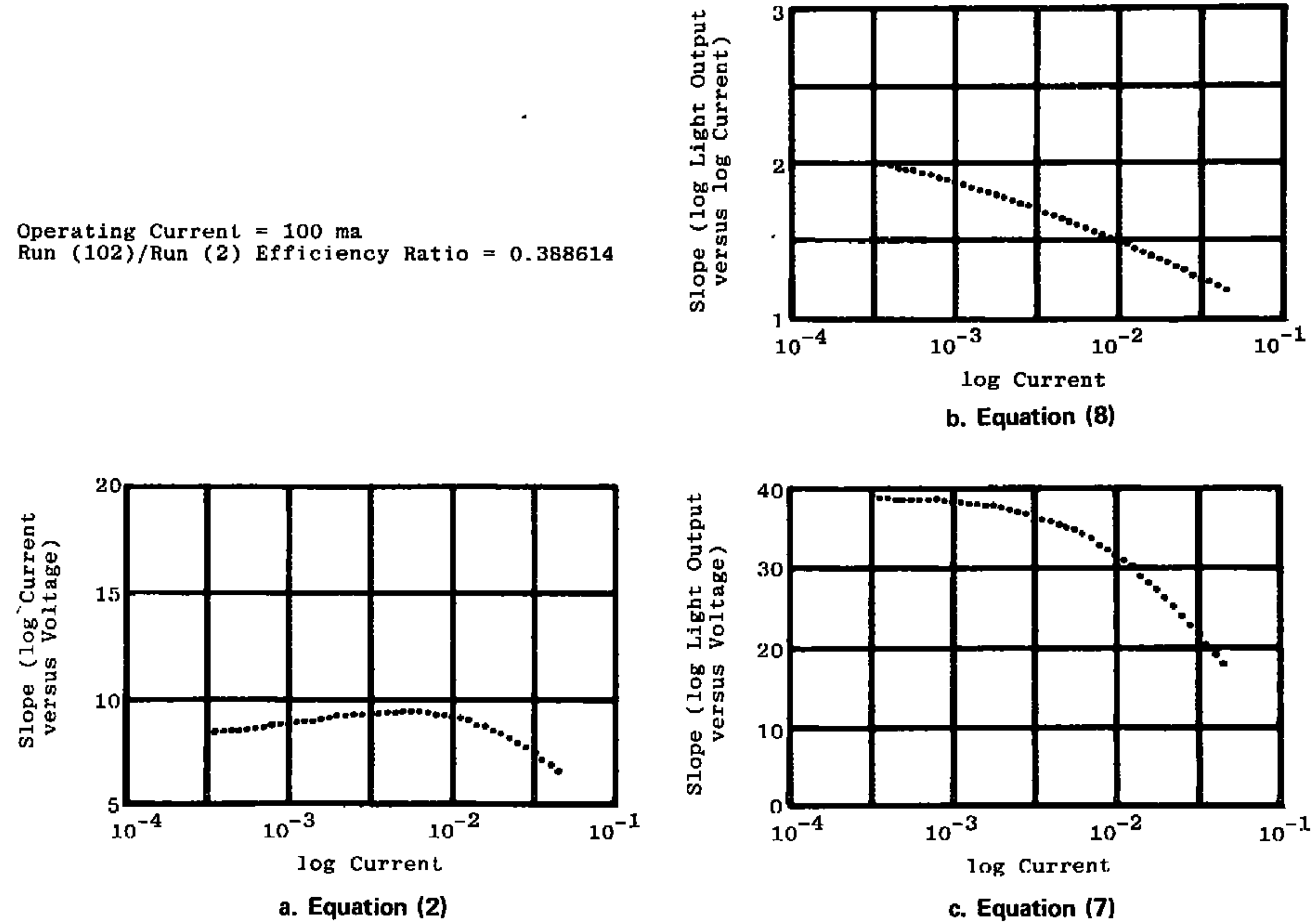

Figure 51. Plots of pretest parameters — SPX 2231.

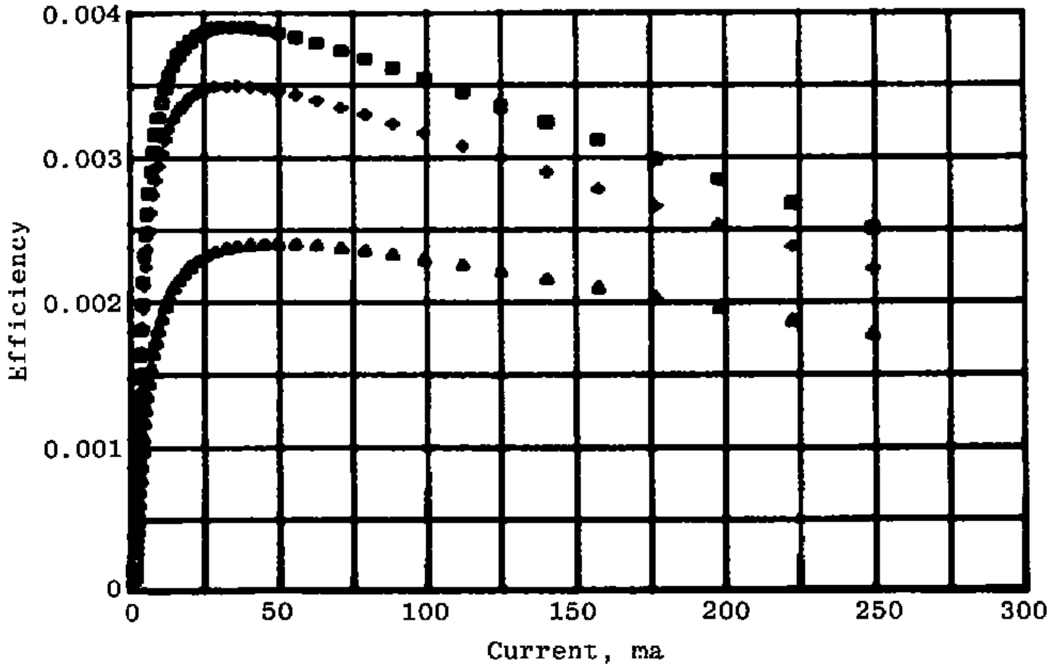

Figure 52. Efficiency vs current – RCA C30123, Diode Nos. 7, 8, and 9.

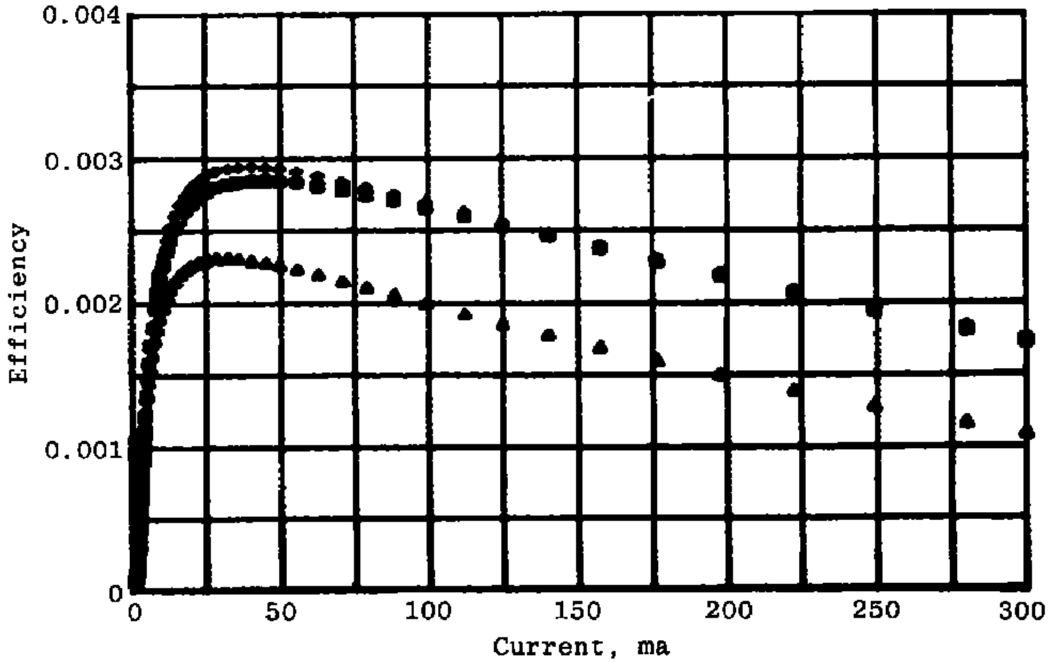

Figure 53. Efficiency vs current – RCA C30123, Diode Nos. 10, 11, and 12.

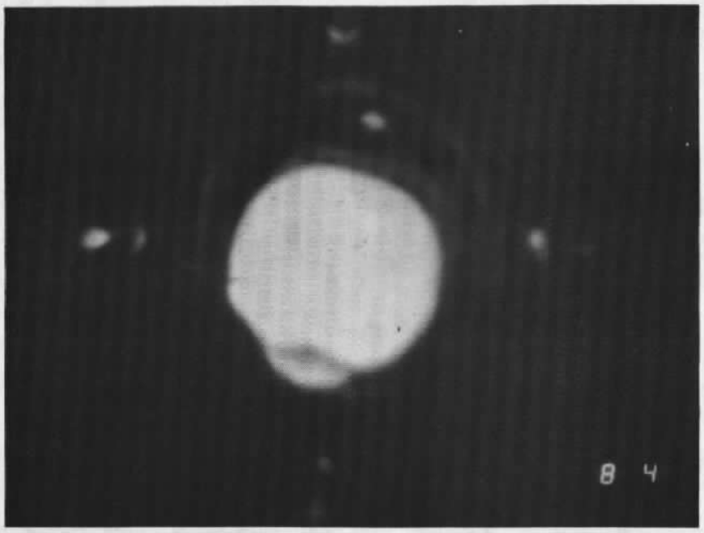

Pretest Light Output Power 8 mw

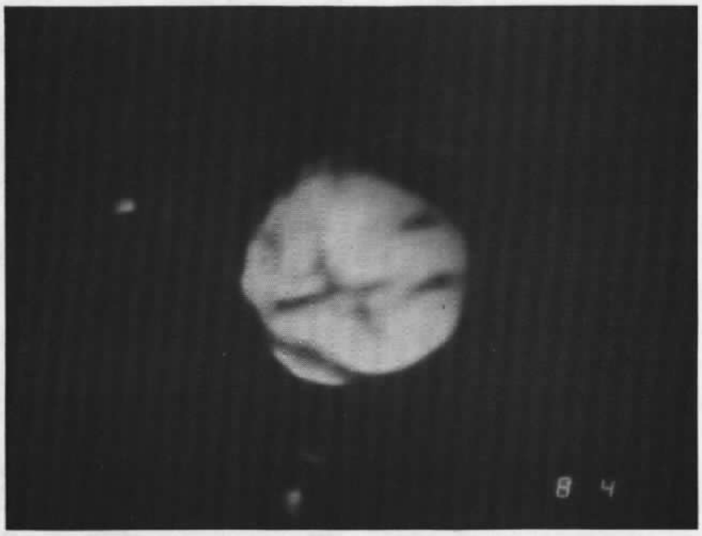

Posttest Light Output Power 0.49 mw

Figure 54. Pretest and posttest IR microphotographs – TIXL 35.

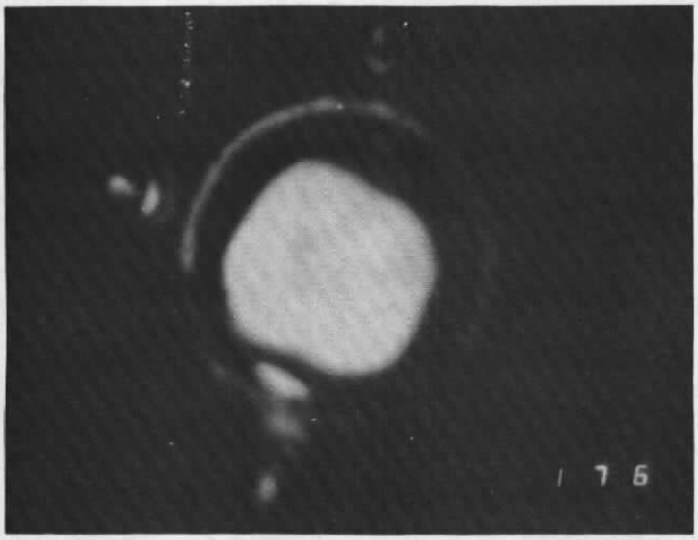

Pretest Light Output Power 1.1 mw

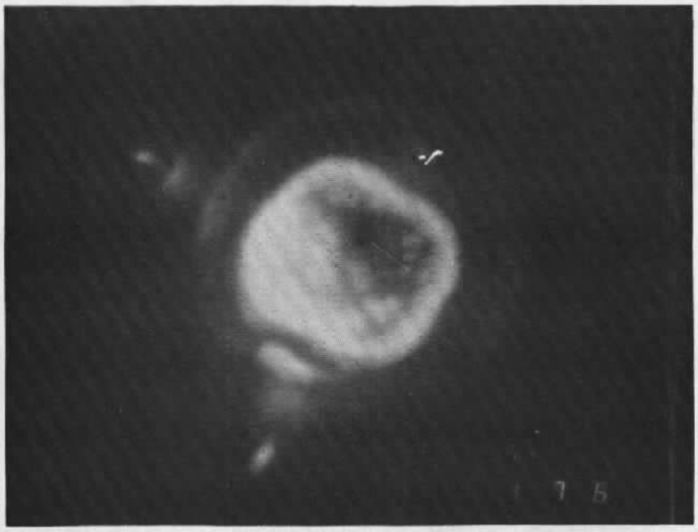

Posttest Light Output Power
3.4×10^{-3} mw

Figure 55. Pretest and posttest IR microphotographs – TIXL 35.

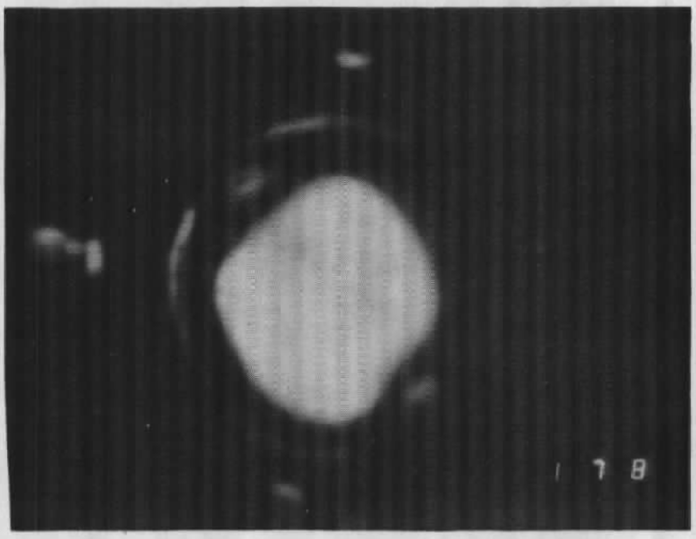

Pretest Light Output Power 1.1 mw

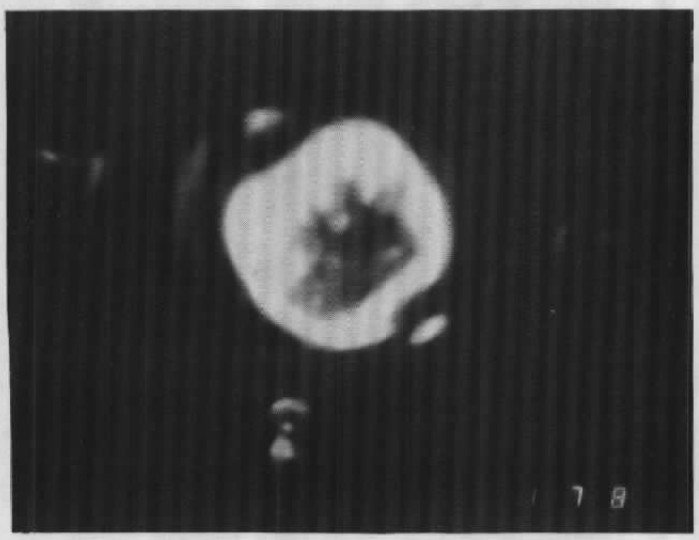

Posttest Light Output Power
4.8×10^{-3} mw

Figure 56. Pretest and posttest IR microphotographs – TIXL 35.

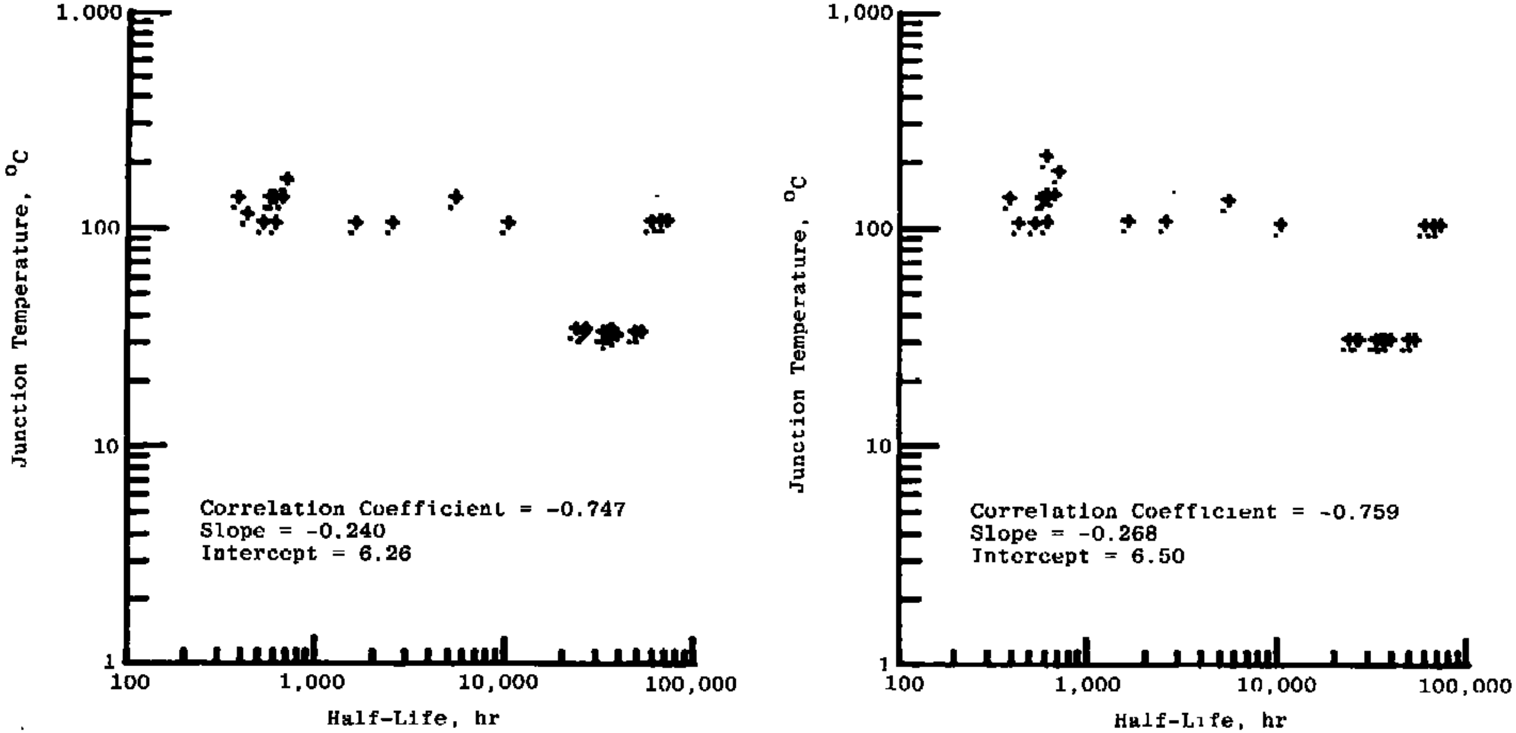

a. **Junction temperature ΔT_j**

b. **ΔT = IVZ**

Figure 57. Junction temperature vs half-life — RCA C30123.

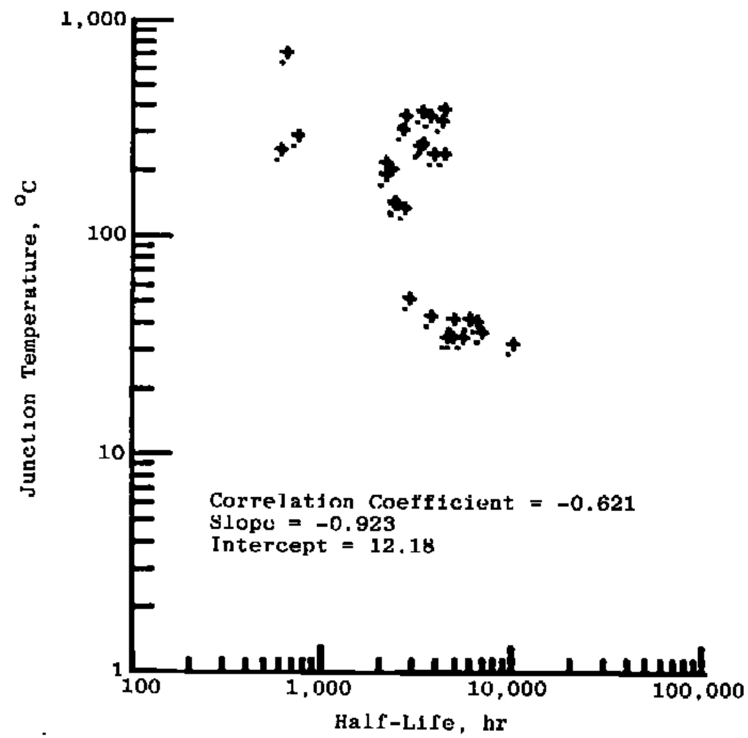

a. Junction temperature ΔT_j

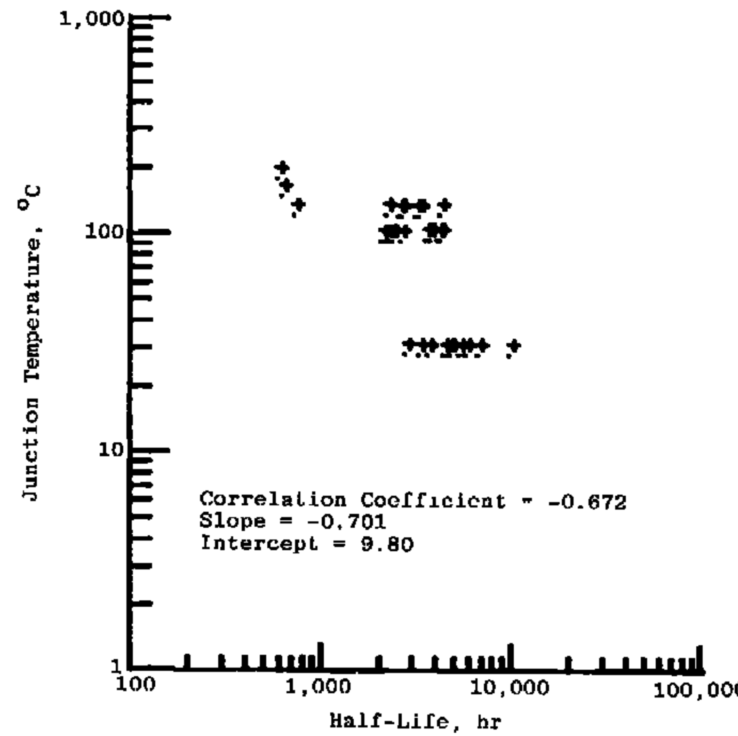

b. ΔT = IVZ

Figure 58. Junction temperature vs half-life — RCA C30119.

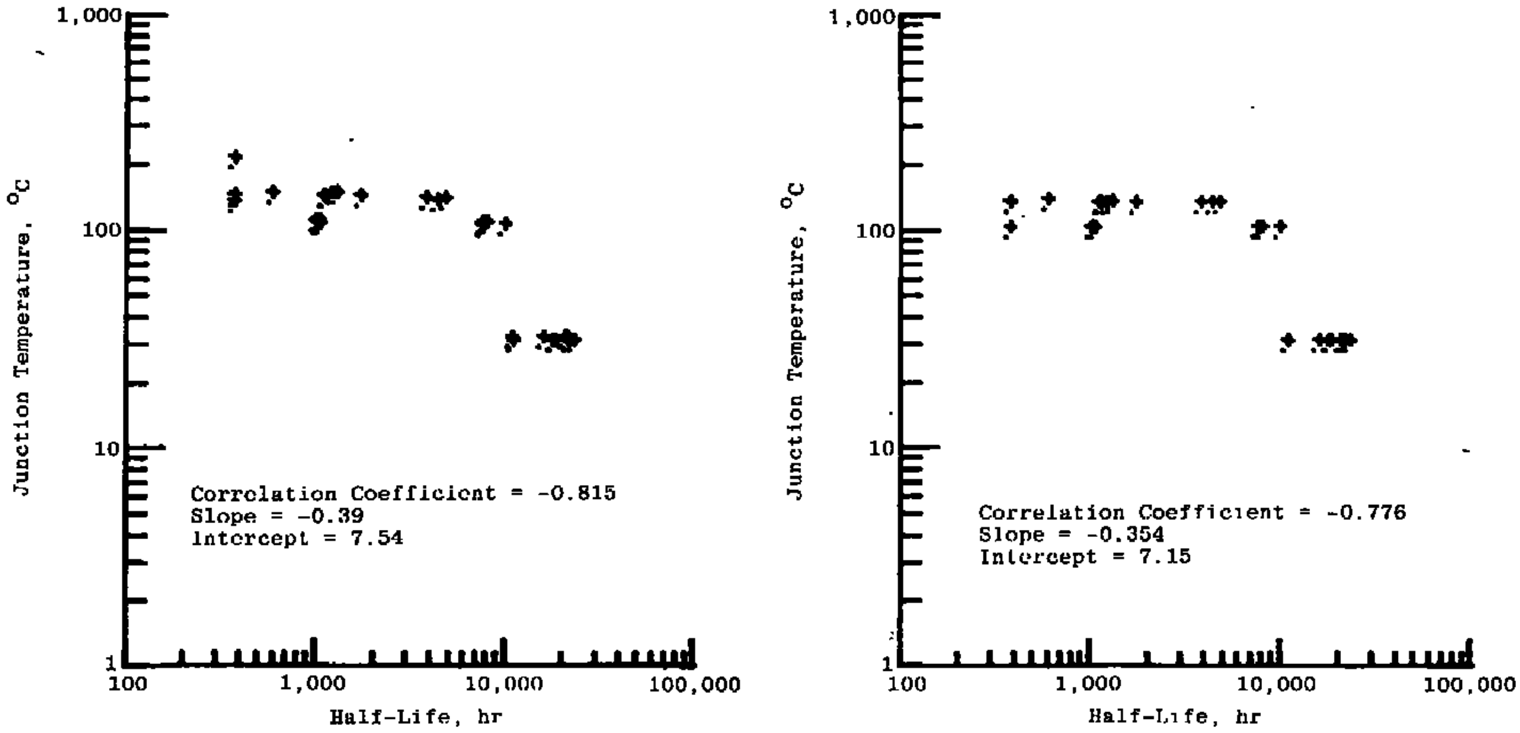

a. Junction temperature ΔT_j

b. ΔT = IVZ

Figure 29. Junction temperature vs half – life SPX 2231.

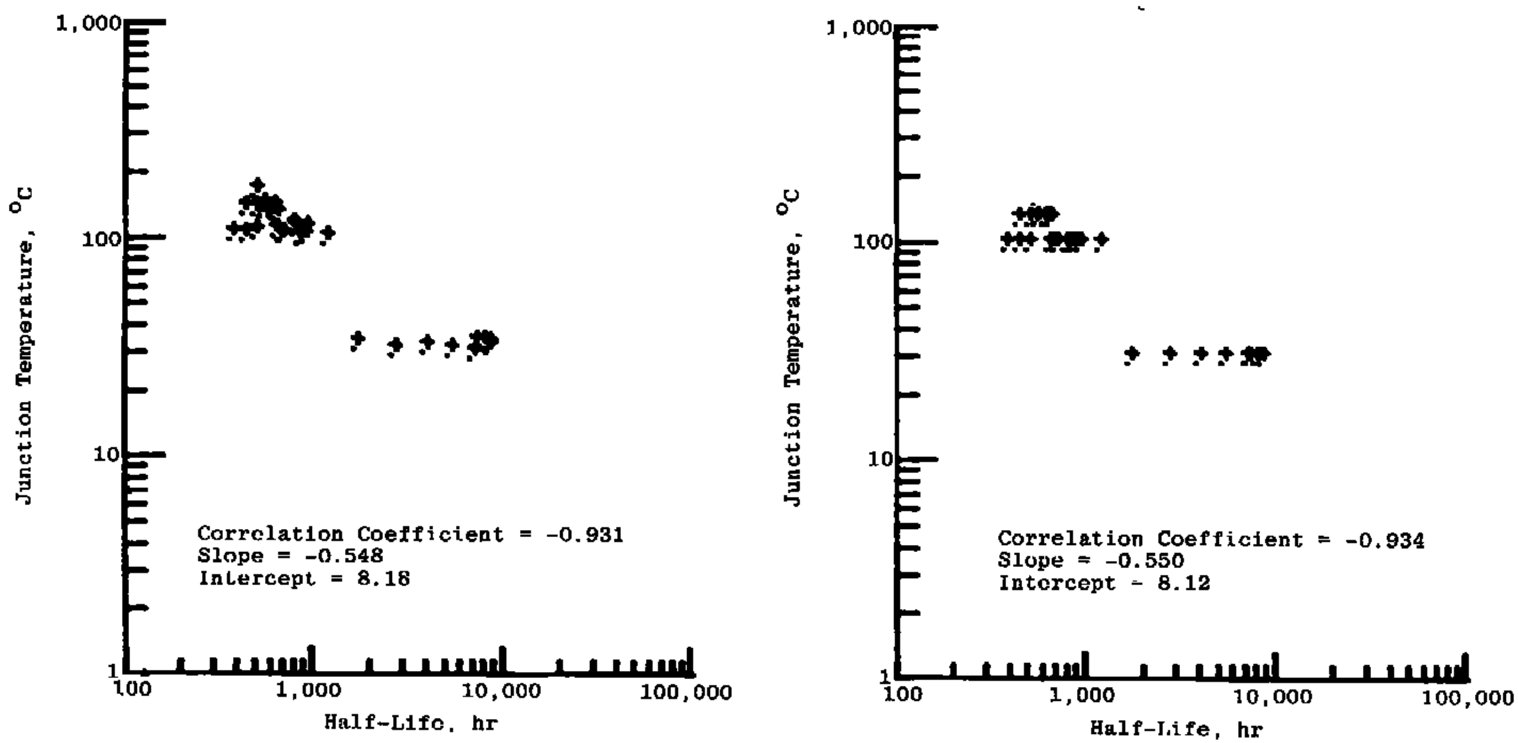

a. Junction* temperature ΔT_j

b. ΔT = IVZ

Figure 60. Junction temperature vs half-life – SPX 2231F.

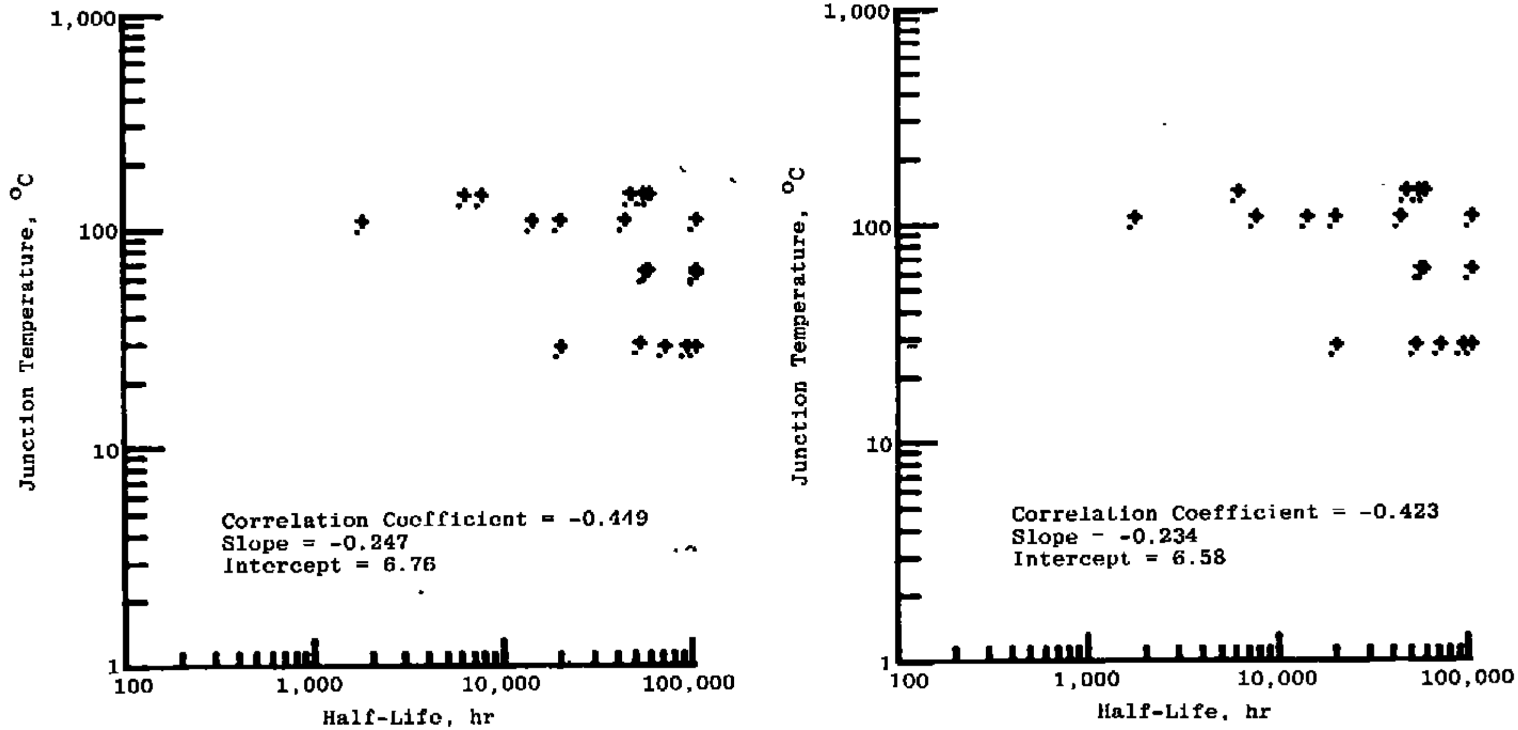

a. Junction temperature ΔT_j

b. ΔT = IVZ

Figure 61. Junction temperature vs half-life — MEK 104.

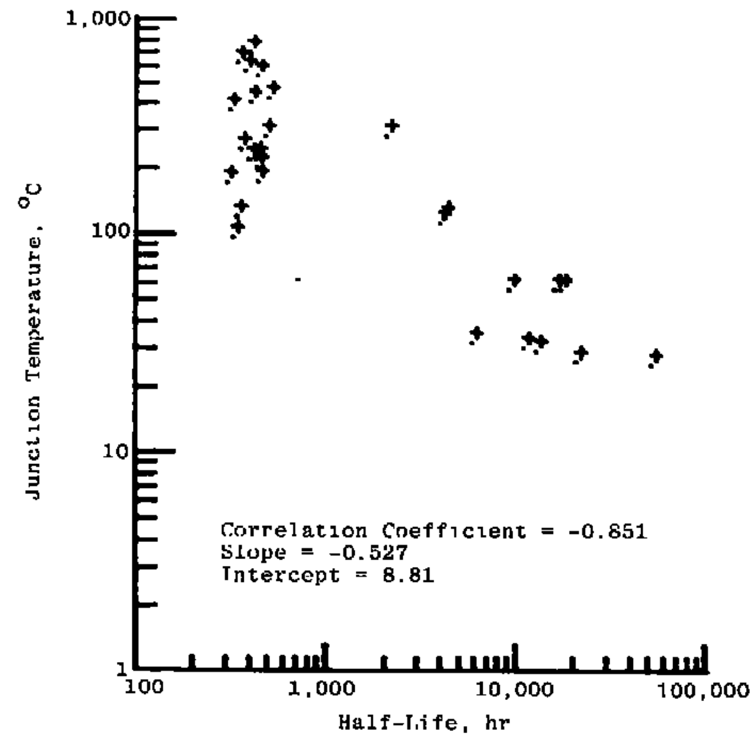

a. Junction temperature ΔT_j

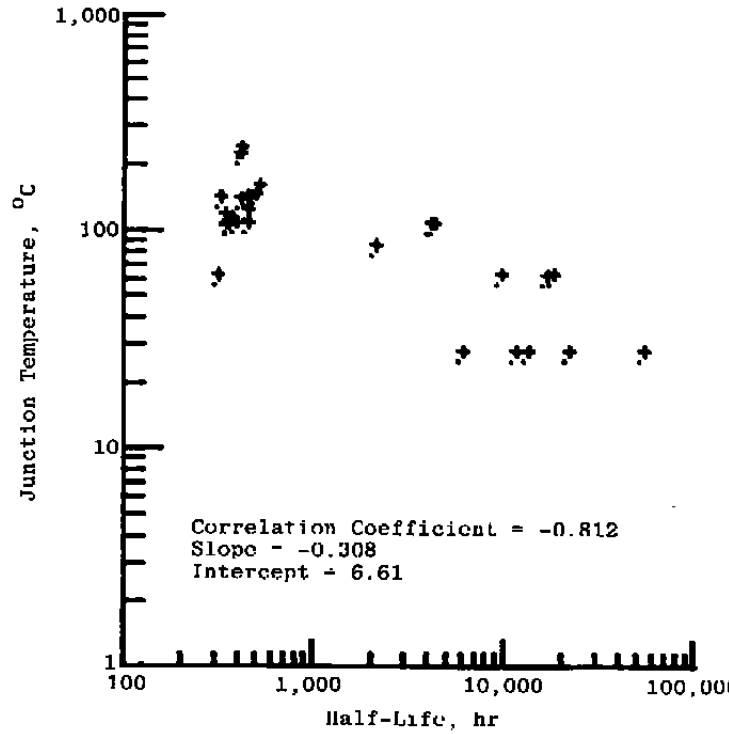

b. $\Delta T = IVZ$

Figure 62. Junction temperature vs half-life — TIES 35.

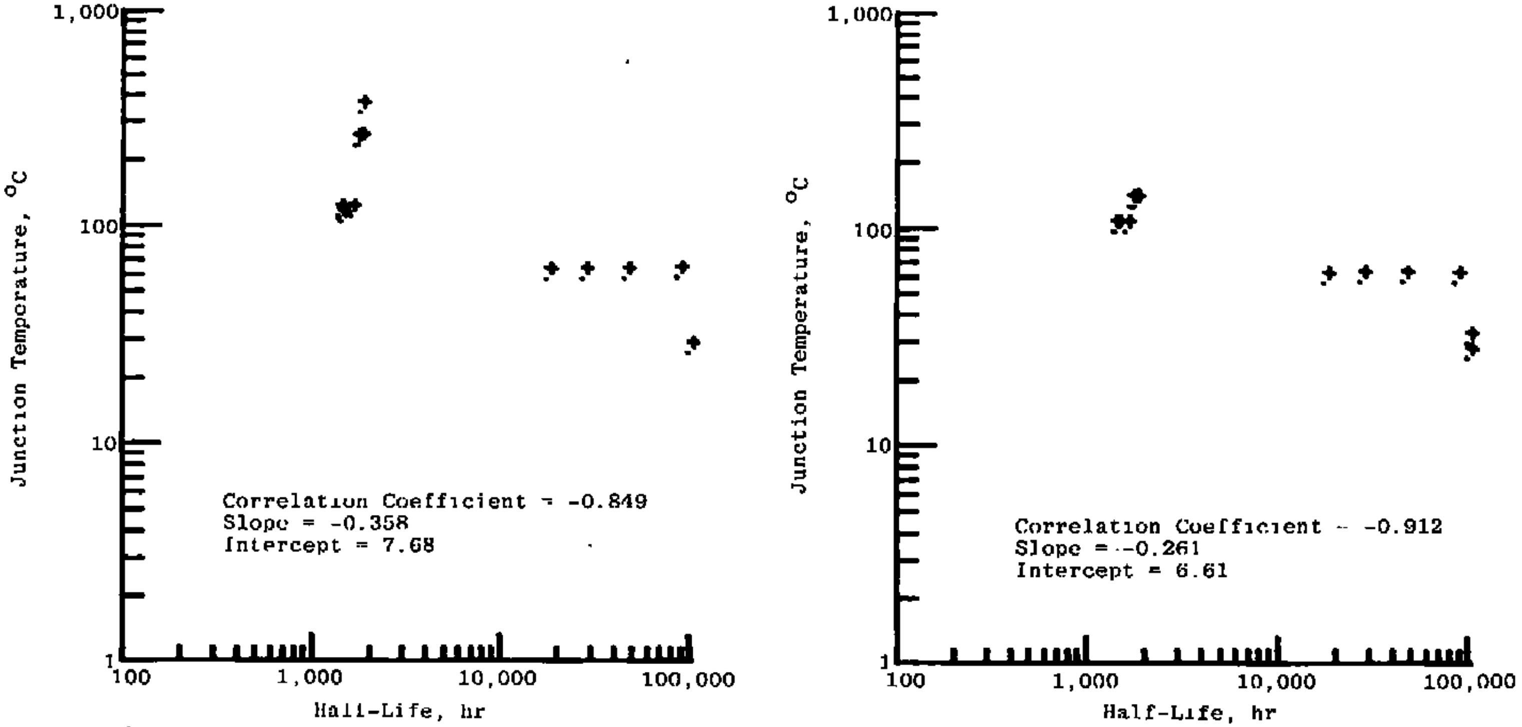

a. Junction temperature ΔT_j

b. ΔT = IVZ

Figure 63. Junction temperature vs half-life — TI Special.

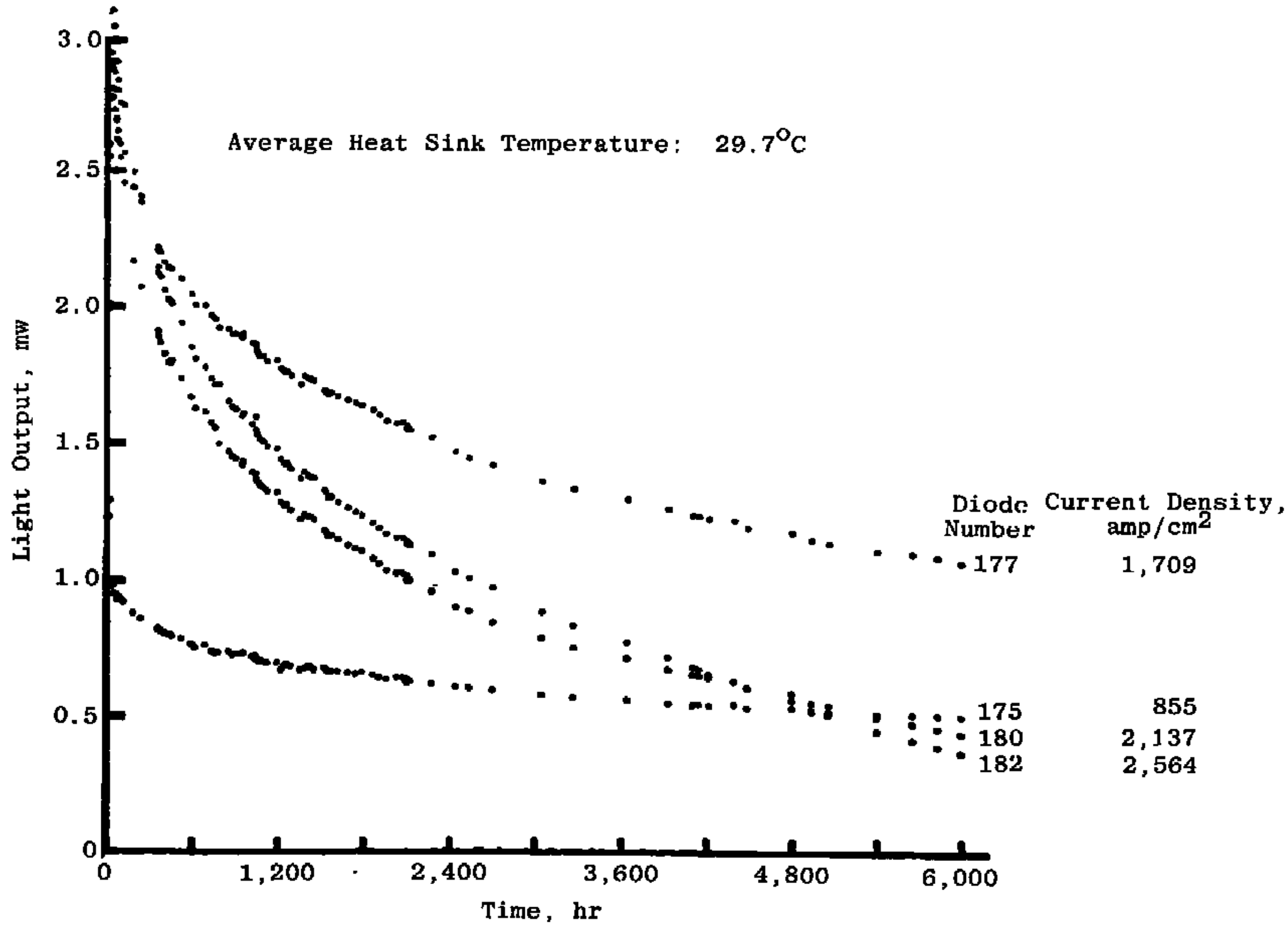

Figure 64. Light output power vs time — TIXL 35.

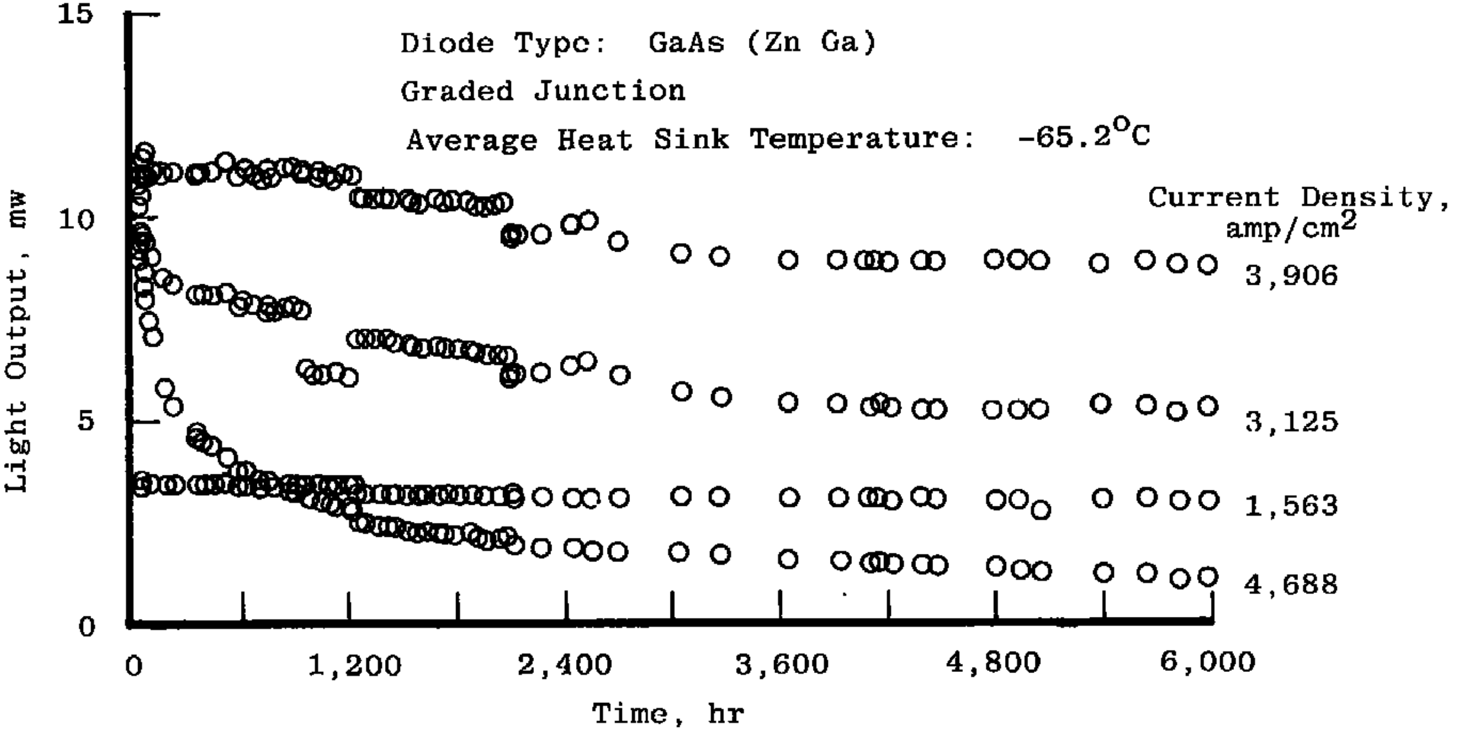

Figure 65. Light output power vs time — SPX 2231, -65°C.

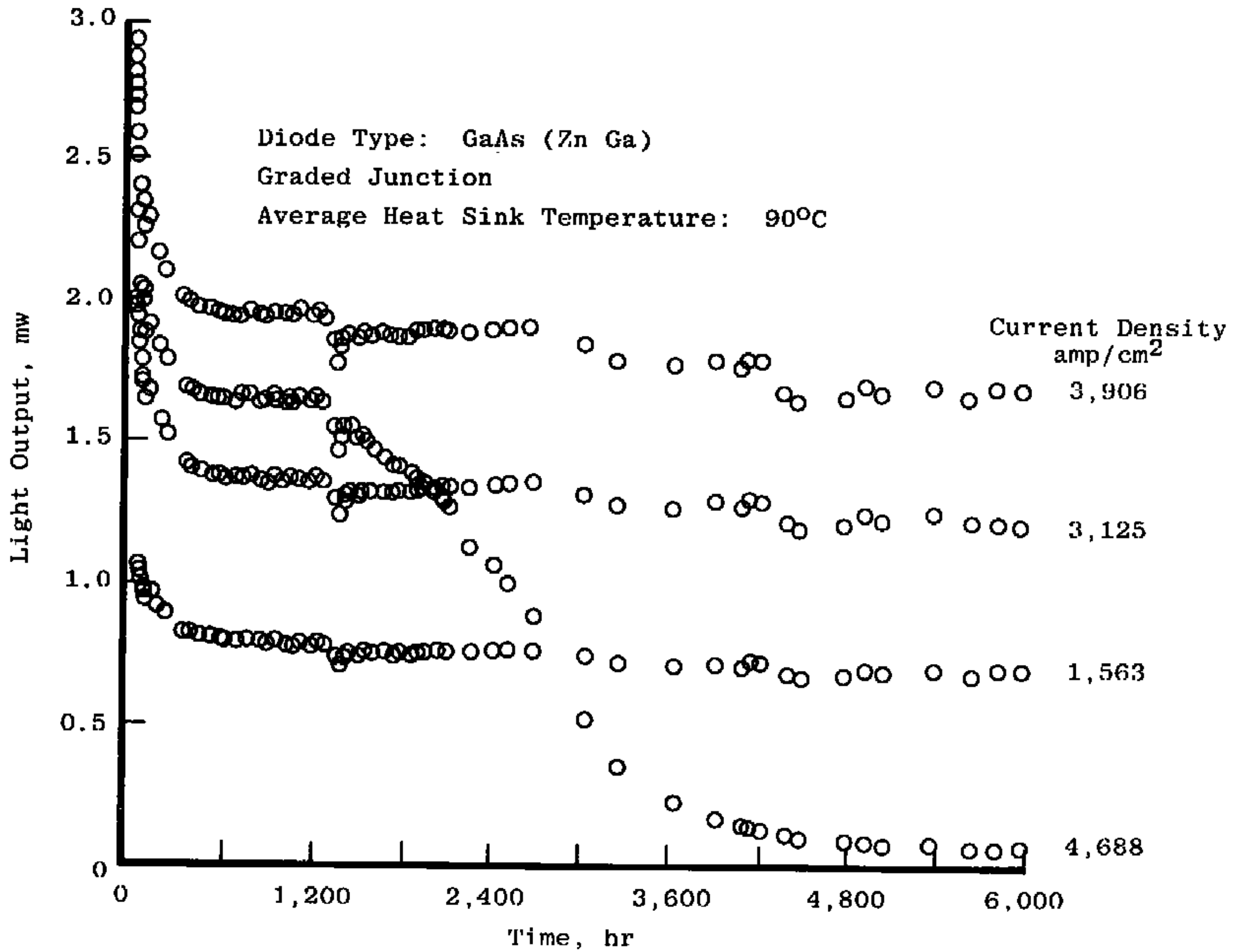

Figure 66. Light output power vs time – SPX 2231, 90°C.

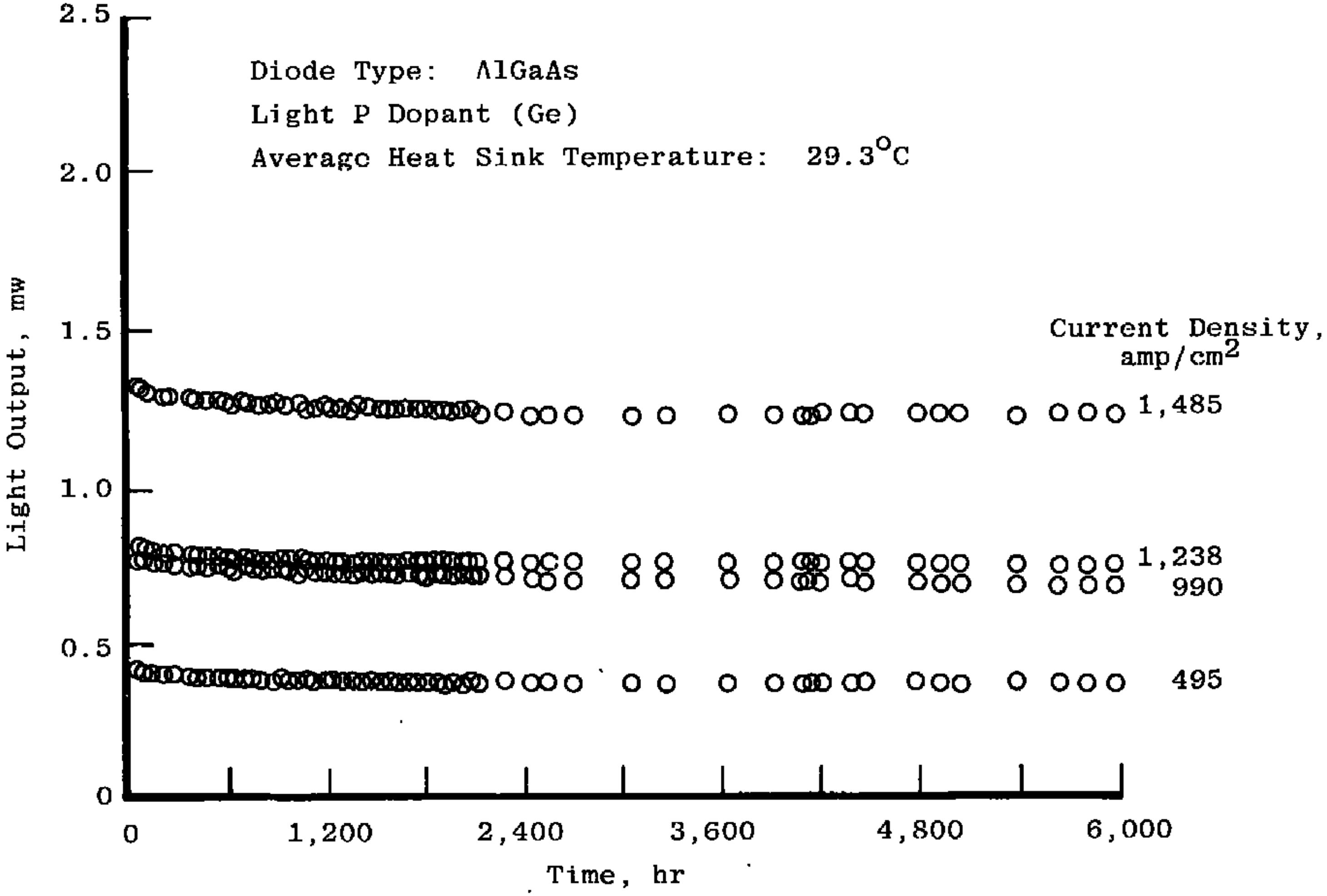

Figure 67. Light output power vs time — RCA C30123, 30°C.

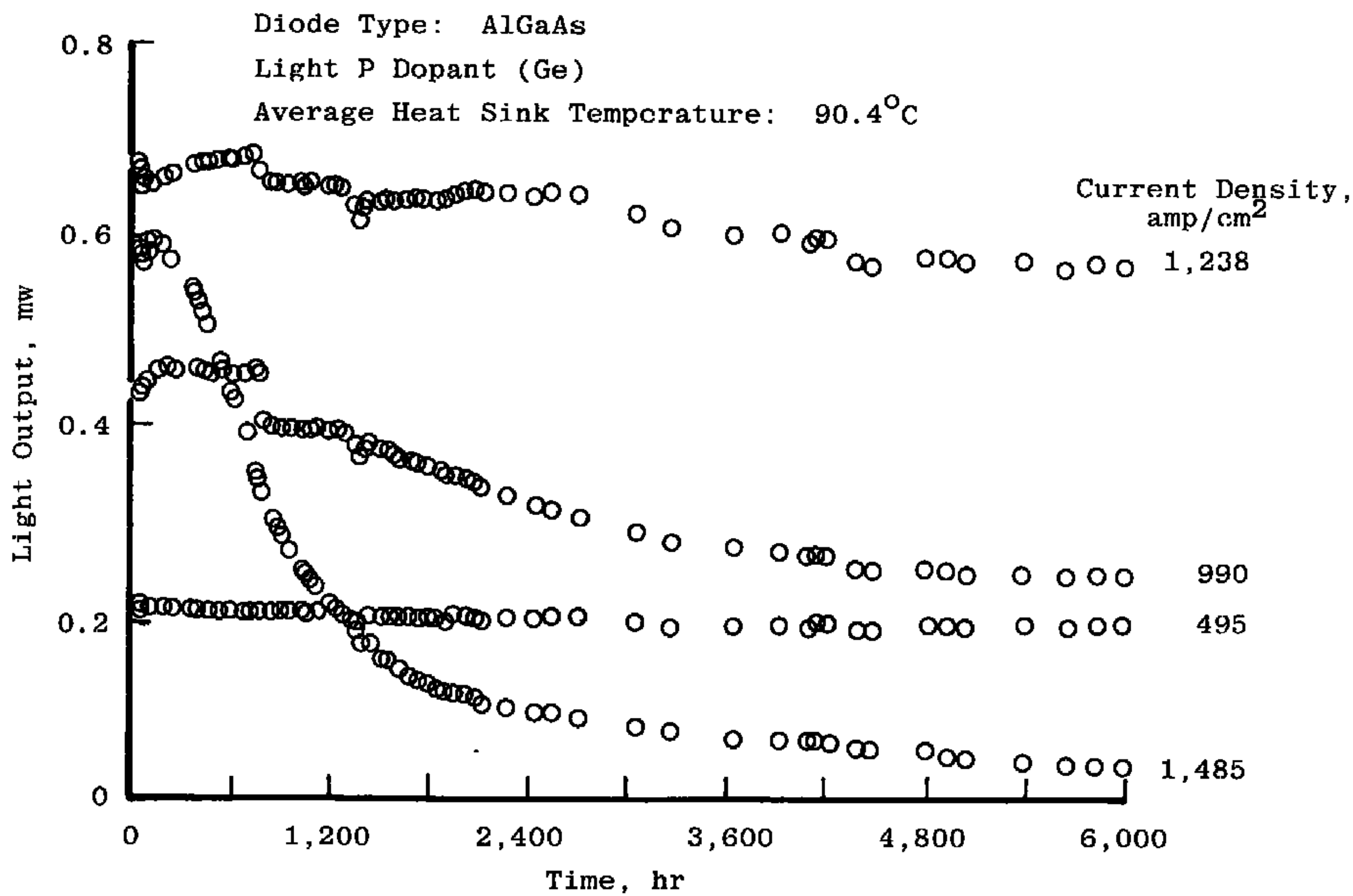

Figure 68. Light output power vs time – RCA C30123, 90°C.

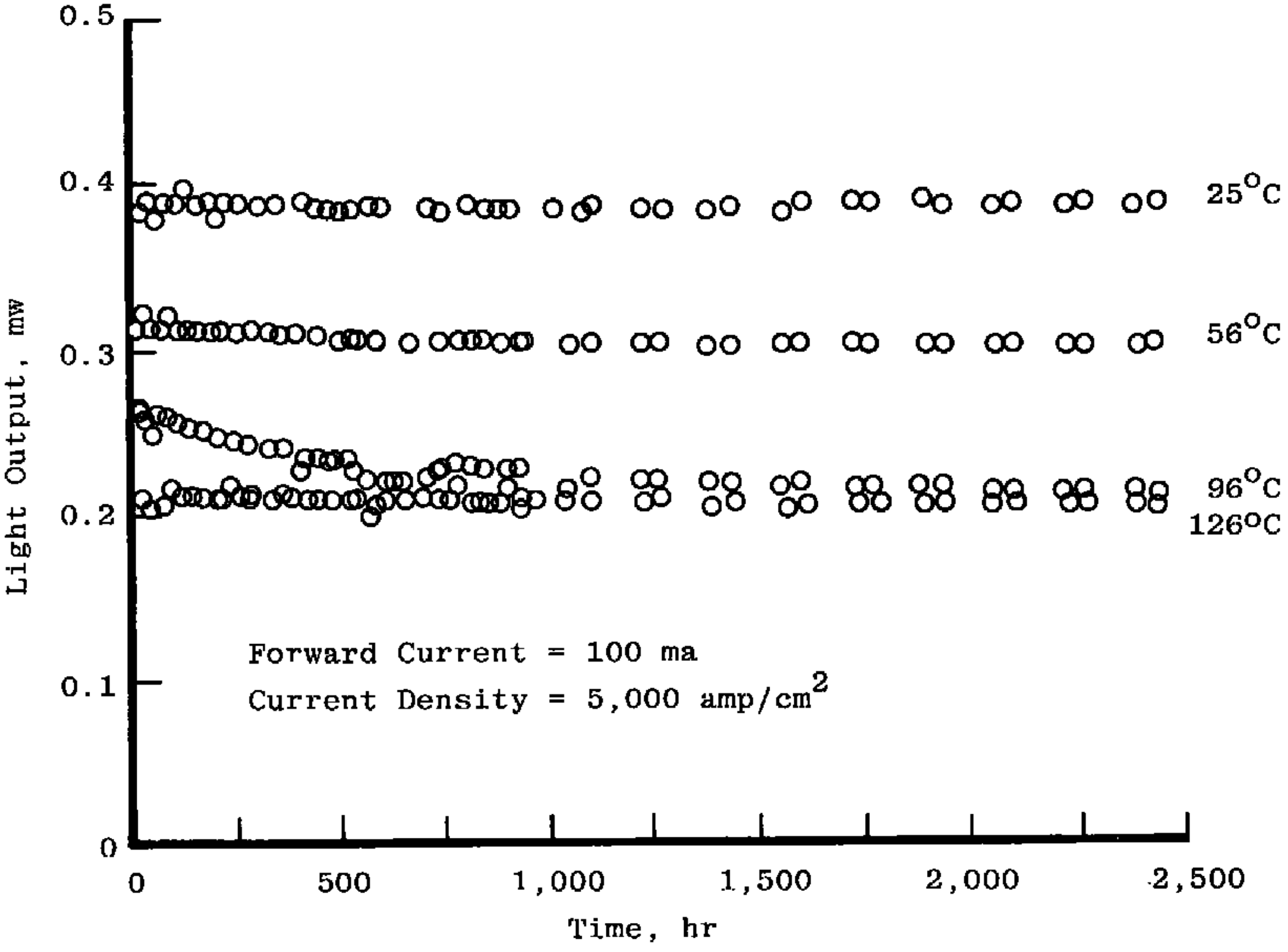

Figure 69. Light output power vs time — MEK 104.

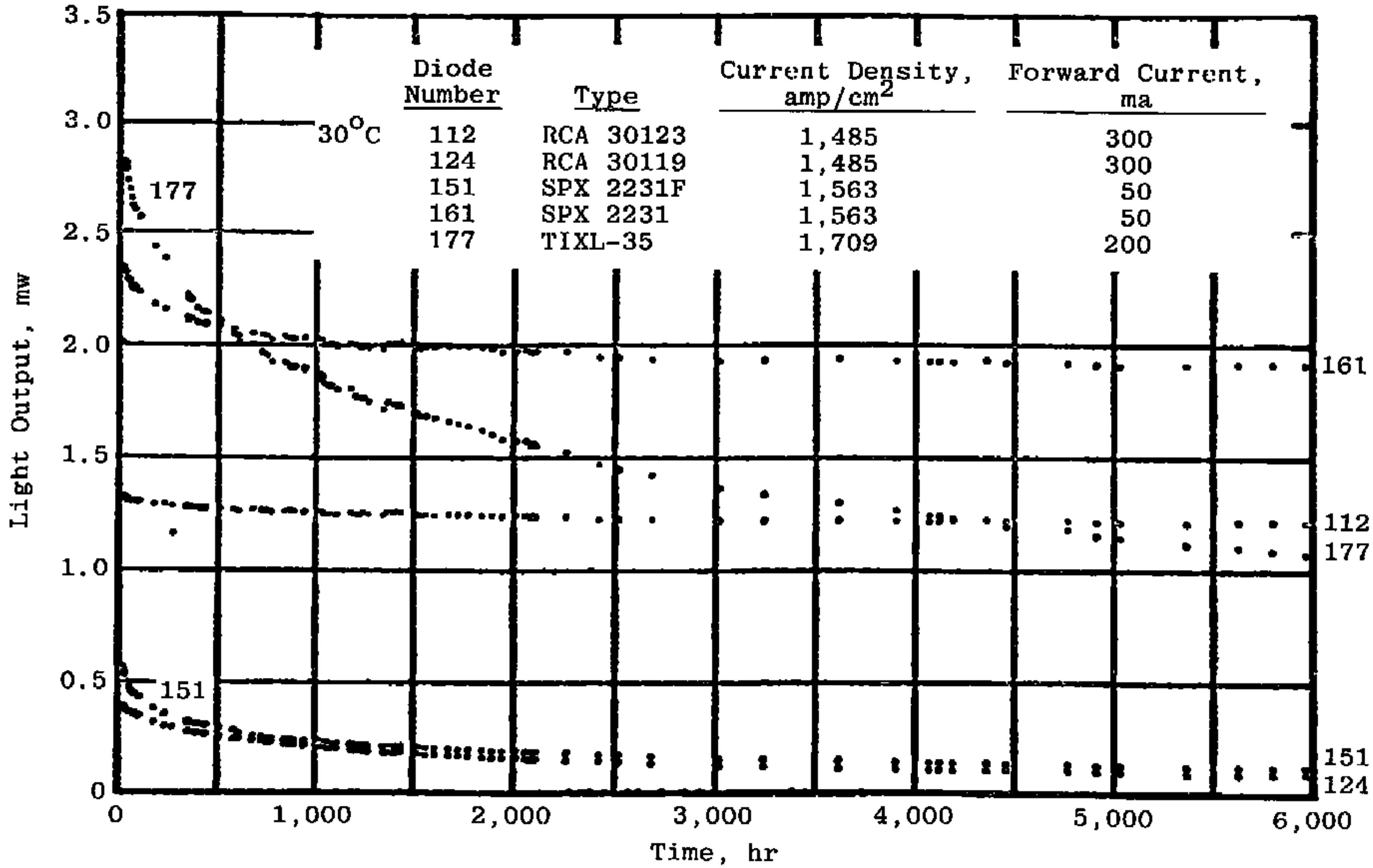

Figure 70. Light output power vs time — summary, 30°C.

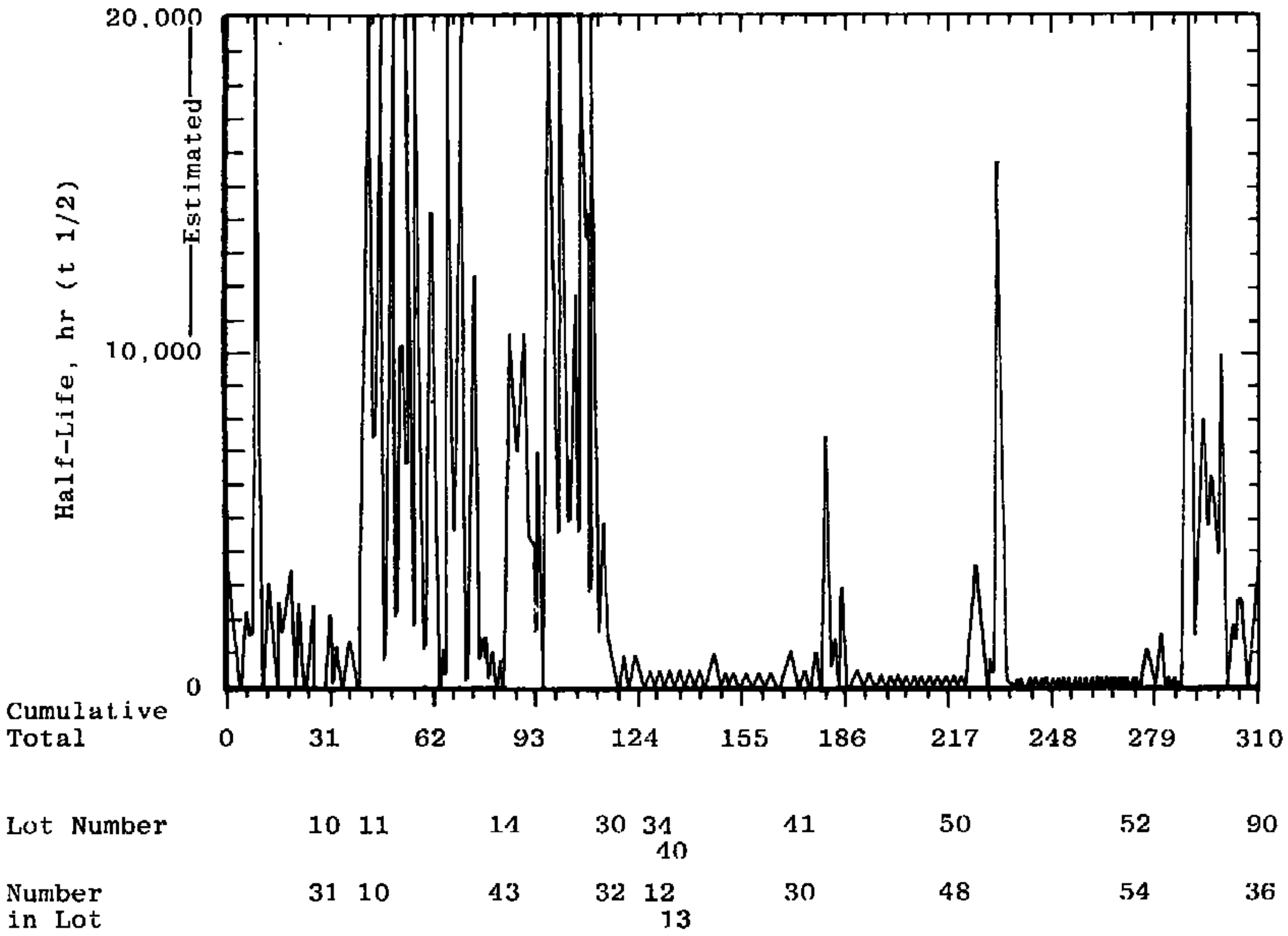

Figure 71. Half-life vs LED type and number.

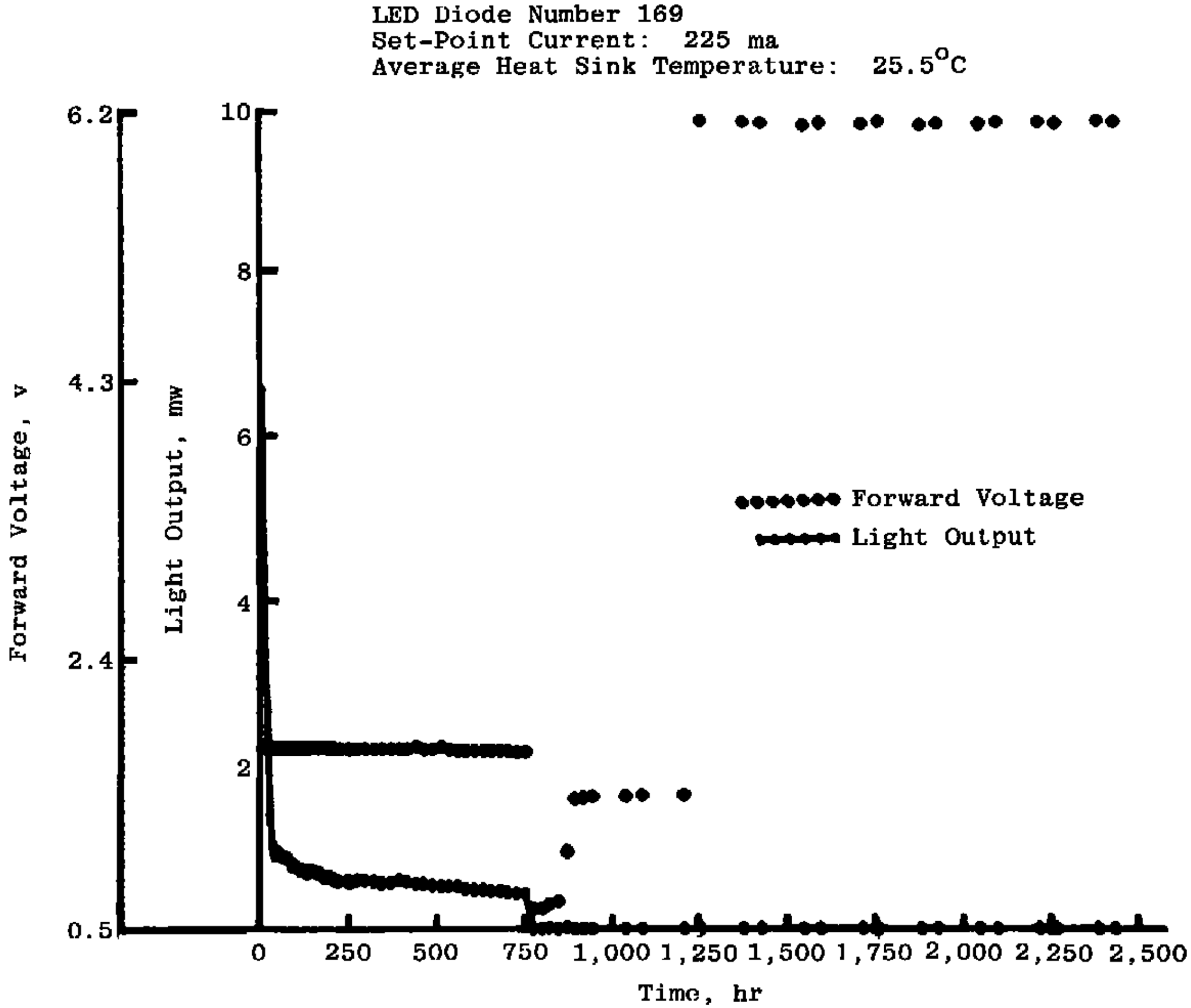

Figure 72. Light output vs time — injection laser diode.

Table 1. Diode Types and Number in Test Chambers, Continuous Test

Diode Type	Lot No.	Chamber Designation					Total Number of Diodes
		A (50°C)	B (20°C)	C (90°)	D (120°C)	E (cycling)	
RCA							
C30123	30	11	11	6	4	0	32
C30119	90	12	12	6	2	4	36
Mitsubishi							
MEK-104	14	10	7	8	9	9	43
Spectronics							
SPX 2231	10	7	8	10	4	2	31
SPX 2231F	11	5	6	0	0	0	11
SPX 2234	34	3	3	3	3	0	12
SPX 2254	40	0	0	6	7	0	13
SPX 2354F	41	4	3	13	10	0	30
Texas Instruments							
TIES 35	50	9	12	12	12	9	54
TI Special	52	7	3	4	4	34	52
TOTAL		68	65	68	55	58	314

Table 2. Summary of Correlation Attempts, First Test

Characteristic	Variables	Objective	Results	Comment
Arrhenius Relationship	T, t ½	Predict Ambient Life	No Definite Trend	Large Error Bands
Thermal Resistance	Z_T (Pretest) Z_T (Posttest, t ½)	Identify Bulk Changes	No Definite Trend	Data Scattered
Switching Optical	Rise Time, Fall Time, Light Output	Change in Recombination Mechanism	No Definite Trend	Data Not Consistent
Light Output Low Currents	Curve Slope, Bulk Resistance	Change in Bulk Crystal	No Correlation	R_B Too Small
Light Output Lowest Detectable	I_F, V_F, Degradation	Correlate Life with Threshold	No Correlation	Receiver Noise
Forward Voltage at Operating Current	ΔV_F, I_F, ΔT	Change in Bulk or Junction	No Definite Trend	First 200 hr
Light Output L_o I_f	Light Output Forward Current	Curve Shift with Degradation	Possible Trend	Need Online Characteristics
Pretest and Posttest IV, LV	I_f, V_f, L Slope LV	Correlate Slope with percent Degradation	Possible Trend	Study Continues
Output Power Ratio First 200 hr	L(N), L(O) E_A	Correlate Change in Junction Energy with Degradation	Posible Trend	Study Continues

Table 3. Correlation Coefficients of Degradation vs a Number of Parameters — Both Tests

Diode Mfgr. Lot/Type	Degradation $\left(\frac{\text{Light output: 6,000 hours}}{\text{L initial}}\right)$ vs Parameter:						
	$\frac{L(100)}{L_o}$	$\frac{L(200)}{L_o}$	dV, 200	dV, 200	Eff, 200	T_j = IVZ, 100	T_j = IVZ, 200
RCA							
30 C30123	0.320	0.332	0.897	0.844	0.621	0.106	0.380
90 C30119	0.549	0.637	0.404	0.400	0.656	0.896	0.924
Spectronics							
10 2231	0.498	0.483	0.528	0.520	0.619	0.745	0.645
11 2231F	0.420	0.596	0.440	0.459	0.007		0.604
34 2234	0.804		0.484	0.484	0.847	0.807	
40 2354	0.816	0.844	0.113	0.304	0.718		
41 2354F	0.697	0.713	0.238	0.304	0.718		
Mitsubishi							
14 MEK 104	0.875	0.701	0.188	0.173		0.097	0.243
Texas Instruments							
50 TIES 35	0.740	0.836	0.599	0.592		0.817	0.760
51 TIXL 35							
52 TI Special	0.581	0.673	0.331	0.333		0.808	0.870

Table 4. Summary of 200-hr Screening Test

Diode Type	Number in Lot	Number of Predicted Failures (100 hr)	Number of Predicted Failures (200 hr)	Number of Actual Failures (2,000 hr)	Number of Actual Failures (5,000 hr)	Type of Failures Screen Test
RCA C30123	36	12 (33%)	14 (39%)	8 (22%)	14 (39%)	Voltage
RCA C30119	36	24 (67%)	25 (68%)	24 (67%)	29 (81%)	Light Output
SPX 2231	36	3 (8%)	23 (64%)	16 (44%)	19 (53%)	Light Output
SPX 2231F	36	4 (11%)	35 (97%)	32 (89%)	32 (89%)	Light Output
SPX 2234	12	9 (75%)	11 (92%)	11 (92%)	12 (100%)	Light Output
SPX 2354	13	6 (46%)	9 (69%)	9 (69%)	11 (85%)	Light Output
MEK 104	31	3 (10%)	3 (10%)	3 (10%)	4 (13%)	Light Output
TI Special	18	4 (22%)	9 (50%)	9 (50%)	9 (50%)	Light Output
TIES 35	44	28 (64%)	31 (70%)	32 (73%)	36 (82%)	Light Output; Voltage
TIXL 35	42	15 (38%)	23 (59%)	23 (59%)	41 (100%)	Light Output
	304	108 (36%)	173 (57%)	167 (55%)	207 (68%)	

Results: 173 predicted failures, 167 actual failures (2,000 hr).
Test is 95-percent effective.

Table 5. Table of Correlation Coefficients--Half-Life, t ½ vs Parameters

Diode Mfgr. Lot/Type	Half-Life (t ½) vs				
	ΔT_j = IVZ	ΔT_j = $\Theta\ \ell n(L)$	dV, 200	MTTF, hr	J at Peak Efficiency, amp/cm^2
RCA					
30 C30123	0.759	0.747	0.719	30,000*	900
90 C30119	0.672	0.923	0.637	6,000	900
Spectronics					
10 2231	0.776	0.815	0.583	16,000*	2,500
11 2231F	0.934	0.931	0.331	4,000	1,500
34 2234				400	4,000
40 2354				1,200	250
41 2354F				1,200	
Mitsubishi					
MEK 104	0.423	0.450	0.107	60,000*	3,000
Texas Instruments					
50 TIES 35	0.812	0.852	0.430	400	1,200
51 TIXL 35	Bad Lot				
52 TI Special	0.912	0.849	0.271	8,000*	200

T_j = Junction temperature at 200 hr
ΔT_j = Change in junction temperature at 200 hr
V = Change in voltage at 200 hr
MTTF = Mean time to failure, hr (if greater than 5,000 hr, then extrapolated)
J = Current density amp/cm^2
* = Estimated

NOMENCLATURE

d	Derivative
I	Current, amp
I_o	Saturation current
k	Boltzmann constant
L_o	Pretest light output, mw
L(1)	Initial light output power, (first test point), MW
L (100, 200, 6,000, t)	Light output power (at 100, 200, and 6,000 hr, t hours), MW
Ln	Natural log
n	Number, $1 \leq n \leq 3$
q	Charge on electron
R	Bulk resistance, ohms
T	Temperature, °C or °K
T_a	Ambient temperature, °C
T_j	Junction temperature, °C
V_j	Junction voltage
Z	Thermal resistance, impedance °C/w
T_F	Fall time, sec
T_R	Rise time, sec
Δ	Change in
ΔT_R	Change in rise time, sec
η	External quantum efficiency
θ	Empirically determined temperature coefficient of efficiency, °C
λ	Decay rate, hr^{-1}